

# **STRUCTURAL AND PHOTOPHYSICAL PROPERTIES OF CHROMOPHORES-EMBEDDED POLY(LACTIDE)S**

by

**GANDU VIRAT**

**Registration No: 10CC17A39006**

A thesis submitted to the  
Academy of Scientific and Innovative Research  
for the award of the degree of  
**DOCTOR OF PHILOSOPHY**  
in  
**SCIENCE**

Under the Supervision of

**Dr. E. BHOJE GOWD**



**CSIR-National Institute for Interdisciplinary Science and Technology**

(CSIR-NIIST), Thiruvananthapuram- 695 019, Kerala, India



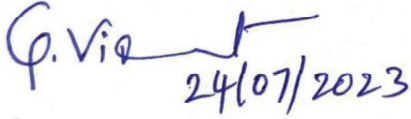
**Academy of Scientific and Innovative Research**

AcSIR Headquarters, CSIR-HRDC campus, Sector 19, Kamla Nehru Nagar,  
Ghaziabad, U.P.- 201002, India

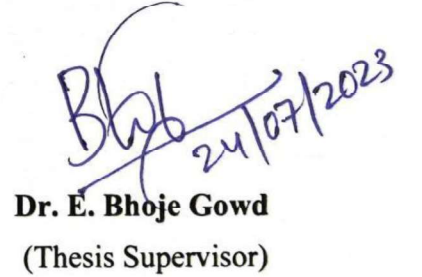
**July 2023**

## CERTIFICATE

This is to certify that the work incorporated in this Ph.D. thesis entitled, "*Structural and Photophysical Properties of Chromophores-Embedded Poly(Lactide)s*" submitted by **Mr. Gandu Virat** to the Academy of Scientific and Innovative Research (AcSIR) in fulfilment of the requirements for the award of the *Degree of Doctor of Philosophy in Science*, embodies original research work carried out by the student under my supervision and guidance. We further certify that this work has not been submitted to any other University or Institution in part or full for the award of any degree or diploma. Research material obtained from other sources has been duly acknowledged in the thesis. Any text, illustration, figures, table etc., used in the thesis from other sources, have also been duly cited and acknowledged.

  
24/07/2023

**Gandu Virat**  
Thiruvananthapuram  
24<sup>th</sup> July 2023

  
24/07/2023

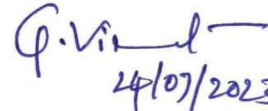
**Dr. E. Bhoje Gowd**  
(Thesis Supervisor)



डॉ. इ. भोजे गौड / Dr. E. BHOJE GOWD  
वरिष्ठ प्रधान वैज्ञानिक / Senior Principal Scientist  
पदार्थ विज्ञान तथा प्रौद्योगिकी प्रभाग  
Materials Science & Technology Division  
सी एस आई आर- राष्ट्रीय अंतरविषयी विज्ञान तथा प्रौद्योगिकी संस्थान  
CSIR - National Institute for Interdisciplinary  
Science and Technology (NIIST)  
तिरुवनन्तपुरम / Thiruvananthapuram-695 019

## STATEMENTS OF ACADEMIC INTEGRITY

I, **Gandu Virat.**, a Ph.D. student of the Academy of Scientific and Innovative Research (AcSIR) with Registration No. 10CC17A39006 hereby undertake that the thesis entitled "**Structural and Photophysical Properties of Chromophores-Embedded Poly(Lactide)s**" has been prepared by me and that the document reports original work carried out by me and is free of any plagiarism in compliance with the UGC Regulations on "*Promotion of Academic Integrity and Prevention of Plagiarism in Higher Educational Institutions (2018)*" and the CSIR Guidelines for "*Ethics in Research and in Governance (2020)*".

  
24/07/2023  
**Gandu Virat**

24<sup>th</sup> July 2023

Thiruvananthapuram

---

It is hereby certified that the work done by the student, under my supervision, is plagiarism-free in accordance with the UGC Regulations on "*Promotion of Academic Integrity and Prevention of Plagiarism in Higher Educational Institutions (2018)*" and the CSIR Guidelines for "*Ethics in Research and in Governance (2020)*".

  
24/07/2023  
**Dr. E. Bhoje Gowd**

24<sup>th</sup> July 2023

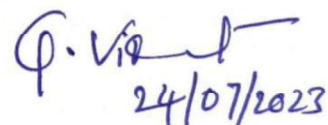
Thiruvananthapuram



## DECLARATION

I, **Gandu Virat.**, bearing AcSIR Registration No. 10CC17A39006 declare

- (i) that my thesis entitled, “**Structural and Photophysical Properties of Chromophores-Embedded Poly(Lactide)s**” is plagiarism free in accordance with the UGC Regulations on “*Promotion of Academic Integrity and Prevention of Plagiarism in Higher Educational Institutions (2018)*” and the CSIR Guidelines for “*Ethics in Research and in Governance (2020)*”.
- (ii) that I would be solely held responsible if any plagiarised content in my thesis is detected, which is violative of the UGC regulations 2018.

  
24/07/2023  
**Gandu Virat**

24<sup>th</sup> July 2023

Thiruvananthapuram

## ACKNOWLEDGEMENTS

With thanks to.....

*Dr. E. Bhoje Gowd, my research supervisor, for his invaluable guidance, continuous support and encouragement throughout my doctoral journey. His deep subject knowledge, expertise and constructive feedback have been instrumental in shaping my research work. I am grateful for his unwavering commitment and patience in sharing his time and resources with me. I am truly honored to have such a dedicated and supportive supervisor who has challenged me to attain my fullest potential. I owe him a debt of gratitude for his contributions to complete this thesis.*

*Dr. C. Anandharamakrishnan & Dr. A. Ajayaghosh, present and former directors, CSIR-NIIST, for providing the necessary facilities and infrastructure to carry out this investigation.*

*Dr. S. Ananthakumar, Dr. M. Ravi, Dr. S. Savithri, Dr. Harikrishna Bhat & Dr. P. Prabhakar Rao present and former Heads, Materials Science and Technology Division, for their valuable help and suggestions.*

*Dr. V. Karunakaran, Dr. C. H. Suresh & Dr. R. Luxmi Varma, present and former AcSIR coordinators for the help they provided me to successfully complete my coursework and other academic activities.*

*Dr. Saju Pillai, Dr. K.P. Surendran & Dr. Biswapriya Deb, DAC members, for their valuable comments and suggestions throughout my Ph.D. programme.*

*All the scientists and technical staff of CSIR-NIIST for their timely help. Especially I convey my sincere gratitude to Dr. K.K Maiti, Dr. T.P.D Rajan, Dr. U.S Hareesh, Dr. V.S. Prasad, Dr. Sanjib Banerjee, Dr. Sahoo, Dr. Subrata das, Dr. Joshy Joseph, Dr. V.K Praveen, Dr.*

*Sreejith Shankar, Dr. Ramesh, Mr. Peer Mohamed, Mr. Kiran Mohan, Ms. Soumini, Mr. Harish & Mr. Robert for their help in various characterization.*

*I am deeply and forever indebted to Dr. Shaiju P, Dr. Baku Nagendra, Dr. S. Nagarajan, Dr. Angel Mary Joseph, Dr. Sijla Rosely, Dr. Deepthi Krishnan, Dr. Jerin, Mr. Sivaprasad, Mr. Amal Raj, Dr. Praveena, Dr. Vipin G. Krishnan, Mrs. Sruthi, Mrs. Ashitha, Mrs. Akhila, Ms. Jefin, Ms. Mumthaz & Mr. Nasik for their constant love, care, motivation and support. This accomplishment would not have been possible without them.*

*My sincere gratitude to Mrs. Athmaja and Mr. Mukesh for the help they provided for the successful completion of my CSIR societal programme.*

*Special thanks to Dr. Gourab, Dr. Chinnadurai, Mr. Basavaraja, Ms. Drishya, Mr. Vijay Kumar and Mr. Dipak, for their timely help and support during my entire research period.*

*My sincere gratitude to Dr. Sandeepa, Dr. Arun, Dr. Ashish, Dr. Molji, Dr. Nimisha, Dr. Manu, Mr. Shamjith, Ms. Remya, Mr. Rahul, Ms. Tessy, Ms. Roshima, Mr. Thejus P.K, Ms. Krishna Priya, Ms. Parvathi, Ms. Sangeetha, Ms. Shisina, Ms. Sreevalsa, Ms. Ragi, Ms. Anjali.N, Ms. Hasna, Mr. Rishad & Ms. Haritha*

*I am thankful to all my friends at CSIR-NIIST for their help and cooperation. I Would also like to extend huge, warm thanks to Mr. Merin & Ms. Aswathi for their timely help in the AcSIR proceedings.*

*Finally, I thank CSIR-India for financial assistance.*

# TABLE OF CONTENTS

	<b>Page</b>
<b>Certificate</b>	i
<b>Statements of Academic Integrity</b>	iii
<b>Declaration</b>	v
<b>Acknowledgements</b>	vii
<b>Table of Contents</b>	ix
<b>List of Abbreviations</b>	xiii
<b>Preface</b>	xv

---

<b>Chapter 1</b>	<b>Introduction</b>	<b>1-35</b>
------------------	---------------------	-------------

---

1.1.	<a href="#">Luminescence</a>	2
1.2.	<a href="#">Aggregation Caused Quenching</a>	4
1.3.	<a href="#">Aggregation-Induced Emission</a>	6
1.4.	<a href="#">Applications of Fluorescence</a>	9
1.5.	<a href="#">Tunable Emission</a>	10
1.6.	<a href="#">Fluorescent Polymers</a>	12
1.6.1.	<a href="#">Conjugated Fluorescent Polymers</a>	12
1.6.2.	<a href="#">Non-conjugated Fluorescent Polymers</a>	13
1.7.	<a href="#">Polylactic Acid</a>	14
1.8.	<a href="#">Polymer Crystallization</a>	16
1.8.1.	<a href="#">Polymorphism in PLLA</a>	18
1.8.2.	<a href="#">Melt Crystallization of PLLA</a>	19
1.8.3.	<a href="#">Solvent-Induced Crystallization of PLLA</a>	20
1.8.4.	<a href="#">Gels of PLLA</a>	21
1.8.5.	<a href="#">Single Crystals of PLLA</a>	22
1.8.6.	<a href="#">Chromophore-Embedded PLLA</a>	23
1.8.7.	<a href="#">Polymer Crystallization Induced Chirality Transfer to Achiral Chromophore in Chromophore-Embedded PLLA</a>	23

1.8.8.	<a href="#">Polymer Crystallization Controlled Emission Properties in Chromophore-Embedded PLLA</a>	25
1.8.9.	<a href="#">Crystallization-Driven Self-assembly of Chromophore-Appended PLLAs</a>	26
1.9.	<a href="#">Scope and Objectives of the Present Thesis</a>	28
1.10.	<a href="#">References</a>	29

---

<b>Chapter 2</b>	<b>Poly(L-lactide)s with Tetraphenylethylene: Role of Polymer Chain Packing on Aggregation-Induced Emission Behavior of Tetraphenylethylene</b>	<b>36-69</b>
------------------	---	--------------

---

2.1.	<a href="#">Abstract</a>	36
2.2.	<a href="#">Introduction</a>	37
2.3.	<a href="#">Experimental</a>	40
2.3.1.	<a href="#">Materials</a>	40
2.3.2.	<a href="#">Synthesis of One-armed, Two-armed and SSPLLA</a>	41
2.3.3.	<a href="#">Sample Preparation</a>	41
2.3.3.1.	<a href="#">Preparation of SSPLLA Gel</a>	41
2.3.3.2.	<a href="#">Preparation of SSPLLA Precipitates</a>	42
2.4.	<a href="#">Characterization</a>	42
2.5.	<a href="#">Results and Discussion</a>	44
2.5.1.	<a href="#">Structural and Thermal Properties of One-armed, Two-armed and Four-armed PLLAs with Tetraphenylethylene as Core</a>	44
2.5.2.	<a href="#">Photophysical Properties of SSPLLA</a>	49
2.5.3.	<a href="#">Aggregation-Induced Emission One-armed, Two-armed and SSPLLA</a>	51
2.5.4.	<a href="#">Effect of Crystal-to-crystal Transition on Emission Behavior of SSPLLA</a>	55
2.5.5.	<a href="#">Cytotoxicity and Antibacterial Properties of SSPLLA</a>	62
2.6.	<a href="#">Conclusions</a>	64
2.7.	<a href="#">References</a>	65

---



---

<b>Chapter 3</b>	<b>Polymer Crystallization Enabled Excimer Emission in Anthracene-Appended Poly(L-lactide)s</b>	<b>70-97</b>
------------------	---	--------------

---

3.1.	<a href="#">Abstract</a>	70
3.2.	<a href="#">Introduction</a>	71
3.3.	<a href="#">Experimental Section</a>	74
3.3.1.	<a href="#">Materials</a>	74
3.3.2.	<a href="#">Synthesis of Anthracene-Appended PLLA- 1 (AAP-1)</a>	74
3.3.3.	<a href="#">Synthesis of Anthracene-Appended PLLA- 2 (AAP-2)</a>	75
3.3.4.	<a href="#">Sample Preparation</a>	75
3.3.4.1.	<a href="#">Preparation of Semicrystalline Sample of AAP-1</a>	75
3.3.4.2.	<a href="#">Preparation of Single Crystals of AAP-1</a>	75
3.3.4.3.	<a href="#">Preparation of AAP-1 Gel</a>	75
3.4.	<a href="#">Characterization</a>	76
3.5.	<a href="#">Results and Discussion</a>	77
3.5.1.	<a href="#">Structural and Thermal Properties of Anthracene-Appended PLLAs</a>	77
3.5.2.	<a href="#">Impact of Polymer Chain length on Anthracene Excimer Formation</a>	80
3.5.3.	<a href="#">Impact of Polymer Chain Packing on Anthracene Emission</a>	82
3.5.4.	<a href="#">Influence of Crystallization of AAP-1 on Anthracene Excimer Emission</a>	85
3.5.5.	<a href="#">Role of Polymorphism of AAP-1 on Anthracene Excimer Emission</a>	88
3.6.	<a href="#">Conclusions</a>	92
3.7.	<a href="#">References</a>	93

---

<b>Chapter 4</b>	<b>Impact of Polymer Chain Packing and Crystallization on Emission Behavior of Curcumin-Embedded Poly(L-lactide)s</b>	<b>98-125</b>
------------------	---	---------------

---

4.1.	<a href="#">Abstract</a>	98
------	--------------------------	----

4.2.	<a href="#">Introduction</a>	98
4.3.	<a href="#">Experimental Section</a>	101
4.3.1.	<a href="#">Materials</a>	101
4.3.2.	<a href="#">Synthesis of Curcumin-PLLA</a>	102
4.3.3.	<a href="#">Preparation of Isothermally Melt-crystallized Samples</a>	102
4.3.4.	<a href="#">Preparation of Single Crystals of Curcumin-PLLA</a>	102
4.3.5.	<a href="#">Preparation of Curcumin-PLLA Gel</a>	102
4.4.	<a href="#">Characterization and Measurements</a>	103
4.5.	<a href="#">Results and Discussion</a>	103
4.5.1.	<a href="#">Structural and Thermal Properties of Curcumin-PLLA</a>	103
4.5.2.	<a href="#">Influence of Polymer Chain Conformation and Crystallization Conditions</a>	107
4.5.3.	<a href="#">Effect of Isothermal Crystallization of Curcumin-PLLA on Emission of Curcumin</a>	109
4.5.4.	<a href="#">Emission behaviour of Curcumin-PLLA Single Crystals</a>	115
4.5.5.	<a href="#">Emission behaviour of Curcumin-PLLA Gel</a>	117
4.6.	<a href="#">Conclusions</a>	121
4.7.	<a href="#">References</a>	122

---

<b>Chapter 5</b>	<b>Overall Summary and Future Perspectives</b>	<b>126-130</b>
------------------	--	----------------

---

5.1.	<a href="#">Overall Summary</a>	126
5.2.	<a href="#">Future Perspectives</a>	129
	<b>Abstract</b>	<b>131</b>
	<b>List of Publications</b>	<b>133</b>
	<b>List of Conference Presentations</b>	<b>135</b>
	<b>Attachment of the Photocopy of Publications</b>	<b>137</b>

## LIST OF ABBREVIATIONS

$\omega$	Angular frequency
$D$	Dispersity index
AFM	Atomic force microscopy
CD	Circular dichroism
$\text{CDCl}_3$	Deuterated chloroform
CPO	Cyclopentanone
DMA	N,N-dimethylacetamide
DMF	N,N-dimethylformamide
DSC	Differential scanning calorimetry
FTIR	Fourier transform infrared spectroscopy
$G'$	Storage modulus
$G''$	Loss modulus
GPC	Gel permeation chromatography
iPrOH	Isopropanol
IR	Infrared
$L$	Long period
$l_a$	Amorphous thickness
$l_c$	Lamellar thickness
$M_n$	Number-average molecular weight
$M_w$	Weight-average molecular weight
NMR	Nuclear magnetic resonance
PDI	Polydispersity Index
PDLA	Poly( <i>D</i> -lactide)

PDLLA	Poly ( <i>DL</i> -lactide)
PL	Photoluminescence
PLA	Poly lactic acid
PLLA	Poly( <i>L</i> -lactide)
POM	Polarized optical microscopy
Ppm	Parts per million
SAXS	Small-angle X-ray scattering
SSPDLA	Star-shaped Poly( <i>D</i> -lactide)
SSPLLA	Star-shaped Poly( <i>L</i> -lactide)
$T_c$	Crystallization temperature
$T_{cc}$	Cold crystallisation temperature
TEM	Transmission electron microscopy
$T_g$	Glass transition temperature
THF	Tetrahydrofuran
TPE	Tetraphenylethylene
$T_m$	Melting temperature
TMS	Tetramethylsilane
UV-Vis	Ultraviolet-visible
WAXD	Wide-angle X-ray diffraction
WAXS	Wide-angle X-ray scattering
$X_c$	Degree of crystallinity
XRD	X-ray diffraction

## PREFACE

Fluorescent materials have garnered significant attention in recent decades owing to their extensive scope of applications. The incorporation of fluorescent molecules into polymers is anticipated to further extend the potential uses of these materials. This covalent approach offers various benefits such as enhanced processability, solubility, mechanical stability, thermal stability, and structural diversity. The rationale behind choosing the poly(L-lactide) is briefly described in **Chapter 1**. Poly(L-lactide) is a biocompatible and biodegradable polymer. Presently, the development of biocompatible and biodegradable fluorescent polymers that exhibit well-understood fluorescence characteristics has emerged as a highly desirable goal. The properties and performance of these materials are inherently linked to their molecular and hierarchical structures, necessitating a thorough comprehension of the structure-property relationship for the rational design of hybrid materials exhibiting optimized fluorescent properties and promoting their potential applications.

Inspired by the brilliant pieces of work in the area of polymer crystallization, we have designed and synthesized one-armed, two-armed, and four-armed poly(L-lactide)s utilizing hydroxyl-modified tetraphenylethylene (TPE) as a macroinitiator in **Chapter 2** with the aim of studying the role of polymer chain packing on aggregation-induced emission behavior of tetraphenylethylene. Star-shaped poly(L-lactide) (SSPLLA) exhibits stronger fluorescence as compared to one-armed and two-armed PLLAs in the gel state. For SSPLLA gels in N, N-dimethylformamide (DMF), PLLA crystallized into the  $\epsilon$  form, and the larger TPE molecules are excluded from the crystalline phase, emitting a cyan color at room temperature. Heating of the gel leads to the phase transition from the  $\epsilon$  to  $\alpha$  form over a broad temperature range. This crystal-to-crystal transition of PLLA causes the

rotation of the phenyl rings of TPE and results in a significant blue shift in the fluorescence of SSPLLA due to the shorter conjugation length. However, further heating even in the semicrystalline state ( $\alpha$  form) causes a complete quenching of emission because of the free rotation of phenyl rings of TPE. Unlike gel, the SSPLLA precipitates in N,N-dimethylacetamide (DMA) crystallized into the  $\alpha$  form, shows decreased fluorescence emission with increasing temperature, and the blue shift being observed at higher temperatures because of the increased mobility of amorphous chains.

Then we attempted to tune the excimer formation of anthracene by synthesizing anthracene-appended poly(L-lactide) polymers having different molecular weights in **Chapter 3**. We successfully demonstrated that the crystallization and polymorphism of polymers dictated the photophysical properties of the anthracene-appended PLLAs. The amorphous (melt-quenched) polymer predominantly emits in the dark blue region mainly from its monomeric state due to the fine dispersion of anthracene moieties throughout the polymer matrix. Crystallization of the polymer expels the anthracene moieties into the amorphous region or on the surface of crystals (in the case of single crystals). Crystallization of the PLLA chains into diamond-shaped crystals regulates the anthracene moieties to locate on the surface of the crystals and no evidence of  $\pi$ - $\pi$  stacking of anthracene moieties was observed in this case resulting in the dark blue emission similar to the amorphous thin films. In the semicrystalline state (melt-crystallized  $\alpha$  form and gel state ( $\varepsilon$  form)), covalently-linked anthracene moieties reside at the interface of crystalline and amorphous domains by either dipolar interactions or  $\pi$ -stacking. The  $\alpha$  form emits fluorescence in the cyan region that is mainly arising from both anthracene excimers and monomers. But in the case of gels ( $\varepsilon$  form), exclusive excimer emission was observed where the emission bands are located at 473, 505, and 560 nm indicating the formation of three types of excimers (i.e., anthracene moieties overlapping at an angle of  $55^\circ$  to each

other, T-shaped excimers and sandwich-type excimers). These results suggested that the molecular arrangement of anthracene moieties can be modulated by changing the structure and morphology of anthracene-appended PLLA in different forms (amorphous, semicrystalline, single crystals, and gels).

**Chapter 4** focuses on the development of biodegradable and biocompatible curcumin-embedded poly(L-lactide) systems, catering to the burgeoning need for bioactive fluorescent materials. Similar to previous work, the crystal structure and polymer chain conformation in PLLA strongly influenced their photophysical properties. The fluorescence behavior of curcumin-PLLA was found to be reliant upon the crystallization conditions of the polymer, as demonstrated by isothermal crystallization studies from the melt state. The changes in the emission behavior of curcumin-PLLA were attributed to the rotation of two phenyl rings with respect to the central keto-enol group induced by the covalently linked helical PLLA chains, as well as the average intermolecular distance of curcumin molecules on the crystalline folding surface in the semicrystalline morphology. The salient features of the overall work were summarized in chapter 5 along with the future perspectives.





# Chapter 1

---

---

## Introduction

---

---

## 1.1. Luminescence

Luminescence is a natural phenomenon that occurs when certain materials emit light without producing heat. It encompasses a wide range of technologies, including fluorescence, phosphorescence, bioluminescence, and chemiluminescence. A scientific theory or concept refers to a notion or framework that elucidates certain natural phenomena and plays a significant part in the establishment of novel subjects. As one searches for substantiation, the theory is revised, verified, and leads to further progression in the field. Sir George G. Stokes first witnessed the luminescence phenomenon in 1852. As per his observation, certain substances would emit light of a different color than the light they absorbed. How and why certain substances emit light is one of many questions raised by Stokes's discovery.<sup>1</sup>

Prior to the discovery of Stokes, numerous researchers noticed the enchanting luminescent behavior. Notably, researchers like Galileo, Boyle, Edward D. Clarke, and Newton endeavored to explicate it.<sup>2</sup> For instance, Edward D. Clarke discovered a luminescent substance called "Durham fluor" in Cambridge in 1819. The crystal of this substance displayed dichroic behavior, appearing as a deep sapphire blue in reflected light and intense emerald green in transmitted light,<sup>3</sup> as shown in Figure 1.1. Nevertheless, because of insufficient knowledge in photophysics, the studies on luminescence were not comprehended well during that duration.<sup>4</sup> Similar to other scientific disciplines, scientific inquiry into luminescence entails observing the phenomenon to summarize the laws on the macro-scale, studying the mechanism on the microscale, and ultimately achieving a total comprehension of the phenomenon.

---

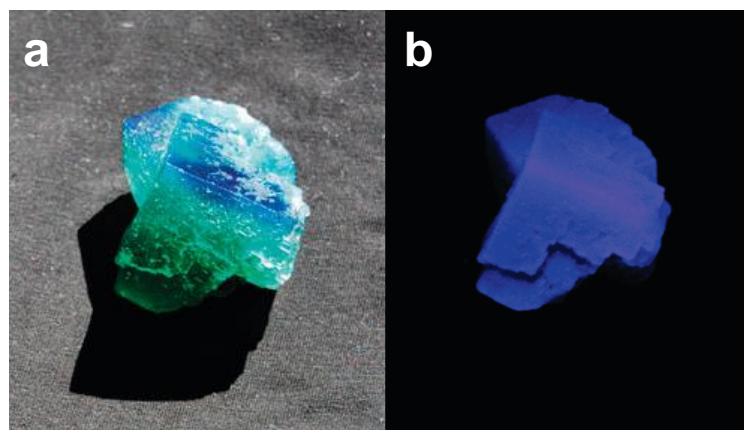


**Figure 1.1.** Images of green fluorite crystals (a) under daylight and (b) under UV light.<sup>3</sup>(from Rogerley, Weardale, Durham County, England).

In the decades following Stokes's discovery, scientists began to study luminescence more extensively. In 1896, Henri Becquerel discovered that certain minerals would emit light when exposed to radiation, laying the foundation for the study of radioactive materials. In 1911, Marie Curie and Andre Debierne discovered that radium emitted a type of radiation that caused nearby air molecules to luminous,<sup>5</sup> which helped them to better understand the properties of radioactivity.

After centuries of uninterrupted investigation into luminescence occurrences and luminescent substances, particularly at the molecular scale, a more profound comprehension of the workings of luminescence has emerged. Scientists have concluded that the luminescent characteristic of a substance originates from the deactivation of the energized state of the molecule that takes in light energy.<sup>6</sup> This knowledge has paved the way for significant progress in the field, culminating in the introduction of the Jablonski diagram<sup>7</sup> in 1933, which depicts the probable processes that a molecule, upon exposure to light, undergoes, encompassing photon absorption, vibrational relaxation (VR), fluorescence, internal conversion (IC), intersystem crossing (ISC), delayed fluorescence, and phosphorescence (Figure 1.2). One of the most well-known examples of luminescence

---

is fluorescence, which is the emission of light by a material when it is excited by a light source of a shorter wavelength. The fluorescence qualities of a substance may be affected by numerous factors, like chemical structure, environment, and interaction with other elements. The notion of fluorescence at the molecular level has enriched the comprehension of the topic and offered a framework for the progress in fluorescence science.

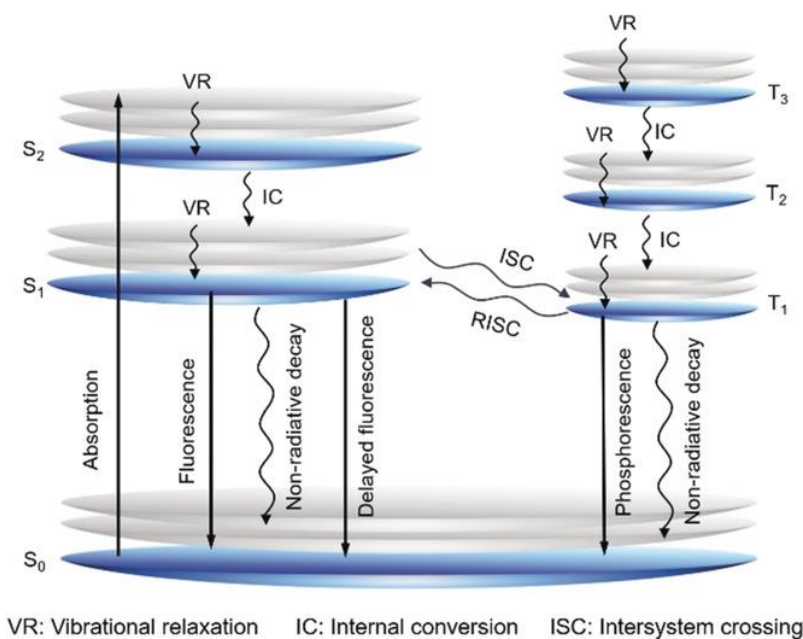


**Figure 1.2.** *Jablonski diagram.*<sup>2</sup>

## 1.2. Aggregation Caused Quenching

Fluorescent materials can potentially be applied in all physical forms, which include gas, liquid, and solid.<sup>8</sup> Classical fluorescence studies have been executed in the solution state<sup>9,10,11,12,13</sup> wherein photophysical parameters, including exciton lifetime, fluorescence efficiency, and decay rate, are measured in highly diluted solutions. The isolated chromophore molecules in these solutions are not significantly disturbed by chromophoric interactions and can be analyzed better. Although, the findings derived from diluted solution data are not applicable to concentrated solutions. A lot of organic fluorophores behave differently with regard to light emission in both concentrated and diluted solutions. Traditional fluorophores, such as flat molecules with discotic shapes, demonstrate efficient

fluorescence when they are molecularly dispersed or genuinely dissolved in their solvent. Chromophore molecules, when laid or agglomerated tightly, usually encounter strong  $\pi$ - $\pi$  interactions in the solid or aggregate state. Consequently, the fluorescence often diminishes. The formation of aggregations mechanistically causes quenching, possibly because the quenching effect is often mentioned as "aggregation-caused quenching" (ACQ).

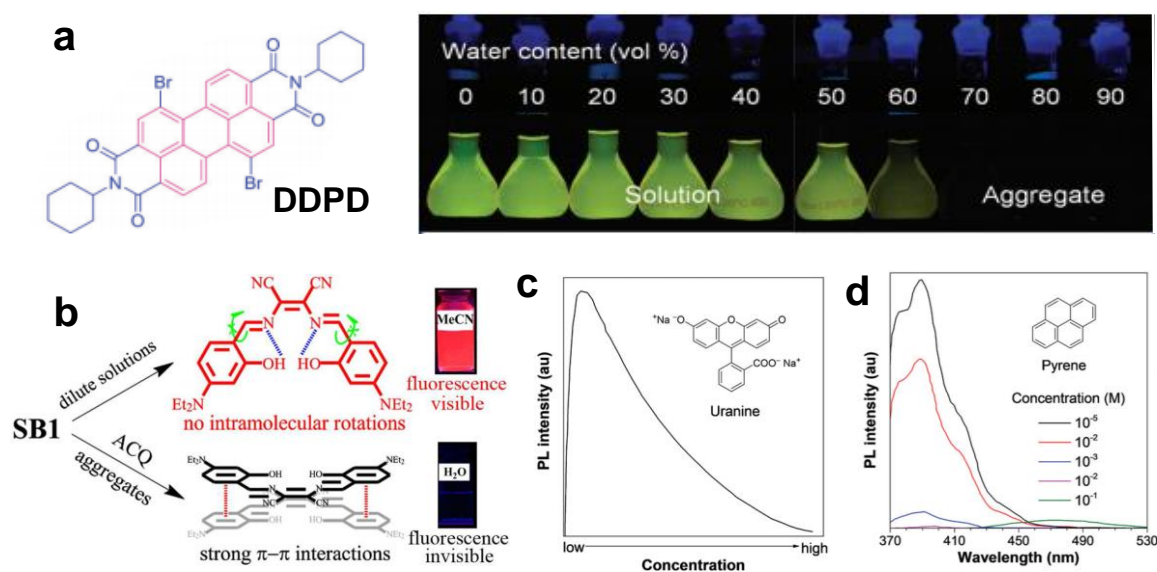


**Figure 1.3.** a) Chemical structure and photographs of ACQ behavior of DDPD,<sup>14</sup> b) ACQ behavior of SB1 molecule,<sup>15</sup> c) and d) plot of fluorescence intensity versus concentration of uranine solution and fluorescence spectra of pyrene in THF at various concentrations, respectively.<sup>16</sup>

Figure 1.3a illustrates a case of the ACQ phenomenon whereby the fluorescence of the dilute perylene diimide derivative (DDPD) in tetrahydrofuran (THF) (at 10  $\mu$ M) is very strong. However, due to DDPD's insoluble nature in water and the formation of DDPD molecular aggregates, the fluorescence becomes weaker with the addition of water to THF. Once the water content reaches over 60 vol%, there is a poor solvating effect in THF/water

mixture resulting in aggregated DDPD molecules. Consequently, the stacking of DDPD molecules leads to the quenching of the fluorescence.

An additional illustration of ACQ pertains to SB1 (salicylaldehyde-based Schiff base), possessing high emission when diluted in acetonitrile; however, as shown in Figure 1.3b, the aggregation of SB1 in water leads to nonemissive behavior due to strong  $\pi$ - $\pi$  interactions.<sup>15</sup> Similarly, uranine and pyrene exhibit high emissions in diluted solutions, but a decrease in emission arises with the rise in concentration,<sup>16</sup> as shown in Figures 1.3c and 1.3d, respectively. Because the planar aromatic rings are electronically conjugated, the ACQ behavior is common in most of the traditional fluorophores. This ACQ behavior is a problematic hurdle for making efficient light-emitting diodes (LEDs), where fluorophores are used as solid thin films. The use of fluorophores as sensors in physiological buffers and as probes to monitor ionic species is also problematic due to the ACQ nature. So, the ACQ effect is considered detrimental to real-world applications.

Numerous research groups recognize the detrimental effects of the ACQ on practical applications and therefore have taken a variety of measures to combat the problem, including using chemical reactions<sup>17</sup> and/or physical methods<sup>18</sup> to impede the formation of chromophoric aggregates or utilize aggregation to enhance the fluorescence property. Moreover, research on molecular luminescence shows that luminescence occurs at the level of a single molecule, and the properties of that molecule determine its luminescence characteristics. In turn, this means that the characteristics of tiny molecules are also present in their macroscopic materials.<sup>19</sup>

### **1.3. Aggregation-Induced Emission**

It is crucial to note that certain endeavors run counter to natural processes since chromophore molecules hold a natural inclination towards aggregate in highly concentrated solutions or the solid state. Therefore, an approach to tackling this problem needs a

---

fundamental change as it is impractical to work against forces beyond our control. Tang and his colleagues discovered an exceptional fluorescent system that utilized aggregation building rather than tearing down, as seen in traditional systems. This discovery involved a variety of silole derivatives that are non-fluorescent in diluted solutions but immensely fluorescent when these fluorophores are aggregated in very concentrated solutions or solid-state. This process was termed "aggregation-induced emission" (AIE) since the formation of aggregates enhanced fluorescence.<sup>20</sup>

Hexaphenylsilole (HPS), one of the initial compounds in the silole derivatives category, was an archetypal AIE luminogen. Diluted HPS molecules exhibit a nonemissive behavior when dissolved in THF, whereas their aggregation in THF/water mixture exhibits highly emissive behavior<sup>21</sup> (Figures 1.4a and 1.4b). Structural inspection showed that HPS, unlike conventional luminophores, is a molecule with non-planar shape resembling a propeller. This distinct molecular structure is responsible for the disparity in fluorescence behavior. Due to its molecular structure, HPS molecules cannot undergo  $\pi$ - $\pi$  stacking and the movement of its aromatic rings is substantially limited, preventing intramolecular rotations. Consequently, this restricted rotation hinders the non-radiative pathway and allows the radiative channel to open, thus rendering HPS molecules emissive when they are in an aggregate state.

With the advent of numerous AIE systems following the discovery of the phenomenon by HPS, scientists have approached different ways to achieve AIE. One way involves manipulating the conformation of fluorophores. For instance, Mina et al. designed an AIE system using an azobenzene derivative that was nonemissive in its trans isomeric form (Figure 1.4c). However, by transforming it into a cis isomeric form through UV light exposure, they were able to induce strong emission behavior.<sup>22</sup> Another approach involves modifying the covalent modification of the fluorophore by introducing substituents to

---

control their stacking, leading to strong emission. For example, 1,4-di[(E)-styryl]benzene is a planar ACQ-type molecule that is nonemissive in an aggregated state (Figure 1.4d), its modification with two methyl groups results in a twisted AIE-type molecule that enhances emission upon aggregation<sup>23</sup> (Figure 1.4e).

The AIE effect creates the possibility to study fluorescence behavior even in aggregate or solid state, thereby learning more about the structure-property relationship as well as about the underlying mechanisms. Such knowledge can reveal instructive structural design methods for efficient luminogens. Due to the fact that the AIE is a photophysical effect connected to solid-state light emission, it has the potential to inspire technological advances that were previously unthinkable. It is essential to note that diverse photophysical properties have been thoroughly examined in diluted solutions, but luminescence behaviors in the aggregate state remain greatly understudied.

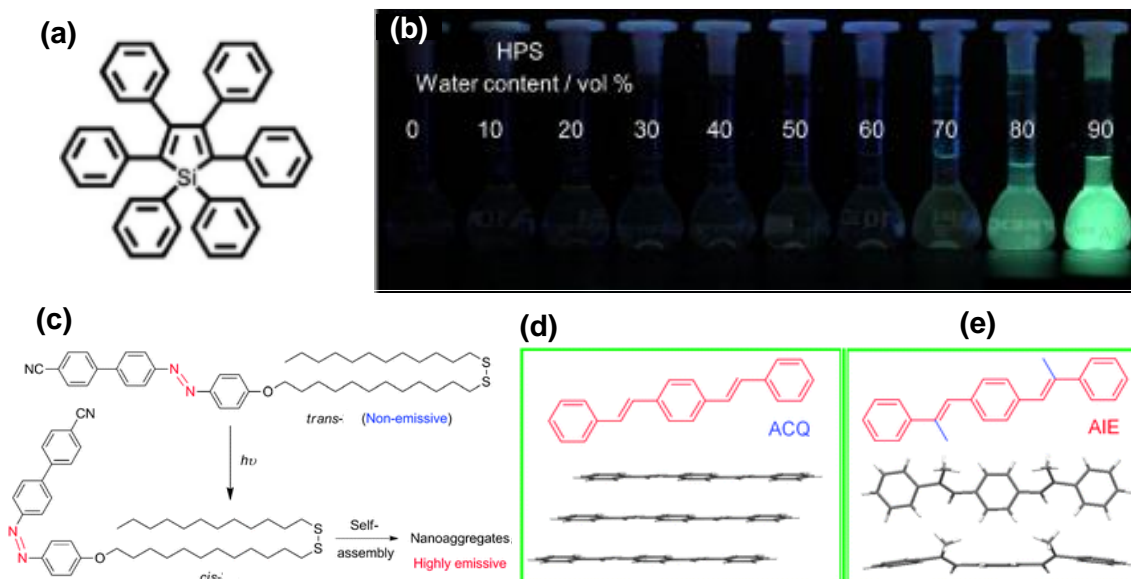


**Figure 1.4.** a) Chemical structure and b) photographs of AIE behavior of hexaphenylsilole in THF/water mixtures with various water content,<sup>21</sup> (c) influence of trans-to-cis isomerization on the fluorescence of azobenzene derivative.<sup>22</sup> (d) stacking behavior of 1,4-di[(E)-styryl]benzene and (e) its dimethylated derivative of 1,4-di[(E)-styryl]benzene.<sup>23</sup>



## **1.4. Applications of Fluorescence**

Fluorescence has become integral to several fields, especially in the biological and medical sciences, due to its non-invasive approach to studying biological processes in living tissues and cells. Fluorescence imaging, which has become an effective tool for cell biology, enables the depiction of cellular functions like protein localization, signaling pathways, and gene expression in real-time and high-resolution using microscopy-based methods like confocal microscopy.<sup>24</sup>

The development of fluorescence biosensors as molecular probes allows for detecting changes in the biological system or molecules.<sup>25</sup> These sensors are engineered proteins or peptides that undergo a change in their fluorescence properties in response to a particular stimulus or target molecule. With their potential in examining protein-protein interactions, enzyme activities, and intracellular signaling pathways, fluorescence biosensors are vital in studying environmental changes and providing early warning systems for potential health risks by monitoring the surroundings for specific pollutants.

The significance of fluorescence-based assays in medical diagnostics continues to increase since the high sensitivity and specificity of these assays make them a suitable fit for quantitatively detecting low levels of analytes in complex biological samples. Fluorescence-based assays have found applications in a broad array of areas ranging from drug discovery to disease diagnosis and monitoring disease progression, screening of drug molecules, for instance, detecting specific antigens or antibodies in blood samples to diagnose infectious conditions and imaging tumors *in vivo* for cancer diagnosis.<sup>26</sup>

Another major application of fluorescence is the invention of light-emitting diodes (LEDs) and due to its advances such as less energy consumption, trustworthy<sup>27</sup> and environmental convenience,<sup>28</sup> these devices have a huge effect on our life. The design and synthesis of LEDs have raised increasing interest because of their potential application

---

in residential lighting,<sup>29</sup> healthcare,<sup>30, 31</sup> horticulture lighting,<sup>32</sup> architecture,<sup>33</sup> optoelectronic devices,<sup>34</sup> facades<sup>35</sup> and industrial purposes.<sup>36</sup> As advancements continue in the development of fluorescent molecules and imaging techniques, fluorescence is becoming more prominent and indispensable, establishing itself as a primary tool across fields from life sciences to industrial applications.

## 1.5. Tunable Emission

Tunable emission is a property of materials that allows them to modify their emission wavelength or intensity, and there is an increasing demand for developing molecular systems with diverse emission properties. This is particularly important for a wide range of smart molecular materials, including sensors,<sup>37</sup> bioimaging,<sup>38</sup> and LEDs.<sup>39</sup> Initially, the development of tunable emission primarily involved chemical modification of fluorescent molecules to change their energy levels or generate charge transfers.<sup>40</sup> However, drawbacks to this strategy include challenges associated with chemical synthesis, rigid molecular structures, and nonadjustable emission properties, which are not ideal for smart fluorescent materials. Fortunately, the discovery of AIE has created new opportunities for diverse fluorescence studies, particularly for multicolor fluorescence systems. The capacity of fluorescent materials to display tunable emissions is a unique benefit, making it suitable for multiple applications.

Tuning the emission color of fluorescent systems is of great importance, and it can be achieved in several ways. For example, organic dyes can exhibit tunable fluorescence through changes in their molecular structure or conformation, while inorganic materials such as quantum dots (Figure 1.5a) exhibit tunable fluorescence through changes in their size, shape, and composition.<sup>41, 42, 43</sup> The emission properties of fluorophores can also be tuned by applying external electrical fields or mechanical force (Figure 1.5b).<sup>44,45, 46</sup> This method has the advantage of being non-invasive and reversible, making it useful for

---

applications such as sensing. Few fluorophores exhibit temperature-dependent fluorescence, where the emission wavelength or intensity changes with temperature and such materials can be used for temperature sensing applications<sup>47, 48</sup> (Figure 1.5c). pH is another parameter that can be used to tune the fluorescence emission of certain fluorophores (Figure 1.5d).<sup>49, 50</sup> Further, some fluorophores exhibit solvatochromic fluorescence and are highly sensitive to changes in the chemical environment, making them useful for applications such as chemical sensing<sup>51,52</sup> (Figure 1.5e). For practical applications, designing light-emitting materials with tunable fluorescence, particularly in solid or aggregate states, is a crucial area of interest.

The conformation of fluorescent molecules strongly depends on molecular assembly, packing forces and rigidity of the system, which can also be controlled by crystallinity. However, poor solubility and processability of fluorescent molecules pose different challenges and limit their application. Among different methods, the covalent incorporation of various fluorophores in polymers to achieve different emission wavelengths attracted the attention of researchers. The changes in the fluorescence behavior are mainly due to the charge transfer (CT),<sup>53</sup> twisted intramolecular charge transfer (TICT),<sup>54</sup> excimer states,<sup>55</sup> or excited state intramolecular proton transfer (ESIPT).<sup>56</sup> Despite the potential of incorporating fluorophores into polymers to manipulate molecular fluorescence, there is a lack of a systematic approach obtaining multicolor emission from a single fluorophore in the aggregated state.

---

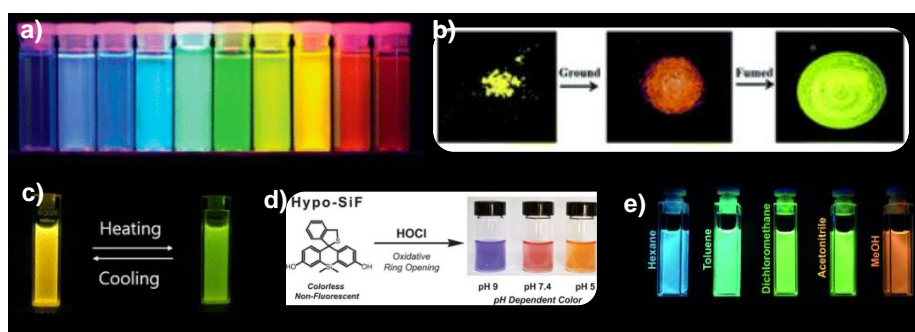


**Figure 1.5.** a) Tunable emission from size-tunable ZnS-capped CdSe QDs,<sup>42</sup> b) photographs of tunable emission behavior of TPE-SQ2 (pristine, after grinding and after fumed ether),<sup>46</sup> c) fluorescence images of V-EO7DCS nanoparticles upon heating in water,<sup>48</sup> d) pH-dependent fluorescence response of Hypo-SiF,<sup>50</sup> and e) color tunable property of pyrene derivative in different solvents.<sup>51</sup>

## 1.6. Fluorescent Polymers

Fluorescent polymers, also known as luminescent polymers, are typically conjugated polymers or polymers that have covalently incorporated fluorophores within their backbone or chain ends. Fluorescent polymers exhibit various benefits over traditional fluorophores, such as high stability, strong fluorescence intensity, and unmatched tunability. By varying the structure of the polymer, one can customize the optical properties, including the emission wavelength,<sup>57</sup> quantum yield,<sup>58</sup> and lifetime.<sup>59</sup> Fluorescent polymers can be used in a variety of applications due to their distinguishing features.

### 1.6.1 Conjugated Fluorescent Polymers

Conjugated polymers have been extensively used within optoelectronic devices owing to their unique properties and solution processability.<sup>60</sup> Although these materials have the potential to serve as next-generation displays, their limited lifetime and low light-emitting efficiency present the biggest obstacle.<sup>61</sup> The photophysical characteristics of

conducting polymers are influenced by the conformation and energy migration effectiveness of the polymer chain. These decisive elements are, sadly, very dependent on the synthesis circumstances, film processing, and photo-oxidation effects.<sup>62</sup> The aggregated polymer chains result in the aggregation quenching of the excited state and decrease the quantum yield. Controlling interchain interactions has the potential to improve polymeric LEDs' electrical and optical characteristics.<sup>63</sup> The singlet oxygen and molecular water alter the ionization levels of conducting polymer chains causing electron trapping and leading to polymer degradation, which eventually influences the stability, fluorescence efficiency and lifetime.<sup>64</sup> Further, their opacity, inability to form films by thermal processing, and nonbiodegradability are some of the limiting factors of these systems when using them in certain applications.

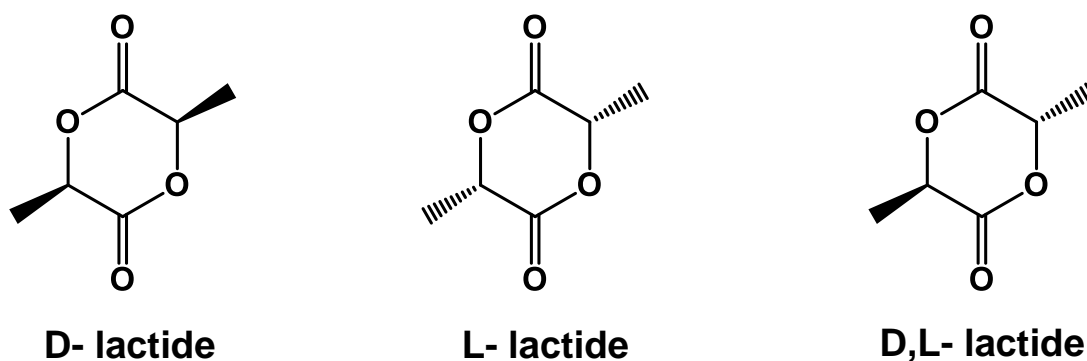
### **1.6.2 Non-conjugated Fluorescent Polymers**

Another approach for fluorescent polymers is to incorporate fluorescent dyes or chromophores into the polymers. This can be obtained either by covalent bonding or physical blending.<sup>65, 66</sup> Polymers can be customized to have specific optical, mechanical, and electrical properties, making them suitable for various applications such as wavelength emission, intensity, and lifetime. Polymers can be designed for high thermal and photochemical stability, which makes them applicable in solid-state lighting,<sup>67</sup> sensors,<sup>68</sup> and displays.<sup>69</sup> The processability of fluorescent polymer materials is simpler than small organic compounds such as solution casting,<sup>70</sup> spin-coating,<sup>71</sup> and inkjet printing.<sup>72</sup> By tailoring fluorescent polymers to be biodegradable, non-toxic, and non-immunogenic, researchers have broadened their utilization in various biological and drug delivery studies, where they can be used as diagnostic or therapeutic agents. In this respect, polymeric fluorescent materials have drawn significant attention.

---

## 1.7. Polylactic Acid

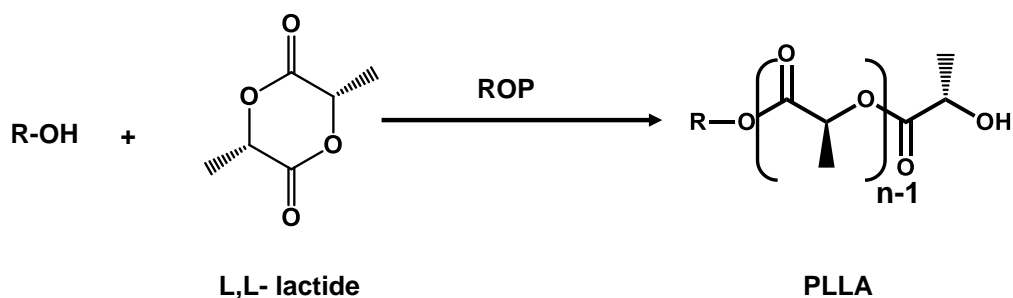
Polylactic acid (PLA) belongs to the family of aliphatic polyesters, which is produced from bioresources.<sup>73</sup> It is a polymer that has been approved by the United States Food and Drug Administration (FDA). Because of its biodegradable and biocompatible nature, this polymer is widely used for the development of degradable and medicinal applications like packaging,<sup>74</sup> drug delivery,<sup>75</sup> bioimplants,<sup>75</sup> etc. Polylactic acid is synthesized from the lactic acid monomer. Lactide is a cyclic dimer of lactic acid that is utilized in the ring-opening polymerization (ROP) process to synthesize PLA.



**Scheme 1.1.** Chemical structures of *D*-lactide, *L*-lactide and *D,L*-lactide.

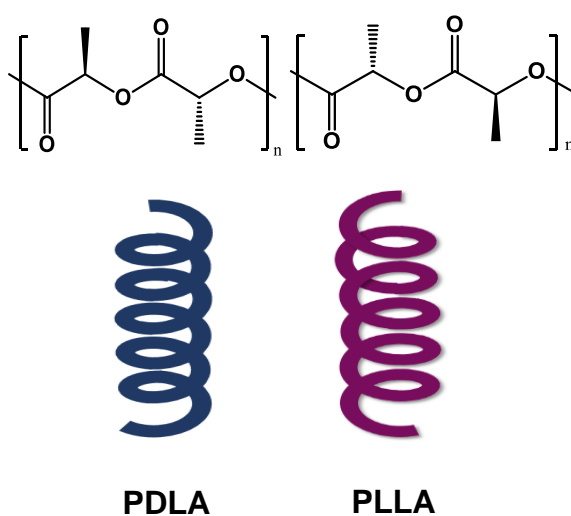
Lactide possesses the crucial characteristic of existing in three different forms (two optically active forms and one inactive form), i.e., *D*-lactide, *L*-lactide and *D, L*-lactide (Scheme 1.1). The polymers synthesized from *D*-lactide, *L*-lactide, and *D, L*-lactide are referred as poly(*D*-lactide) (PDLA), poly(*L*-lactide) (PLLA) and poly(*D, L*-lactide) (PDLLA), respectively. PLA can be prepared in two different ways. One method is condensation of lactic acid, which will give brittle, low molecular weight PLA. The second approach ring-opening polymerization of lactide which produces high molecular weight PLA. It is a controlled polymerization technique where cyclic monomers are transformed into a linear polymer. Poly(*L*-lactide) is formed by ring-opening polymerization of *L*-lactide

in the presence of a hydroxy functionalized initiator and stannous octoate, as depicted in Scheme 1.2. To ensure proper PLA production, it is crucial to maintain the optical purity of lactide since even minute quantities of enantiomeric impurities can significantly alter properties such as crystallinity and biodegradability.<sup>76, 77</sup>



**Scheme 1.2.** Ring-opening polymerization of poly(L-lactide) from L-lactide.

PDLLA is a non-crystalline polymer because of the irregular arrangement of L and D units, which is referred as a racemic mixture. Conversely, PLLA and PDLA are semicrystalline polymers, which come in two optically active forms (chiral) and exhibit similar features. Notably, as illustrated in Scheme 1.3, PDLA displays right-handed helicity, while PLLA exhibits left-handed helicity.



**Scheme 1.3.** Right-handed helicity of PDLA (left side) and left-handed helicity of PLLA (right side).

PLLA is the most commonly used isomer of PLA. PLLA is a thermoplastic polymer with a melting point ( $T_m$ ) of 160 -180 °C and a glass transition temperature ( $T_g$ ) of around 60 °C, which differ based on impurities and molecular weight. Interestingly, PLLA has higher crystallinity and tensile strength properties than PDLA.<sup>78</sup> PLLA degradation rate is significantly lower than PDLLA because of the presence of the crystalline region.

## 1.8. Polymer Crystallization

The polymer crystallization process is complicated and it involves the formation of highly ordered and well-defined structures in polymers, which was initially observed via X-ray diffraction investigations performed on both synthetic and natural polymers.<sup>79</sup> Crystallization involves the alignment of polymer chains in hierarchical length scales, where the polymer chains fold together to give ordered regions. At the molecular level, polymer crystallization involves the ordering of the polymer chains into a three-dimensional lattice structure. This ordering process can occur by different mechanisms, including nucleation and growth, chain folding, and lamellar thickening.<sup>80, 81</sup> Crystallization of polymers is determined by many circumstances, including the chemical structure,<sup>82</sup> intermolecular forces, small and regular pendant groups, and processing conditions.<sup>83</sup> Crystallization is an important feature of polymer science and technology, as it can significantly affect the mechanical,<sup>84</sup> thermal,<sup>85</sup> and electrical<sup>86, 87</sup> properties of the resulting materials. Additionally, polymer crystals can influence the optical properties of the material, like refractive index<sup>88</sup> and birefringence.<sup>89</sup> By controlling the degree of crystallinity and the ordering of the polymer chains, it is possible to create materials with definite properties. Despite the importance of polymer crystallization, it is still a complex and challenging process that requires careful control of the processing conditions. Researchers continue to study the fundamental mechanisms of polymer crystallization and develop new techniques to improve our ability to control and manipulate these processes.

---



The hierarchical structural development can be viewed at three different length scales in semicrystalline polymers (Figure 1.6). Techniques like electron diffraction and wide-angle X-ray diffraction (WAXD) can be used to understand the structural information of the unit cell, which is in the order of a fraction of nanometers. Upon the crystallization, polymer chains are folded together to form an ordered region called lamella and these lamellae are interconnected by the amorphous region. Lamellae are flat platelets that range in thickness from 100 to 200 and have lateral diameters of many microns. Small-angle X-ray scattering (SAXS) and transmission electron microscopy (TEM) are used to collect information about the dimensions of lamellae. The lamellae are comprised of spherical aggregates (spherulites) and their sizes range from microscopic to a few millimeters in diameter. Small-angle light scattering (SALS) and polarized optical microscope are generally used to observe the spherulites formation and their dimensions.

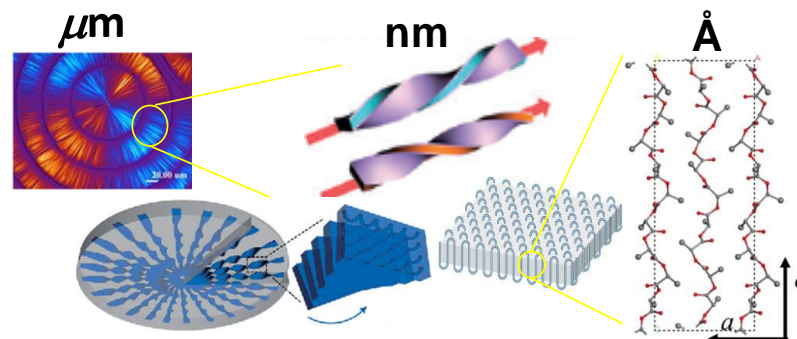


**Figure 1.6.** *The hierarchical structure of the semicrystalline polymer.*

The phenomenon of polymeric crystallization in assorted polymorphic forms is very common. This process can be explained through fundamental principles of thermodynamics and kinetics, which govern polymer crystallization. Polymorphism in polymers arises from the formation of various ordered conformations of macromolecules, coupled with their packing in distinct crystalline lattices. Predominantly, PLLA crystallizes

from either a melt or solvent state under specific crystallization conditions. PLLA can crystallize into different polymorphic forms on the manner in which crystallization occurs.

### 1.8.1. Polymorphism in PLLA

Polymorphism is a phenomenon characterized by the potential of a material to assume multiple crystal structures with different arrangements in the crystal lattice. Polylactic acid exists in various crystal polymorphs that include  $\alpha$ ,  $\alpha'(\delta)$ ,  $\alpha''$ ,  $\beta$ ,  $\gamma$ , and  $\varepsilon$  forms.<sup>90-94</sup> As shown in Figure 1.7a, the  $\alpha$  form is the crystalline polymorph of PLLA with an orthorhombic unit cell that has lattice parameters  $a = 1.07$  nm,  $b = 0.645$  nm, and  $c = 2.78$  nm. In contrast, the  $\beta$  form has polymer chains that are arranged in a trigonal unit cell with lattice parameters  $a = 1.052$  nm,  $b = 1.052$  nm, and  $c = 0.88$  nm. Similarly, in the  $\gamma$  form, polymer chains are packed in an antiparallel fashion in an orthorhombic unit cell, with lattice parameters  $a = 0.995$  nm,  $b = 0.625$  nm, and  $c = 0.88$  nm.<sup>93, 95, 96</sup> The PLLA polymer chains in the  $\alpha'$  form are loosely packed, with a small change in lattice parameters ( $a = 1.080$  nm,  $b = 0.620$  nm, and  $c = 2.880$  nm) compared to the  $\alpha$  form. According to Marubayashi et al., PLLA crystallizes in  $\alpha''$  form (disordered form of  $\alpha$ ) after treatment with  $\text{CO}_2$ . Also, PLLA crystallizes into the  $\varepsilon$  form by forming co-crystals with specific solvents like DMF, THF, CPO,  $\gamma$ -butyrolactone or 1,4 dioxane. The most stable crystalline form of PLLA is  $\alpha$  form, with a  $10_3$  helical conformation, these chains are packed upward and downward direction in an orthorhombic unit cell that consists 10 monomeric units with 3 turns around the chain axis in each unit cell (Figures 1.7b and 1.7c) whereas in PLLA/DMF cocrystals, along with PLLA polymer chains, DMF solvent molecules also presented in the orthorhombic unit cell (Figures 1.7d and 1.7e) with lattice parameters  $a = 1.5\text{--}1.6$  nm,  $b = 1.2\text{--}1.3$  nm,  $c = 2.8\text{--}2.9$  nm. Among these forms,  $\alpha$  and  $\alpha'$  forms are most common in PLLA crystallization. There are different ways to induce polymorphism in the PLLA material. One common method is the control of the processing conditions through melt

crystallization. Another method is to use solvent-induced crystallization method by using different solvents or solvent mixtures for the crystallization process.

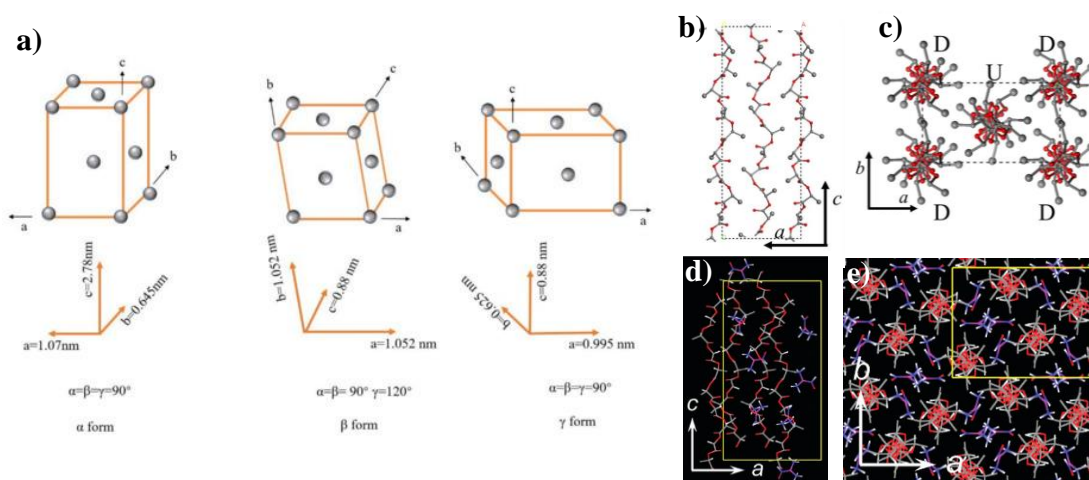


**Figure 1.7.** a)  $\alpha$ ,  $\beta$ ,  $\gamma$  crystal form models of PLLA,<sup>97</sup> b) and c) Packing models of PLLA chains in  $\alpha$  form,<sup>96</sup> d) and e) Packing models of PLLA polymer chains and DMF molecules in the PLLA/DMF complex. Carbon atoms in PLLA polymer chains (gray color) and DMF molecules (blue color).<sup>98</sup>

### 1.8.2. Melt Crystallization of PLLA

Melt crystallization is a process in which highly entangled polymer melt is converted into a semicrystalline state during the cooling process. This process can be used to create polymer products with controlled crystalline structures and properties. If the polymer is allowed to cool from its melt at a slow rate under proper conditions, a few polymers are found to be crystallized through the formation of three-dimensional spherical structures called spherulites. These spherulites are originated from chain-folded lamellae. The polymer crystallization process was found to be strongly influenced by the nucleation and growth process. Nucleation in polymers occurs by homogenous nucleation or heterogeneous nucleation. Homogenous nucleation requires a greater degree of supercooling, whereas heterogeneous nucleation requires only a low degree of

supercooling. Different theories were proposed to describe the crystallization of polymer from the melt. According to Strobl's theory, the crystallization from the melt is a multistep process. Melt crystallization of PLLA is thoroughly investigated and it was found that the cooling rate influences the degree of crystallinity of PLLA and the melt crystallization temperature influences the crystal structure of PLLA. Numerous studies have indicated the feasibility of obtaining  $\alpha$  and  $\alpha'$  polymorphs of PLLA from isothermal crystallization through rapid cooling from the melt state. The resulting crystalline products depend on the annealing temperature, with high temperatures ( $>120^{\circ}\text{C}$ ) leading to the exclusive crystallization of the  $\alpha$  form and low temperatures ( $<90^{\circ}\text{C}$ ) favoring the development of  $\alpha'$  form. The coexistence of both  $\alpha$  and  $\alpha'$  forms can be observed within samples that are crystallized between the aforementioned temperature ranges.

### 1.8.3. Solvent-Induced Crystallization of PLLA

Polymers frequently encounter solvents during polymerization and processing, particularly in advanced polymer processing techniques such as electrospinning, spinning, and wet spinning. Solvent-induced crystallization in polymers involves various steps, including solvent diffusion into the polymer matrix, polymer swelling, and crystallization. The interaction of the solvent molecules and polymers reduces the  $T_g$  and facilitates segmental mobility by disrupting intermolecular cohesive forces between the polymer chains. The matching of solubility parameters between the polymer and solvent plays a crucial role in controlling polymer crystallization.

Two possibilities exist based on the interactions of polymer and solvent molecules: the solvent molecules may facilitate segmental mobility and induce crystallization, or they may be trapped within the polymer's crystal lattice to form co-crystals during crystallization. PLLA can crystallize in both ways, forming either the  $\alpha$  or  $\varepsilon$  form

---

depending on the solvent used for crystallization. Solvent-induced crystallization of amorphous PLLA in solvents like toluene, acetone, methanol, and propanol typically results in the  $\alpha$  form.<sup>98, 99</sup> However, the  $\varepsilon$  form of complex PLLA crystals with  $10_7$  (left-handed  $10_3$ ) helical conformation resembling the  $\alpha$  form can be achieved using specific solvents such as THF, DMF, or CPO at below ambient temperatures.

#### 1.8.4. Gels of PLLA

As described in the preceding section, PLLA is known to form cocrystals/complexation with a specific solvent at low temperatures. This complexation in PLLA occurs via noncovalent interaction, PLLA acts as a host and the solvent molecule acts as a guest. This complex crystal is termed as  $\varepsilon$  form in which four PLLA chains are arranged in a unit cell, along with eight guest solvent molecules (Figure 1.8a). Marubayashi et al. reported that PLLA forms cocrystals with DMF at lower temperatures and proposed that weak interactions between PLLA and DMF are responsible for stable PLLA/DMF complex.<sup>98</sup> It has been reported that certain solvents which favor the formation of  $\varepsilon$  form could help in forming PLLA gels by dissolving PLLA at higher temperatures and then cooling the solutions to room temperature or below ambient temperatures. As shown in Figure 1.8b solvent desorption causes the transformation of  $\varepsilon$  form crystal structure to  $\alpha$  form crystal structure. It has also been stated that the crystal-to-crystal transition occurs with the rise in the temperature and exchange of solvents in polymer gels with other solvents (Figure 1.8c) which can be confirmed by using WAXD and Fourier transform infrared spectroscopy (FTIR).<sup>100</sup>

---

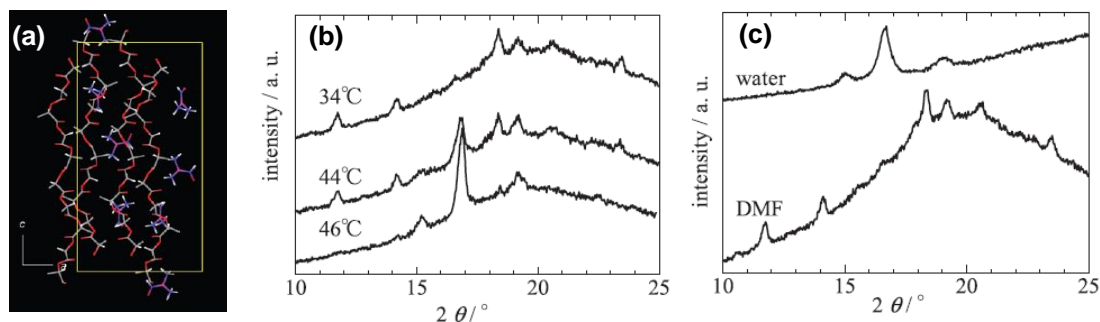


**Figure 1.8.** a) Scheme of PLLA polymer chains and DMF molecules in the PLLA/DMF complex. Carbon atoms in PLLA polymer chains (gray color) and DMF molecules (blue color).<sup>98</sup> b) WAXS of PLLA gel in DMF at various temperatures and c) WAXS of PLLA gel in DMF and PLLA gel after solvent exchange with water.<sup>100</sup>

### 1.8.5. Single Crystals of PLLA

In polymer single crystals, flexible polymer chains are rapidly folded and regularly stacked in one crystal. This particular folding structure produces both intermolecular and intramolecular stacking. In order to ascertain the crystal structure of polymers, polymer single crystals are typically utilized. The polymer single crystals are obtained by dilute polymer solutions and the polymer chains were crystallized into sheets-like lamellae with an average thickness  $\sim 10$  nm and of  $10 \mu\text{m}$  in the perpendicular directions (Figure 1.9).

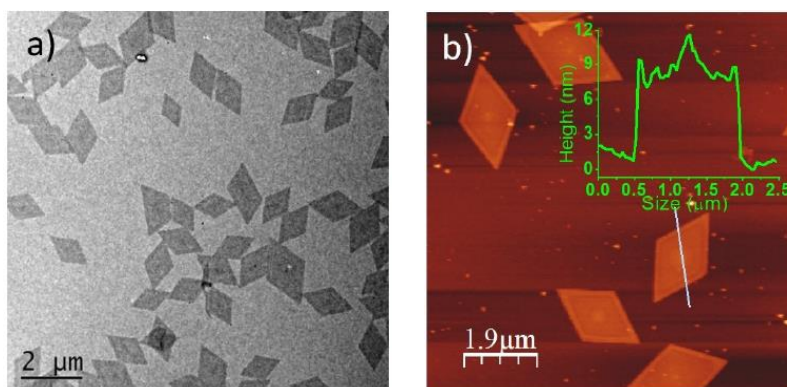


**Figure 1.9.** a) TEM and b) AFM images of single crystals of merocyanine appended poly(L-lactide) in isopropanol.<sup>101</sup>

### **1.8.6. Chromophore-Embedded PLLA**

Embedding the chromophores into insulating thermoplastic polymers via chemical methods can be broadly classified into three categories: (i) inclusion of chromophores within polymer chain backbone, (ii) end-capping of polymer chains with chromophores, and (iii) incorporation of chromophores as the central unit in a star-shaped polymer. The crucial benefit of this method is the facile fabrication of thin films and devices under mild conditions via solution processing techniques. While few thermoplastic polymers containing chromophores have been synthesized and studied their photophysical characteristics, the application of biodegradable and biocompatible polymers is intriguing due to their potential in real-time bioimaging. Among these materials, PLLA is commonly favored for chromophore incorporation, yielding unique properties and functionalities. The chiral nature of PLLA's asymmetric carbon results in its helical conformation, inducing optical activity. Consequently, these optically active polymer chains possess promising potential for advanced optoelectronic applications. Furthermore, the resultant hybrid materials ranging from solubility, processability, mechanical stability, and thermal stability to structural diversity have numerous benefits.

### **1.8.7. Polymer Crystallization Induced Chirality Transfer to Achiral Chromophore in Chromophore-Embedded PLLA**

A few research groups have explored the incorporation of chromophores into PLLA, with the aim of chirality transfer from helical PLLA polymer chains to non-helical chromophores and studied the impact of induced helicity on photoluminescence properties of chromophore-incorporated polymers. For instance, the induced helicity of vanillin was reported by Kia et al. when it was embedded into helical polymers like PDLA and PLLA.<sup>102</sup> Nisha et al. reported the effect of the helical PLLA chains on the assembly of oligo(p-

---

phenylenevinylene) (OPV) chromophores in OPV-embedded PLLA (Figure 1.10a).<sup>103</sup> They observed that the induced circular dichroism (ICD) signal from the chromophore occurred as PLLA crystallized. Further, OPV aggregates in the crystalline form resulted in the red-shift of fluorescence. The formation of helical structures of the stacked OPV segments was confirmed by CD, AFM and SEM analyses.

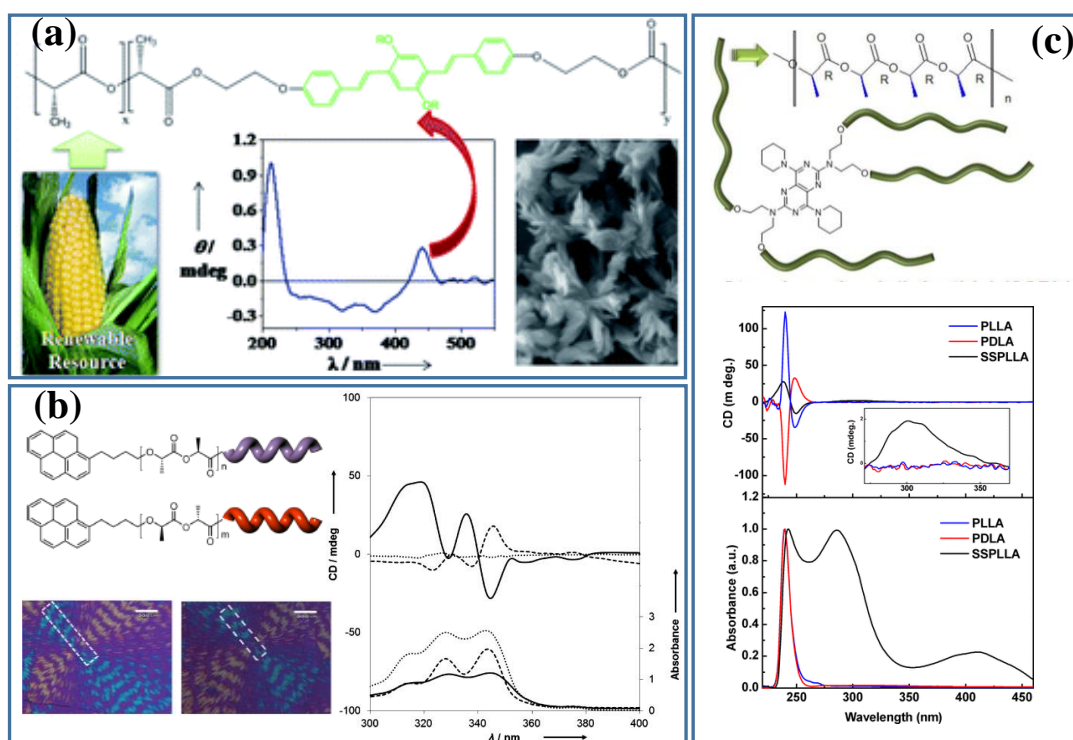


**Figure 1.10.** a) Induced helicity behavior from PLLA-OPV system, its CD and corresponding SEM image,<sup>103</sup> b) study of helical transformation from the molecular level to macroscopic level in pyrene end-capped PLAs,<sup>104</sup> c) study of polymer helical chains on photophysical properties of star-shaped PLLA as dipyrromethane core.<sup>105</sup>

Ho and co-workers systematically investigated the chirality transfer from the molecular level to the macroscopic level (in different length scales) in pyrene end-capped PLAs (Figure 1.10b). They used vibrational circular dichroism to understand the ICD of pyrene in pyrene end-capped PLAs at the molecular level (conformational chirality) and



this ICD behavior resulted from the twisting of lamellae in the polymer spherulites (hierarchical chirality).<sup>104</sup> Nagarajan et al. reported the role of polymer crystallization and morphology on the fluorescence properties of the dipyridamole fluorophores in star-shaped PLLA (SSPLLA). They demonstrated that the incorporation of dipyridamole molecules in SSPLLA could enhance the emission due to the chirality transfer from the PLLA polymer chains to the dipyridamole, as well as the molecular-level dispersion of dipyridamole in the amorphous phase of semicrystalline PLLA (Figure 1.10c).<sup>105</sup>

### **1.8.8. Polymer Crystallization Controlled Emission Properties in Chromophore-Embedded PLLA**

The crystallization process is associated with the arrangement of polymer chains in hierarchical length scales of polymers and it plays a very significant role in determining the polymer properties. In chromophore-embedded PLLA, the crystallization of PLLA was found to impact the emission behavior of chromophores. For instance, Tai-shen et al. investigated the fluorescence behavior of salicylideneazine (1,2-bis(2,4-dihydroxybenzylidene) hydrazine) after embedding to poly(L-lactide). They have demonstrated that PLLA crystallization controls the aggregation-induced emission behavior of salicylideneazine. This chromophore is highly emissive in PLLA crystalline state compared to the amorphous state of CN-PLLA, due to restricted molecular rotations in the intimately packed PLLA crystalline state (Figure 1.11a and 1.11b).<sup>106</sup> Wei et al., embedded the tetraphenylethenes (TPE) into the PLLA polymer at distinctive positions. Unique fluorescence characteristics were observed in the aggregation and solid states of these polymers. Through their demonstration, it has been proven that when SSPLLA is dissolved in THF, it is non-emissive; however, upon adding a poor solvent, it emits strongly due to the crystallization of PLLA.<sup>107</sup> Tang and co-workers synthesized the donor-acceptor

---

based AIE molecule (tetraphenylethene system linked with pyridinium salt) embedded PLLA (TPE-EP). They have successfully demonstrated that the PLLA crystallization provided the nano-confinement to the chromophore (TPE-EP) and as a result, the polymorphic form of the chromophore changed. Due to this, amorphous and crystalline polymers emitted distinct colors. An amorphous PLLA film emits green color, while a crystalline film emits a yellow color. The variation of fluorescence arises due to the change in the polymorphic form of a chromophore upon the polymer crystallization (Figure 1.11c and 1.11d).<sup>108</sup> Overall, understanding of the polymer structure and morphology is crucial for predicting and controlling the properties of chromophore-incorporated polymers, including their fluorescence behavior.

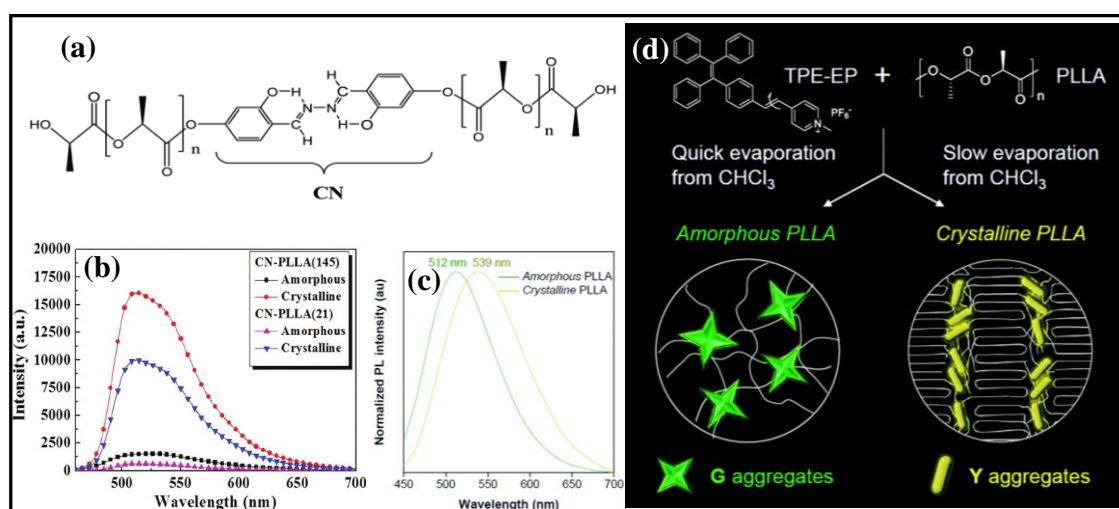


**Figure 1.11.** a) Structure and b) fluorescence spectra of salicylideneazine-PLLA,<sup>106</sup> c) fluorescence spectra and d) schematic representation of amorphous and crystalline TPE-EP incorporated PLLA.<sup>108</sup>

### 1.8.9. Crystallization-Driven Self-assembly of Chromophore-Appended PLLAs

Rajak and Anindita identified the conditions to obtain uniform and discrete diamond-shaped single crystals of chromophore-appended PLLAs using chromophores

like merocyanine (MC), pyrene (PY), naphthalene monoimide (NMI), or benzene (Bn). The process of PLLA crystallization enabled the arrangement of chromophore molecules in an antiparallel stacking orientation, accomplished through dipole-dipole interactions or  $\pi$ -stacking. They have demonstrated that co-crystallization of donor and acceptor embedded PLLAs results in the Förster Resonance Energy Transfer (FRET) on the surface of the crystals. On the other hand, no FRET was observed in the self-sorted assemblies because of their tightly packed crystal structure (Figure 1.12).

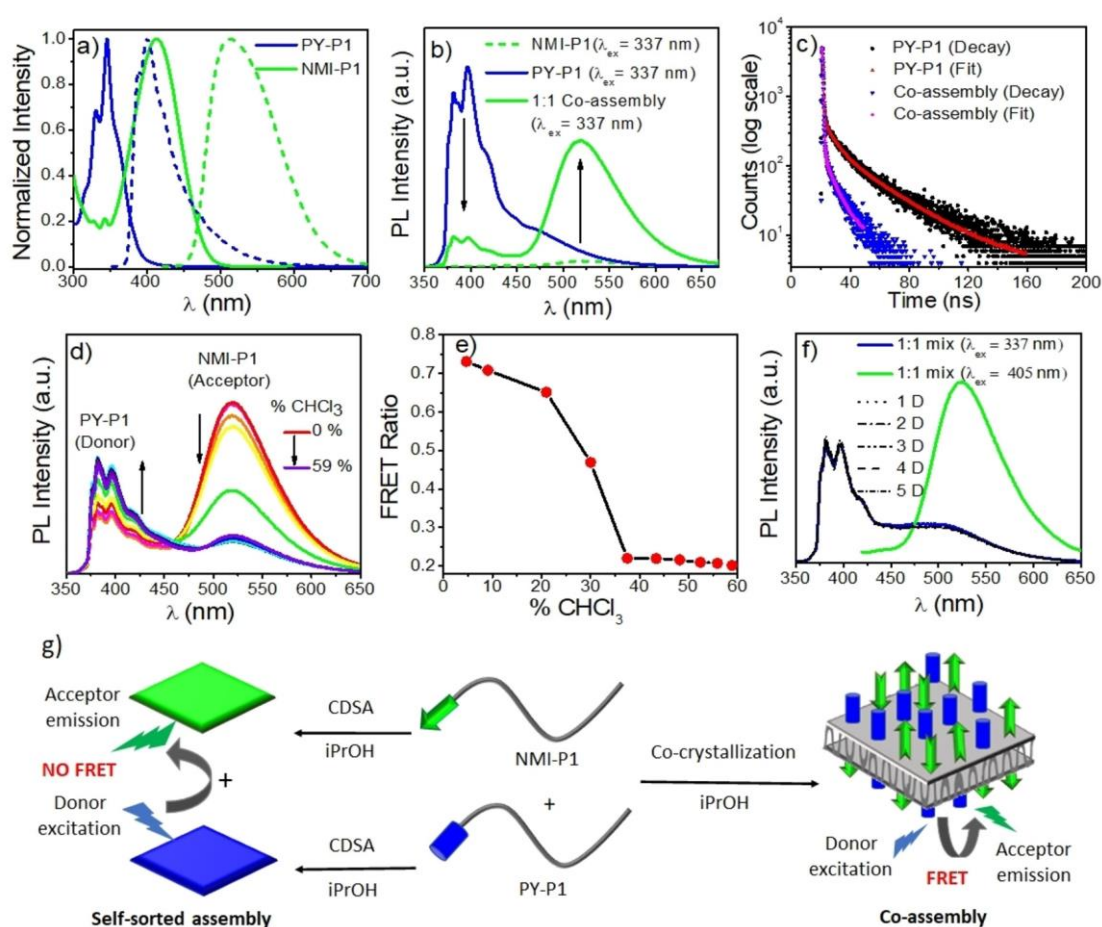


**Figure 1.12.** a) UV-visible (continuous lines) and photoluminescence spectra (dotted lines) of pyrene-PLLA (PY-P1) (blue lines) and naphthalene monoimide-PLLA (NMI-P1) (green lines) in IPA, b) photoluminescence spectra of PY-P1, NMI-P1 and their co-crystallized sample in IPA, c) time-resolved fluorescence decay profiles of PY-P1 and of co-crystallized NMI-P1 and PY-P1 in IPA, d) photoluminescence spectra of co-crystallized

*NMI-PI and PY-PI in IPA as a function of chloroform addition, e) FRET ratio with chloroform percentage plot, f) photoluminescence spectra of mixture of NMI-PI and PY-PI in IPA and g) schematic representation of co-crystallization of NMI-PI and PY-PI in IPA.*<sup>101</sup>

## **1.9. Scope and Objectives of the Present Thesis**

In recent decades, the quest for fluorescent systems with tunable emissive properties has generated significant interest due to their vast range of applications in optical waveguides, biosensors, bio-imaging, mechanochromism, and OLEDs. Incorporating fluorescent molecules covalently into polymers has numerous advantages, such as processability, thermal stability, solubility, mechanical stability, and structural diversity. The conformation and packing of chromophores in hybrid materials dictate their emission properties by promoting interactions among neighboring chromophores. Therefore, an extensive understanding of the structure-property correlation is necessary for the systematic design of hybrid materials to optimize their emission properties. However, thus far, precisely controlling the arrangement of chromophore molecules in polymer matrices remains a difficult task. In this context, the present thesis provides an opportunity to gain insights into the role of helical polymer chains and polymer crystallization on the tunable emission of chromophore-embedded biocompatible and biodegradable fluorescent polymers. In two chapters, tunable emission of chromophores was achieved by altering the dihedral angles of the terminal phenyl groups by the chain conformation of covalently attached PLLAs or by tuning the polymorphism of PLLA. In the other chapter, the aggregation (excimer formation) of chromophore was controlled by tuning the crystallization behavior of PLLA.

---

The objective of this thesis is to synthesize various chromophore-embedded PLLA systems and comprehend the impact of polymer chain packing and polymer crystallization on the photophysical properties of hybrid systems. The detailed objectives are given below.

(i) the impact of the number of the substituted polymer chains on the aggregation-induced emission behavior of fluorescent molecules.

(ii) the impact of polymer chain length and packing (polymorphism) on the photophysical properties of chromophores.

(iii) the role of polymer helical chains and crystallization conditions on the morphological and photophysical properties of hybrid systems.

## 1.10. References

1. G. G. Stokes, *Philosophical Transactions of the Royal Society of London*, 1852, **142**, 463-562.
  2. Z. Zhao, H. Zhang, J. W. Y. Lam and B. Z. Tang, *Angew. Chem. Int. Ed.*, 2020, **59**, 9888-9907.
  3. B. Valeur and M. N. Berberan-Santos, *J. Chem. Educ.*, 2011, **88**, 731-738.
  4. T. C. O'Haver, *J. Chem. Educ.*, 1978, **55**, 423.
  5. P. Radvanyi and J. Villain, *Comptes Rendus Physique*, 2017, **18**, 544-550.
  6. B. Valeur and M. N. Berberan-Santos, *Characteristics of Fluorescence Emission*, 2012, pp. 53-74.
  7. A. Jablonski, *Nature*, 1933, 131, 839-840.
  8. I. Djavani-Tabrizi and R. A. Jockusch, *J. Phys. Chem. Lett.*, 2022, 13, 2187-2192.
  9. S. W. Thomas, G. D. Joly and T. M. Swager, *Chem. Rev* 2007, 107, 1339-1386.
  10. F. J. M. Hoeben, P. Jonkheijm, E. W. Meijer and A. P. H. J. Schenning, *Chem. Rev*, 2005, 105, 1491-1546.
  11. U. H. F. Bunz, *Chem. Rev*, 2000, 100, 1605-1644.
  12. F. Hide, M. A. Díaz-García, B. J. Schwartz and A. J. Heeger, *Acc. Chem. Res*, 1997, 30, 430-436.
  13. S. M. Borisov and O. S. Wolfbeis, *Chem. Rev*, 2008, 108, 423-461.
  14. H. Wang, E. Zhao, J. W. Y. Lam and B. Z. Tang, *Materials Today*, 2015, 18, 365-377.
  15. X. Ma, R. Sun, J. Cheng, J. Liu, F. Gou, H. Xiang and X. Zhou, *J. Chem. Educ.*, 2016, 93, 345-350.
  16. H. Zhang, Z. Zhao, A. T. Turley, L. Wang, P. R. McGonigal, Y. Tu, Y. Li, Z. Wang, R. T. K. Kwok, J. W. Y. Lam and B. Z. Tang, *Adv. Mater.*, 2020, 32, 2001457.
  17. L. Zong, Y. Xie, C. Wang, J.-R. Li, Q. Li and Z. Li, *Chem. Commun.*, 2016, 52, 11496-11499.
-

18. Z. Zhang, D. Chen, Z. Liu, D. Wang, J. Guo, J. Zheng, W. Qin and C. Wu, *ACS Appl. Polym. Mater.*, 2020, 2, 74-79.
  19. R. M. Jones, T. S. Bergstedt, D. W. McBranch and D. G. Whitten, *J. Am. Chem. Soc.*, 2001, 123, 6726-6727.
  20. J. Luo, Z. Xie, J. W. Y. Lam, L. Cheng, H. Chen, C. Qiu, H. S. Kwok, X. Zhan, Y. Liu, D. Zhu and B. Z. Tang, *Chem. Commun.*, 2001, DOI: 10.1039/B105159H, 1740-1741.
  21. J. Mei, Y. Hong, J. W. Y. Lam, A. Qin, Y. Tang and B. Z. Tang, *Adv. Mater.*, 2014, 26, 5429-5479.
  22. M. Han and M. Hara, *J. Am. Chem. Soc.*, 2005, 127, 10951-10955.
  23. Y. Hong, J. W. Y. Lam and B. Z. Tang, *Chem. Soc. Rev.*, 2011, 40, 5361-5388.
  24. T. Miyashita, in *Protein-Protein Interactions: Methods and Applications*, ed. H. Fu, Humana Press, Totowa, NJ, 2004, DOI: 10.1385/1-59259-762-9:399, pp. 399-409.
  25. Y. Suzuki and K. Yokoyama, *Journal*, 2015, 5, 337-363.
  26. T. Etrych, O. Janoušková and P. Chytil, *Journal*, 2019, 11.
  27. C. Moon-Hwan, D. Diganta, P. V. Varde and P. Michael, *Microelectron. Reliab.*, 2012, 52, 762-782.
  28. R. Michael, *Leukos*, 10, 77-86.
  29. D. F. de Souza, P. P. F. da Silva, L. F. A. Fontenele, G. D. Barbosa and M. de Oliveira Jesus, *Energy Reports*, 2019, 5, 409-424.
  30. J. Dong and D. Xiong, *Ann. Biomed. Eng.*, 2017, 45, 2509-2523.
  31. Y. Naichia Gary, W. Chia-Hao and C. Ta Chih, *Renew. Sust. Energ. Rev.*, 2010, 14, 2161-2166.
  32. M. A. Jones, *Hortic. Res.*, 2018, 5, 47.
  33. V. G. Chudinova and O. R. Bokova, *IOP Conference Series: Mater. Sci. Eng*, 2017, 262, 012147.
  34. Y. Cai, A. Qin and B. Z. Tang, *J. Mater. Chem. C*, 2017, 5, 7375-7389.
  35. N. Cekic, M. Dacic and A. Kostic, *Facta universitatis - series: J. Archit. Civ. Eng.* 2012, 10, 33-42.
  36. C. Perdahci, H. C. Akin and O. Cekic, *IOP Conference Series: Earth and Environmental Science*, 2018, 154, 012010.
  37. M. Zuo, W. Qian, Z. Xu, W. Shao, X.-Y. Hu, D. Zhang, J. Jiang, X. Sun and L. Wang, *Small*, 2018, 14, 1801942.
  38. L. C. Murfin, M. Weber, S. J. Park, W. T. Kim, C. M. Lopez-Alled, C. L. McMullin, F. Pradaux-Caggiano, C. L. Lyall, G. Kociok-Köhn, J. Wenk, S. D. Bull, J. Yoon, H. M. Kim, T. D. James and S. E. Lewis, *J. Am. Chem. Soc.*, 2019, 141, 19389-19396.
  39. T.-Y. Li, J. Wu, Z.-G. Wu, Y.-X. Zheng, J.-L. Zuo and Y. Pan, *Coord. Chem. Rev.*, 2018, 374, 55-92.
  40. J. Yoshino, A. Furuta, T. Kambe, H. Itoi, N. Kano, T. Kawashima, Y. Ito and M. Asashima, *Chem. – Eur. J.*, 2010, 16, 5026-5035.
  41. P. Ramasamy, N. Kim, Y.-S. Kang, O. Ramirez and J.-S. Lee, *Chem. Mater.*, 2017, 29, 6893-6899.
  42. L. Wen, L. Qiu, Y. Wu, X. Hu and X. Zhang, *Sensors (Basel)*, 2017, 17.
-

43. H. Zhang, Z. Chen, Y. He, S. Yang and J. Wei, *ACS Appl. Nano Mater.*, 2021, 4, 4340-4345.
  44. Y. Sun, M. Shi, Y. Zhu, I. F. Perepichka, X. Xing, Y. Liu, C. Yan and H. Meng, *ACS Appl. Mater. Interfaces*, 2020, 12, 24156-24164.
  45. H. Liu, Y. Gu, Y. Dai, K. Wang, S. Zhang, G. Chen, B. Zou and B. Yang, *J. Am. Chem. Soc.*, 2020, 142, 1153-1158.
  46. W. Qiao, P. Yao, Y. Chen, Q. Xiao, L. Zhang and Z. a. Li, *Mater. Chem. Front.*, 2020, 4, 2688-2696.
  47. T. Jiang, X. Wang, J. Wang, G. Hu and X. Ma, *ACS Appl. Mater. Interfaces*, 2019, 11, 14399-14407.
  48. J. Cui, J. E. Kwon, H.-J. Kim, D. R. Whang and S. Y. Park, *ACS Appl. Mater. Interfaces*, 2017, 9, 2883-2890.
  49. S. Chen, J. Liu, Y. Liu, H. Su, Y. Hong, C. K. W. Jim, R. T. K. Kwok, N. Zhao, W. Qin, J. W. Y. Lam, K. S. Wong and B. Z. Tang, *Chem. Sci.*, 2012, 3, 1804-1809.
  50. Q. A. Best, N. Sattenapally, D. J. Dyer, C. N. Scott and M. E. McCarroll, *J. Am. Chem. Soc.*, 2013, 135, 13365-13370.
  51. Y. Niko, S. Kawauchi and G.-i. Konishi, *Chem. Eur. J.*, 2013, 19, 9760-9765.
  52. J. Yuan, L. Wang, Y. Wang and J. Hao, *Chem. Eur. J.* 2020, 26, 3545-3554.
  53. L. Zhu, C. Zhong, Z. Liu, C. Yang and J. Qin, *Chem. Commun.*, 2010, 46, 6666-6668.
  54. L. Hu, Y. Duan, Z. Xu, J. Yuan, Y. Dong and T. Han, *J. Mater. Chem. C*, 2016, 4, 5334-5341.
  55. X. Shan, W. Chi, H. Jiang, Z. Luo, C. Qian, H. Wu and Y. Zhao, *Angew. Chem. Int. Ed.*, 2023, 62, e202215652.
  56. C.-H. Wang, Z.-Y. Liu, C.-H. Huang, C.-T. Chen, F.-Y. Meng, Y.-C. Liao, Y.-H. Liu, C.-C. Chang, E. Y. Li and P.-T. Chou, *J. Am. Chem. Soc.*, 2021, 143, 12715-12724.
  57. S. Srinivasan, P. A. Babu, S. Mahesh and A. Ajayaghosh, *J. Am. Chem. Soc.*, 2009, 131, 15122-15123.
  58. A. Nagai, K. Kokado, J. Miyake and Y. Chujo, *Polymer Journal*, 2010, 42, 37-42.
  59. H. Megahd, M. Villarreal Brito, A. Lanfranchi, P. Stagnaro, P. Lova and D. Comoretto, *Mater. Chem. Front.*, 2022, 6, 2413-2421.
  60. M. U. Hassan, Y.-C. Liu, K. u. Hasan, H. Butt, J.-F. Chang and R. H. Friend, *Nano Energy*, 2016, 21, 62-70.
  61. A. H. Ribeiro, A. Fasih, B. van der Zee, L. Veith, G. Glaser, A. Kunz, K. Landfester, P. W. M. Blom and J. J. Michels, *J. Mater. Chem. C*, 2020, 8, 6528-6535.
  62. Z. Hu, B. Shao, G. T. Geberth and D. A. Vanden Bout, *Chem. Sci.*, 2018, 9, 1101-1111.
  63. T.-Q. Nguyen, I. B. Martini, J. Liu and B. J. Schwartz, *J. Phys. Chem. B.*, 2000, 104, 237-255.
  64. D. Abbaszadeh, A. Kunz, N. B. Kotadiya, A. Mondal, D. Andrienko, J. J. Michels, G.-J. A. H. Wetzelaer and P. W. M. Blom, *Chem. Mater.*, 2019, 31, 6380-6386.
  65. J. Xu, W. Ji, C. Li, Y. Lv, Z. Qiu, L. Gao, E. Chen, J. W. Y. Lam, B. Tang and L. Jiang, *Adv. Opt. Mater.* 2018, 6, 1701149.
  66. F. Martini, S. Borsacchi, M. Geppi, G. Ruggeri and A. Pucci, *Polym. Chem.*, 2014, 5, 828-835.
-

67. J. Gotta, T. B. Shalom, S. Aslanoglou, A. Cifuentes-Rius, N. H. Voelcker, R. Elnathan, O. Shoseyov and S. Richter, *Adv. Funct. Mater.*, 2018, 28, 1706967.
  68. V. Kumar, B. Maiti, M. K. Chini, P. De and S. Satapathi, *Sci. Rep.* 2019, 9, 7269.
  69. NPG Asia Materials, 2011, DOI: 10.1038/asiamat.2011.66.
  70. M. A. Khan, Z. Hussain, U. Liaqat, M. A. Liaqat and M. Zahoor, *Nanomaterials (Basel)*, 2020, 10.
  71. L. Xu and A. Yamamoto, *Colloids Surf. B.*, 2012, 93, 67-74.
  72. T. Akagi, T. Fujiwara and M. Akashi, *Langmuir*, 2014, 30, 1669-1676.
  73. R. E. Drumright, P. R. Gruber and D. E. Henton, *Adv. Mater.*, 2000, 12, 1841-1846.
  74. M. Cvek, U. C. Paul, J. Zia, G. Mancini, V. Sedlarik and A. Athanassiou, *ACS Appl. Mater. Interfaces*, 2022, 14, 14654-14667.
  75. B. Tyler, D. Gullotti, A. Mangraviti, T. Utsuki and H. Brem, *Adv. Drug Deliv. Rev.*, 2016, 107, 163-175.
  76. P. Song, L. Sang, C. Jin and Z. Wei, *Polymer*, 2018, 134, 163-174.
  77. H. Urayama, T. Kanamori and Y. Kimura, *Macromol Mater Eng.*, 2002, 287, 116-121.
  78. E. Capuana, F. Lopresti, M. Ceraulo and V. La Carrubba, *Journal*, 2022, 14.
  79. J. R. Katz, *Trans. Faraday Soc.*, 1936, 32, 77-94.
  80. N. Wu, S. Lang, H. Zhang, M. Ding and J. Zhang, *J. Phys. Chem. B.*, 2014, 118, 12652-12659.
  81. X. Jiang, G. Reiter and W. Hu, *J. Phys. Chem. B.*, 2016, 120, 566-571.
  82. M. Gilbert and F. J. Hybart, *Polymer*, 1972, 13, 327-332.
  83. J. E. K. Schawe, *J. Therm. Anal. Calorim.*, 2014, 116, 1165-1173.
  84. B. Ma, X. Wang, Y. He, Z. Dong, X. Zhang, X. Chen and T. Liu, *Polymer*, 2021, 212, 123280.
  85. M. Hortós, J. Anakabe, A. Arrillaga, S. Espino and J. J. Bou, *Polym. Int.*, 2019, 68, 1767-1775.
  86. C. M. Gonzalez Henriquez, E. A. Soto Bustamante and W. Haase, Brazil, 2009.
  87. E. Laredo, A. Bello, J. Diaz, M. Grimau, D. Martinez-Tong, D. Wu and L. Wu, *Polymer Composites*, 2013, 34, 67-76.
  88. B. Nagendra, P. Rizzo, C. Daniel and G. Guerra, *Macromolecules*, 2021, 54, 6605-6611.
  89. B. Li, Y. Zhao, X. Chen, Z. Wang, J. Xu and W. Shi, *Macromolecules*, 2022, 55, 3974-3985.
  90. J. Zhang, K. Tashiro, A. J. Domb and H. Tsuji, *Macromol. Symp.*, 2006, 242, 274-278.
  91. B. Eling, S. Gogolewski and A. J. Pennings, *Polymer*, 1982, 23, 1587-1593.
  92. H. Marubayashi, S. Akaishi, S. Akasaka, S. Asai and M. Sumita, *Macromolecules*, 2008, 41, 9192-9203.
  93. L. Cartier, T. Okihara, Y. Ikada, H. Tsuji, J. Puiggali and B. Lotz, *Polymer*, 2000, 41, 8909-8919.
  94. P. Shaiju, N. S. Murthy and E. B. Gowd, *Macromolecules*, 2016, 49, 224-233.
  95. P. De Santis and A. J. Kovacs, *Biopolymers*, 1968, 6, 299-306.
  96. K. Wasanasuk, K. Tashiro, M. Hanesaka, T. Ohhara, K. Kurihara, R. Kuroki, T. Tamada, T. Ozeki and T. Kanamoto, *Macromolecules*, 2011, 44, 6441-6452.
-



- 
97. K. Shi, G. Liu, H. Sun, B. Yang and Y. Weng, *Polymers (Basel)*, 2022, 14.
  98. H. Marubayashi, S. Asai and M. Sumita, *Macromolecules*, 2012, 45, 1384-1397.
  99. M. Syazwan and T. Sasaki, 2018, 18, 331-337.
  100. Y. Matsuda, A. Fukatsu, Y. Wang, K. Miyamoto, J. W. Mays and S. Tasaka, *Polymer*, 2014, 55, 4369-4378.
  101. A. Rajak and A. Das, *Angew. Chem. Int. Ed.*, 2022, 61, e202116572.
  102. K. Kan, M. Fujiki, M. Akashi and H. Ajiro, *ACS Macro Letters*, 2016, 5, 1014-1018.
  103. S. K. Nisha and S. K. Asha, *J. Mater. Chem. C*, 2014, 2, 2051-2060.
  104. M.-C. Li, H.-F. Wang, C.-H. Chiang, Y.-D. Lee and R.-M. Ho, *Angew. Chem. Int. Ed.*, 2014, 53, 4450-4455.
  105. S. Nagarajan and E. B. Gowd, *Macromolecules*, 2017, 50, 5261-5270.
  106. T.-S. Hsiao, P.-C. Huang, L.-Y. Lin, D.-J. Yang and J.-L. Hong, *Polym. Chem.*, 2015, 6, 2264-2273.
  107. W. Zhao, C. Li, B. Liu, X. Wang, P. Li, Y. Wang, C. Wu, C. Yao, T. Tang, X. Liu and D. Cui, *Macromolecules*, 2014, 47, 5586-5594.
  108. M. Khorloo, Y. Cheng, H. Zhang, M. Chen, H. H. Y. Sung, I. D. Williams, J. W. Y. Lam and B. Z. Tang, *Chem. Sci.*, 2020, 11, 997-1005.
-



## Chapter 2

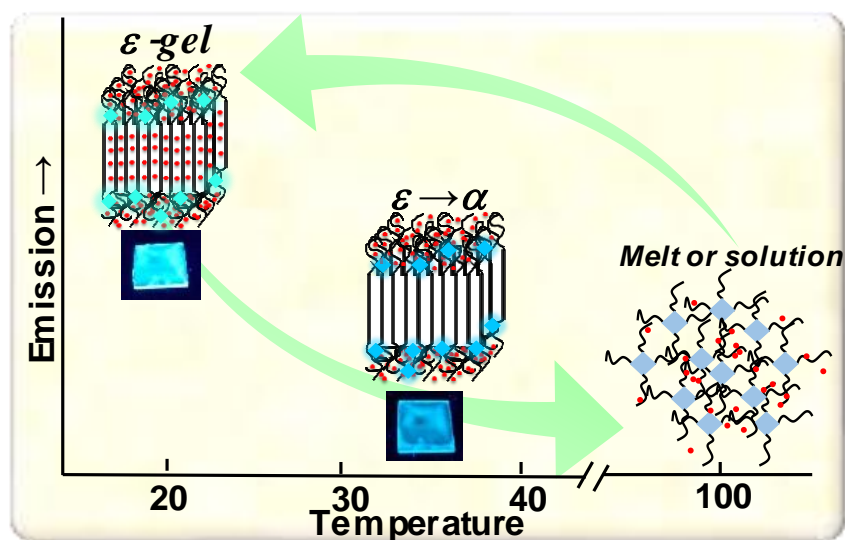
---

---

# Poly(L-lactide)s with Tetraphenylethylene: Role of Polymer Chain Packing on Aggregation-Induced Emission Behavior of Tetraphenylethylene

---

---



This chapter has been adopted from the following publication

**G. Virat** and E. Bhoje Gowd\*

*Polym. Chem.*, **2022**,13, 838-849.

## 2.1. Abstract

*Development of biocompatible and biodegradable fluorescent polymers and understanding their fluorescent characteristics are highly desirable. In this work, we synthesized one-armed, two-armed and four-armed poly(L-lactide)s by ring-opening polymerization of L-lactide using hydroxyl functionalized tetraphenylethylenes (TPE) as a macroinitiator. PLLA with TPE is non-emissive in good solvents and it emits differently in the aggregate and gel states. Star-shaped poly(L-lactide) (SSPLLA) emits strongly compared to the one-armed and two-armed PLLAs in the gel state. Gel of SSPLLA in N,N-dimethylformamide (DMF) crystallized into the  $\epsilon$  form and emitted cyan light under UV illumination at room temperature. Temperature-dependent UV-Vis spectroscopy, photoluminescence spectroscopy, X-ray diffraction and differential scanning calorimetry of SSPLLA/DMF gel in the heating process revealed that the emission behavior is sensitive to the structural changes of PLLA. Upon heating, the crystal structure of the SSPLLA gel transforms from the  $\epsilon$  to  $\alpha$  form over a broad temperature range. Such crystal-to-crystal transition of PLLA resulted in the rotation of phenyl rings of TPE and leads to a significant blue-shift in the fluorescence of SSPLLA due to the shorter intramolecular conjugation length. On further heating, even in the semicrystalline state ( $\alpha$  form), enhanced mobility of the amorphous chains leads to the complete quenching of emission due to the free rotation of phenyl rings of TPE. On the other hand, the precipitate of SSPLLA prepared using N,N-dimethylacetamide (DMA) crystallized into the  $\alpha$  form. Unlike gel, the fluorescence emission decreased gradually with temperature and the blue shift was observed relatively at higher temperatures due to the vigorous mobility of amorphous chains. We believe that bio-based polymers with aggregation-induced emission (AIE) characteristics can find applications in bio-imaging and medical/pharmaceutical fields.*

---

## 2.2. Introduction

Fluorescent materials have attracted immense interest in recent decades due to their enormous applications in biosensors, bio-imaging, mechanochromism, optoelectronic devices, optical waveguides and organic light-emitting diodes.<sup>1-13</sup> Most of the fluorescent molecules exhibit reduced emission or are completely non-emissive in the aggregated or solid states due to self-quenching associated with the strong noncovalent interactions.<sup>14-16</sup> In contrast, some fluorescent molecules are non-emissive in dilute solution and fluorescence increases upon crystallization/self-assembly or aggregation.<sup>1, 17-19</sup> The restricted rotation of chromophores in the aggregate or crystalline states is mainly responsible for the aggregation-induced emission (AIE) due to the radiative decay of excitations.<sup>17, 18, 20-23</sup> This unusual phenomenon has been extensively studied in recent years using many AIE molecules such as tetraphenylethylenes, siloles, stilbenes, distyrylanthracene, phenyleneethylenes, etc.<sup>1,23-34</sup> Among these, tetraphenylethylene (TPE) and its derivatives have been widely used to understand the fundamental emissive mechanism. The free rotation of the phenyl rings and partial twisting of the C=C bond in TPE lead to the fast nonradiative decay and quench the fluorescence emission in dilute solutions. On the other hand, the restriction of intramolecular rotation of the peripheral phenyl rings hinders the path of nonradiative transitions and enhances the fluorescence emission through radiative transitions.<sup>18, 19, 23, 35</sup> Therefore, several strategies have been adopted to address the issue of restriction of intramolecular motions in TPEs up to date and among them, covalent bond fixation of peripheral phenyl rings is one of the sensible strategies. The incorporation of AIE molecules into the polymers is expected to expand the application scope of AIE materials.

The covalent incorporation of AIE molecules into polymers has several advantages such as processability, solubility, mechanical stability, thermal stability and structural

---

diversity. Several synthetic strategies have been developed to synthesize AIE molecules incorporated polymers with different architectures such as linear, block, star, hyperbranched, dendritic, comb and cross-linked.<sup>20, 22, 25, 34, 36-40</sup> Owing to the structural diversity, AIE properties of chromophores in these hybrid systems can be tuned in response to external stimuli such as light, heat, pH, solvents, etc.<sup>11, 24, 28, 34, 36, 37, 41</sup> The emission properties of these hybrid materials are sensitive to the packing structure and aggregation of fluorescent molecules. For example, the importance of molecular design in controlling the photophysical and optoelectronic behaviors are investigated in several star-shaped polymers for various applications.<sup>42-45</sup> Therefore, understanding the structure-property relationship is of great importance for the rational design of hybrid materials with optimized fluorescent properties and to promote their potential applications.

As for the AIE molecules, a few polymers carrying these molecules have been synthesized and tested for their emission behavior in response to multiple external stimuli.<sup>22, 25-28, 34, 36, 41, 46, 47</sup> For example, Taniguchi et al. synthesized poly(dimethylsiloxane) carrying TPE molecules and demonstrated the stimuli-sensitive fluorescence behavior of the hybrid system against organic solvents and temperature.<sup>34</sup> Zhang et al. synthesized AIE active core cross-linked star polymers with polystyrene (PS), polyethylene (PE) or polyethylene-*b*-polycaprolactone (PE-*b*-PCL) and these polymers exhibited temperature responsive emission behavior in tetrahydrofuran (THF)/*n*-hexane mixtures.<sup>27</sup> Using TPE-functionalized PE-based polymers, it was demonstrated that the micelle formation restricts the intramolecular rotation of TPE to enhance the fluorescence emission.<sup>25</sup> Xu et al. showed the reversible thermal-induced fluorescence behavior of TPE-labeled Nylon 6 and at the higher temperature, a blue shift in fluorescence was reported due to the rotation of phenyl rings of TPE.<sup>36</sup> Liang et al. reported the tuning of the fluorescent behavior by polymer crystallization using poly( $\epsilon$ -caprolactone) capped with TPE molecules

and showed that these hybrid materials are sensitive to explosives.<sup>47</sup> Although significant works have been reported on AIE-labeled polymers by several groups, investigation on AIE-incorporated biodegradable and biocompatible synthetic polymers is extremely limited. Particularly, the development of AIE in biomedicine and bio-imaging is of utmost importance and the AIE-incorporated biodegradable and biocompatible polymers have great potential as bioprobes for real-time imaging and sensor applications.<sup>22, 48, 49</sup> Poly(L-lactide) (PLLA) is one of the most successful biodegradable polymers produced from renewable biomass. It exhibits five major crystalline forms, namely,  $\alpha$ ,  $\beta$ ,  $\gamma$ ,  $\delta(\alpha')$ , and  $\epsilon$ .<sup>50-55</sup> Because of its intrinsic properties, many fluorescent molecules have been incorporated into PLLA to afford unique functionalities.<sup>22, 56-62</sup> Hsiao et al. showed that the crystallization of PLLA chains determines the AIE properties of the 1,2-bis(2,4-dihydroxybenzylidene)hydrazine after the incorporation into the backbone of PLLA.<sup>57</sup> Zhao et al. incorporated TPE into the PLLA chains by living chain transfer polymerization and demonstrated that these polymers exhibit unique emission properties in the aggregated states.<sup>22</sup> They have demonstrated that star-shaped PLLA (SSPLLA) was non-luminescent in good solvents like tetrahydrofuran (THF) and emits strongly when the poor solvent (water) was added due to aggregate formation. However, the influence of polymer chain packing and crystal structure of PLLA on the aggregation-induced emission behavior of core molecules in star-shaped polymers has rarely been reported. Further, the influence of solvent molecules on the crystal structure and fluorescent behavior of SSPLLA has not been studied. For the first time, we have studied the influence of the crystal structure of the PLLA chains on the fluorescent behavior of core molecules in SSPLLA using temperature-dependent UV and PL measurements.

This work focuses on the role of polymer chain packing on the emission behavior of TPE molecules in one-armed, two-armed and four-armed PLLAs. Hydroxyl modified

---

tetraphenylethylenes (TPE) were used as a macroinitiator to carry out the ring-opening polymerization of L-lactide. Compared to one-armed and two-armed PLLAs, four-armed PLLA (SSPLLA) shows strong emission in aggregate and gel states. For that reason, SSPLLA was selected for a detailed study to understand the role of polymer chain packing on the emission behavior of the core molecule TPE. SSPLLA shows non-emissive behavior in good solvents (e.g., chloroform) and typical AIE behavior in aggregate and gel states. The fluorescence behavior of SSPLLA could be regulated by multiple factors, including solvents, polymer chain conformation, crystal-to-crystal transition of the host polymer and temperature. The change in the emission behavior of SSPLLA is attributed to the restriction of intramolecular rotation of the peripheral phenyl rings of core molecules induced by the chain conformation of arm PLLAs. We believe that the marriage of AIE molecules with biocompatible/biodegradable polymer will impart remarkable fluorescent properties and guide a new way with fascinating functions and applications in medical and pharmaceutical fields and bio-imaging.

## **2.3. Experimental**

### **2.3.1. Materials**

L-lactide monomer, tin(II) 2-ethylhexanoate  $\text{Sn}(\text{Oct})_2$ , chloroform, dry toluene and hexane were purchased from Sigma-Aldrich chemical company. D-lactide was supplied from Jinan Daigang Biomaterials, China. Methanol, ethyl acetate, N,N-dimethylformamide (DMF), and N,N-dimethylacetamide (DMA) were purchased from Merck Chemicals. L-lactide monomer was recrystallized before polymerization with ethyl acetate as solvent. Hydroxyl modified tetraphenylethylenes (TPE-1-OH, TPE-2-OH and TPE-4-OH) were purchased from TCI chemicals and used without further purification.

---



### 2.3.2. Synthesis of One-armed, Two-armed and SSPLLA

Ring-opening polymerization was used to synthesize one-armed (TPE-1-PLLA), two-armed PLLA (TPE-2-PLLA) and SSPLLA (TPE-4-PLLA). Details of the polymerization of SSPLLA are as follows. A mixture of L-Lactide (3.7 g), TPE-4-OH (10.4 mg), Sn(Oct)<sub>2</sub> (2 drops) and dry toluene (40 ml) was stirred in an inert atmosphere at room temperature for 1 h to remove air. Then the reaction was carried out at 140 °C for 4 h in a nitrogen atmosphere. The obtained polymer was dissolved in chloroform and purified twice by re-precipitation using methanol as a precipitant. The resultant precipitate was filtered and dried under reduced pressure at 40 °C for 12 h. For the purpose of comparison, SSPDLA was synthesized with comparable molecular weight ( $M_n = 9400$  g/mol) by the same procedure using D-lactide as monomer. The same procedure was used to synthesize the other two polymers, TPE-1-PLLA and TPE-2-PLLA using TPE-1-OH and TPE-2-OH as macroinitiators, respectively. The chemical structures of polymers were confirmed by <sup>1</sup>H NMR. The number-average molecular weights of polymers were determined by GPC. In this work, we have prepared the lower molecular weights PLLAs to maintain the concentration of TPE core molecules, so that the influence of polymer chain packing on the emission properties of the core molecules can be studied effectively.

### 2.3.3. Sample Preparation

**2.3.3.1. Preparation of SSPLLA Gel.** 10 wt% of SSPLLA (TPE-4-PLLA) was dissolved in DMF at 120 °C and the solution was poured into a container. It was placed in a freezer overnight at -4 °C for gelation. Gel formation was confirmed by the failure of the solvent to flow while inverting the container. Furthermore, the thermoreversible nature of the gels was confirmed by repeated heating and cooling processes. A similar procedure was used to prepare gels with one-armed (TPE-1-PLLA) and two-armed PLLA (TPE-2-PLLA).

---

**2.3.3.2. Preparation of SSPLLA Precipitate.** 10 wt% of SSPLLA was dissolved in DMA at 120 °C and the solution was poured into a container. It was placed in a freezer overnight at -4 °C. Unlike in DMF, SSPLLA forms precipitate in DMA.

## 2.4. Characterization

<sup>1</sup>H NMR spectra were recorded on a 500 MHz Bruker Advance DPX spectrometer using tetramethylsilane (TMS) as an internal reference. The molecular weight and dispersity ( $\bar{M}_w/\bar{M}_n$ ) of the polymer were determined by GPC using Agilent Technologies-1260 instrument with RI detector, which is equipped with a PL-gel 20  $\mu$ m mixed bed column operated at 30 °C with THF as solvent (flow rate of 1 mL/min). Molecular weight was measured using a standard calibration curve obtained using narrow polystyrene standards. DSC thermograms of solid and gels were carried out using a thermal analyzer (TA instrument Q2000) at a heating and cooling rate of 10 °C/min under N<sub>2</sub> atmosphere. CD measurements were collected on a JASCO-J-810 spectrometer with Peltier thermostatic cell holders using a quartz cuvette of 1.0 cm path length. The concentration of the solution was fixed at 1 mg/ml for SSPLLA chloroform/hexane mixture. Photophysical properties were measured using a 1 cm or 1 mm quartz cuvette. The emission spectra at room temperature were recorded using a SPEX-Fluorolog-3 FL3-221 spectrofluorimeter. Variable temperature fluorescence spectra were recorded on the Spex-Fluoromax FL22 spectrofluorimeter equipped with a double grating 0.22 m Spex 1680 monochromator, a 450 W Xe lamp as the excitation source and a Hamamatsu R928P photomultiplier tube detector. The excitation wavelength was 330 nm. Emission spectra were corrected for source intensity (lamp and grating) by standard correction curves. The absorption spectra were recorded on a Shimadzu UV-2600 UV-Vis spectrophotometer. Variable temperature absorption spectra were recorded using the Shimadzu model S-1700 temperature controller. The sample was allowed to reach thermal equilibrium at every temperature ( $\pm 0.1$  °C) in a

Hellma Analytics 1 cm path length quartz cell in thermostated cell holder of the spectrophotometer. Wide-angle X-ray scattering (WAXS) measurements were carried out on a XEUSS SAXS/WAXS system from Xenocs (operated at 50 kV and 0.60 mA) in transmission geometry using Cu K $\alpha$  radiation (wavelength,  $\lambda = 1.54 \text{ \AA}$ ). The two-dimensional patterns were recorded on a Mar 345 image plate system (detector) and the data was processed using the Fit2D program. Silver behenate was used to calibrate the sample to detector distance. The variable temperature measurements of SSPLLA gels were carried out using a Linkam THMS 600 hot stage fitted to the X-ray system. Rheological measurements were conducted on an Anton Paar modular compact (MCR 150) stress-controlled rheometer equipped with a parallel plate geometry (20 mm diameter) and striated cone. The gap between the cone and the plate was kept fixed between 0.25 mm. AFM images were collected on multimode SPM (Bruker Nanoscope V) in the tapping mode. Antimony doped silicon cantilever with a resonant frequency of 300 kHz and spring constant of  $40 \text{ Nm}^{-1}$  was used. Samples were prepared by drop-casting the diluted gel dispersion on a cleaned silicon wafer surface and dried in the air for 48 hours in a closed petri dish at room temperature. MTT assay was evaluated using human lung fibroblast cell line WI-38. WI-38 cells were kindly gifted from CSIR-IICB, Kolkata, India. Cells were maintained in Dulbecco's modified Eagle medium (DMEM) with 10% fetal bovine serum (FBS) and 5% CO<sub>2</sub> at 37 °C. The growth inhibition capacity was evaluated by MTT assay. Cell suspensions of  $5 \times 10^3$  cells/well (100  $\mu\text{L}$ ) were seeded in a 96 well plate and 100  $\mu\text{L}$  of SSPLLA was added to that at various concentrations (1  $\mu\text{g}/\text{mL}$  to 100  $\mu\text{g}/\text{mL}$ ). The plain medium was used as a negative control, while the clinically used anti-cancer chemotherapeutic agent doxorubicin (Dox, 1  $\mu\text{M}$ ) was employed as a positive control. The plates were incubated for a period of 6 h, 12 h and 24 h in a CO<sub>2</sub> incubator. After incubation, 20  $\mu\text{L}$  MTT (5 mg/mL) was added to each well and incubation was continued for an

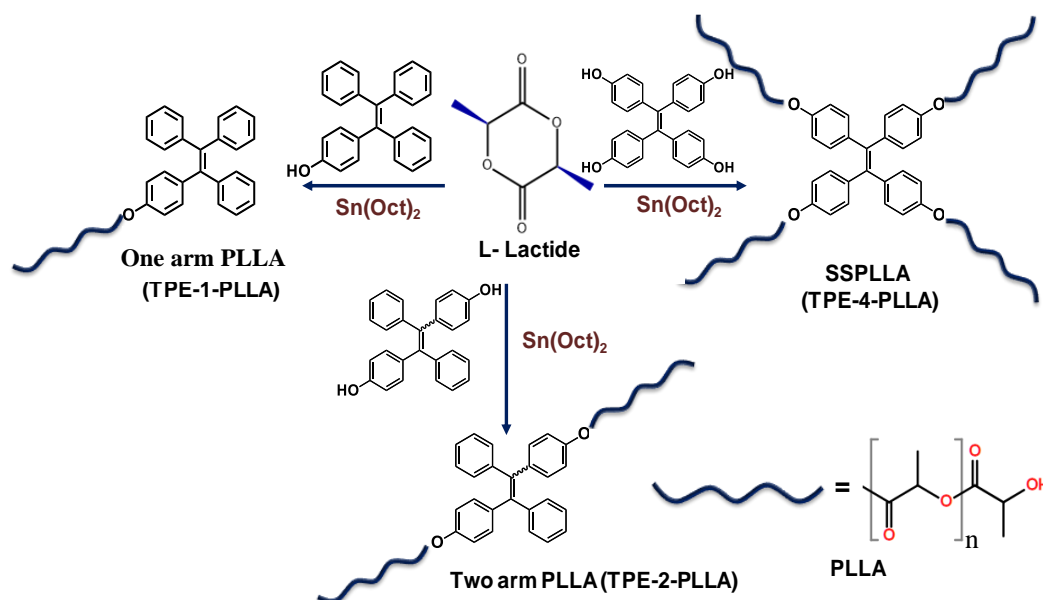
---

additional 2 h. The insoluble formazan crystals formed were solubilized by the addition of 100  $\mu\text{L}$  MTT lysis buffer followed by an incubation of 4 h and the absorbance was measured at 570 nm using a microplate spectrophotometer (BioTek, Power Wave XS). The bacterial growth of SSPLLA against selected Gram-negative and Gram-positive pathogens was carried out by spreading the bacterial strains aseptically on LB agar plates using a sterile cotton swab. Four wells were prepared on the culture smeared agar plates using a sterile cork borer. The disks were loaded with 25  $\mu\text{L}$  of SSPLLA gel in DMF and DMF as the control (2 replicates for each). The disks were then dried inside the biosafety cabinet and incubated at 37  $^{\circ}\text{C}$  for 36 h.

## 2.5. Results and Discussion

### 2.5.1. Structural and Thermal Properties of One-armed, Two-armed and Four-armed

#### PLLAs with Tetraphenylethylene as Core



**Scheme 2.1.** Synthesis of one-armed, two-armed and four-armed PLLAs with tetraphenylethylene.

One-armed, two-armed and four-armed PLLAs were synthesized by ring-opening polymerization of L-lactide using TPE-1-OH, TPE-2-OH and TPE-4-OH, respectively, as macroinitiators and tin(II) 2-ethylhexanoate ( $\text{Sn}(\text{Oct})_2$ ) as the catalyst as depicted in Scheme 2.1. The chemical structures of One-armed, two-armed and four-armed PLLAs were confirmed by  $^1\text{H}$ -NMR (Figure 2.1),  $^{13}\text{C}$ -NMR (Figure 2.2) and FTIR (Figure 2.3).

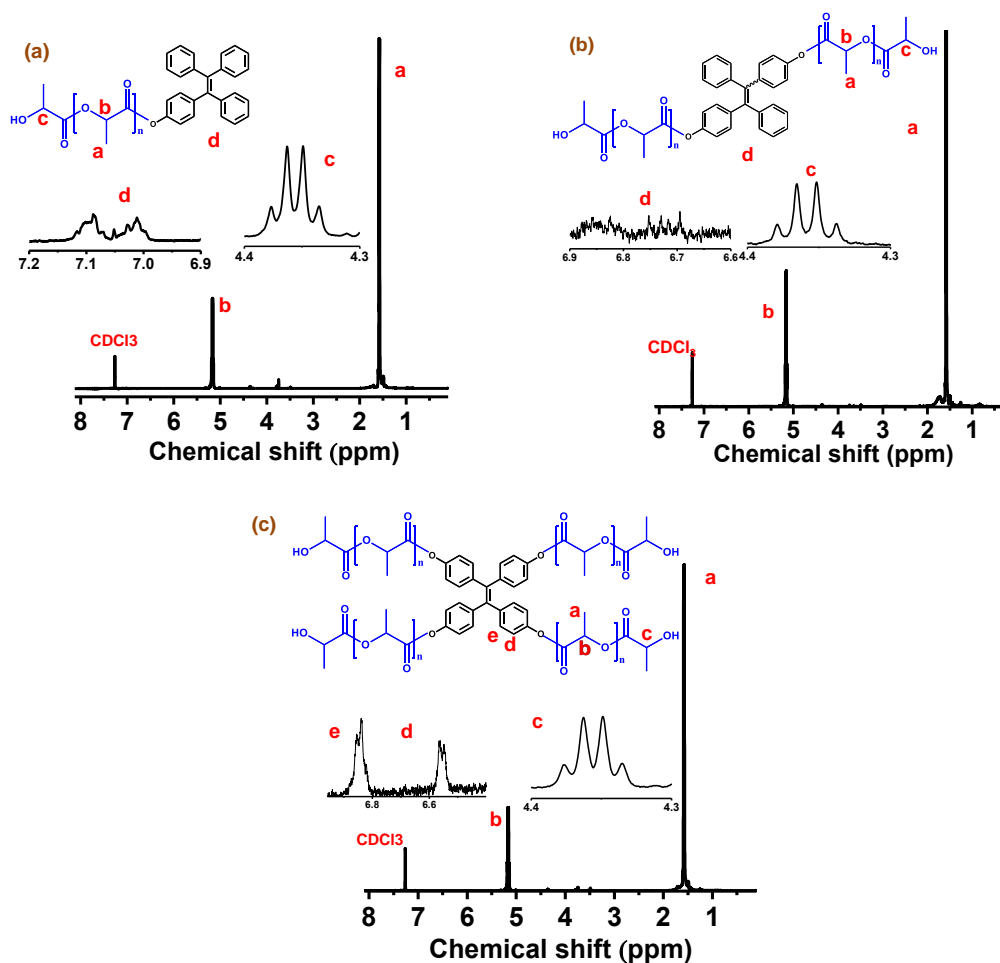


**Figure 2.1.**  $^1\text{H}$  NMR spectrum of (a) one-armed, (b) two-armed and (c) SSPLLA with tetraphenylethylene as the core molecule.

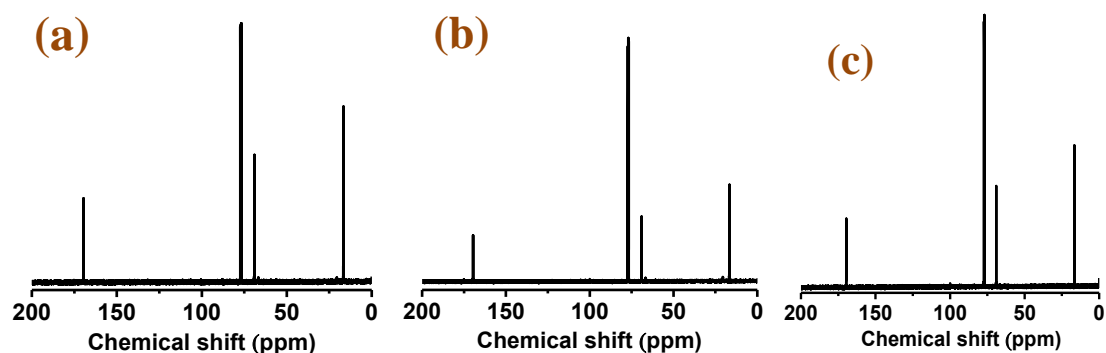


**Figure 2.2.**  $^{13}\text{C}$  NMR spectrum of (a) one-armed PLLA, (b) two-armed PLLA and (c) SSPLLA with tetraphenylethylene as the core molecule.

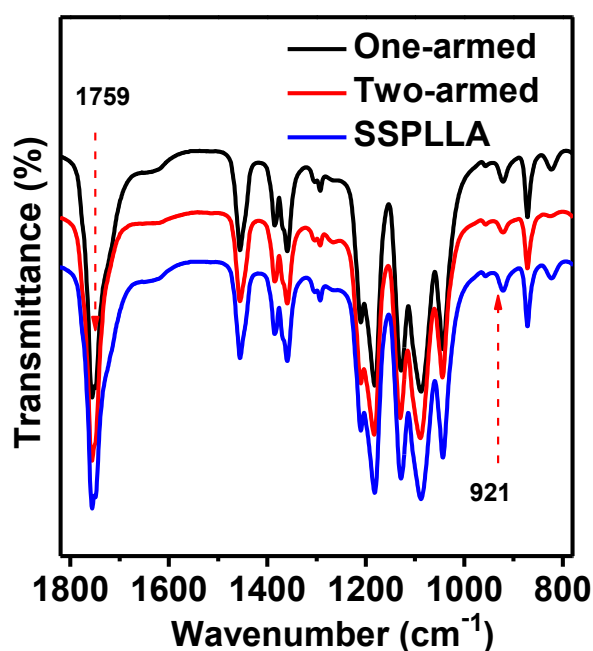


**Figure 2.3.** FTIR spectra of one-armed, two-armed and SSPLLA.

The number average molecular weights ( $M_n$ ) and molecular weight distributions ( $\mathcal{D}$ ) of various PLLAs were measured using GPC (Figure 2.4 and Table 2.1). The absolute molecular weight of various PLLAs were estimated from  $^1\text{H}$  NMR using the reported procedure.<sup>63</sup>

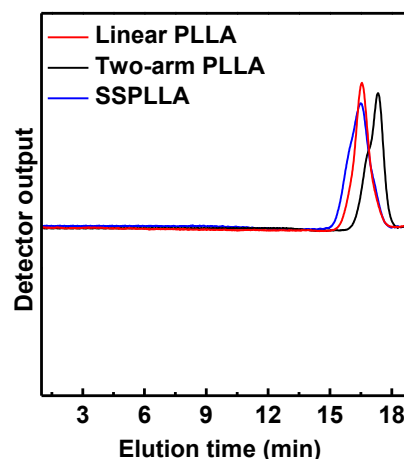


**Figure 2.4.** GPC traces of one-armed PLLA, two-armed PLLA and SSPLLA in THF.

**Table 2.1.** Characterization of PLLAs synthesized in this study.

Sample	$M_n$ (g/mol) <sup>[a]</sup>	$M_n$ (g/mol) <sup>[b]</sup>	$\bar{D}$ <sup>[b]</sup>	$T_g$ (°C)	$T_{cc}$ (°C)	$T_m$ (°C)	$X_c$ (%) <sup>[c]</sup>
One-armed PLLA	8800	9195	1.28	46	90	159	27
Two-armed PLLA	13800	14600	1.32	50	105	162	23
SSPLLA	8900	9100	1.4	46	91	159	17

[a]  $M_n$  was estimated using  $^1H$  NMR [b]  $M_n$  and  $\bar{D}$  were estimated using GPC, and [c]  $X_c$  was estimated using WAXS patterns shown in Figure 2.5.

Differential scanning calorimetry (DSC) thermograms (Figure 2.5a) of one-armed PLLA, two-armed PLLA and SSPLLA show no peaks during cooling, indicating that the crystallization rate of various PLLAs is relatively slow and upon reheating, multiple transitions corresponding to glass transition ( $T_g$ ), cold-crystallization ( $T_{cc}$ ) and melting ( $T_m$ ) are observed (Table 2.1). No traces of crystallization and melting of TPE molecule were observed. The wide-angle X-ray scattering (WAXS) patterns of the cold-crystallized PLLAs (Figure 2.5b) show X-ray reflections corresponding to the  $\alpha$  form of PLLA at  $2\theta = 14.8^\circ$  (010),  $16.8^\circ$  (110/200),  $19.1^\circ$  (203),  $20.8^\circ$  (204),  $22.4^\circ$  (015), and  $27.7^\circ$  (207)<sup>50</sup> and no additional crystalline reflections were observed, indicating the purity of the synthesized samples. In the  $\alpha$  form, left-handed  $10_7$  helical chains are packed in the orthorhombic unit cell.<sup>50, 64</sup> Sakamoto and Tsuji investigated the effect of branching on the crystallization

behavior of one-armed PLLA, two-armed PLLA and branched PLLA and demonstrated that the crystal growth mechanism is not affected by the presence of branching.<sup>63, 65</sup>

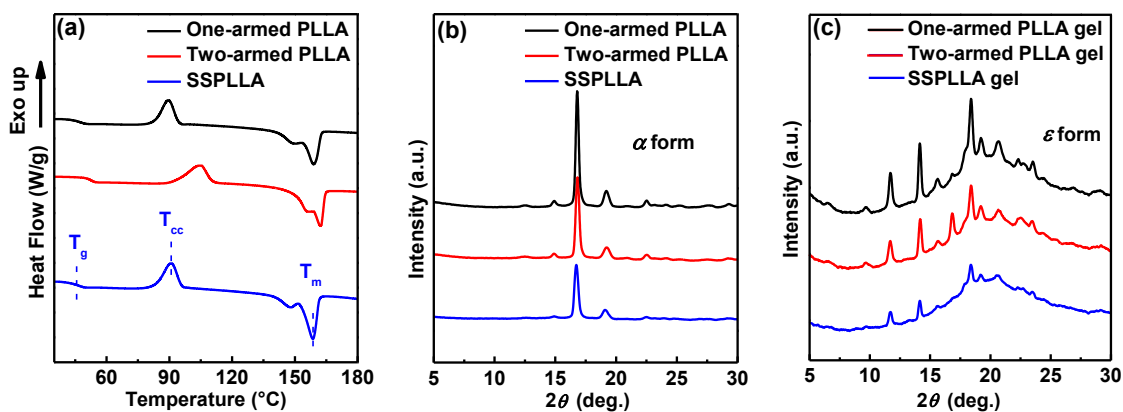


**Figure 2.5.** (a) DSC reheating thermograms obtained at a rate of 10 °C/min, WAXS patterns of (b) cold-crystallized samples and (c) gels (in DMF) of one-armed PLLA, two-armed PLLA and SSPLLA.

PLLA is known to form crystalline complexes or co-crystals ( $\epsilon$  form) with particular solvents such as *N,N*-dimethylformamide (DMF), cyclopentanone (CPO), and THF at temperatures below -5 °C.<sup>53, 55</sup> It was recently reported that the solvents favoring the  $\epsilon$  form could form PLLA gels by dissolving PLLA at higher temperatures and subsequent cooling of the solutions to room temperature or sub-ambient temperatures.<sup>66</sup> Figure 2.5c shows the WAXS patterns of one-armed PLLA, two-armed PLLA and SSPLLA gels in DMF at room temperature. All the WAXS patterns show X-ray reflections at  $2\theta = 9.8^\circ$  (111),  $11.9^\circ$  (200),  $14.1^\circ$  (020),  $15.7^\circ$  (121/114),  $18.5^\circ$  (123),  $19.5^\circ$  (223),  $20.8^\circ$  (116) and  $23.8^\circ$  (117) corresponding to the  $\epsilon$  form of PLLA.<sup>53</sup> In the  $\epsilon$  form, PLLA chains are packed in the orthorhombic unit cell and take the  $10_7$  helical chain conformation. SSPLLA gel formed is quite stable at room temperature.<sup>53</sup> The degree of crystallinity ( $X_c$ ) of PLLA decreased with the increase of the number of arms connected to the TPE (Table



1) and  $X_c$  of one-armed PLLA, two-armed PLLA and SSPLLA gels were estimated to be 27, 23 and 17%, respectively.

### 2.5.2. Photophysical Properties of SSPLLA

With the TPE incorporated PLLAs in hand, we systematically characterized the influence of polymer chains on the optical properties of TPE by UV-Vis absorption spectroscopy, and circular dichroism of SSPLLA as depicted in Figure 2.6. The absorption spectrum of SSPLLA (Figure 2.6a) in chloroform solution (good solvent) shows two bands around 244 nm and 325 nm corresponding to the  $n \rightarrow \pi^*$  transition of the carbonyl groups in PLLA<sup>67</sup> and  $\pi \rightarrow \pi^*$  transition of TPE unit, respectively.<sup>34, 68</sup> When the poor solvent (hexane) was added into the SSPLLA solution, a hypsochromic shift of C=O absorption band (236 nm) occurred due to the aggregation (formation of helical chains of PLLA). Wang et al. reported such a blue-shift of the carbonyl band upon the crystallization of PLLA in bulk.<sup>69</sup> To further confirm the formation of helical PLLA chains, the CD spectrum of SSPLLA was measured in chloroform and a mixture of solvents (chloroform/hexane:25/75 v/v) (Figure 2.6b). The CD spectra show a positive Cotton effect at 236 nm corresponding to the  $n \rightarrow \pi^*$  transition of the carbonyl group of PLLA and polymer chains adopt left-handed helical chain conformation.<sup>67</sup> It has to be noted that in a good solvent such as chloroform, SSPLLA chains adopt majorly random coil conformation (with a few short helices) because of the molecular level dissolution and the CD spectrum is less intense. This is labeled as a solution state. On the other hand, on the addition of the poor solvent shows a large positive Cotton effect and the intensity of the CD band is significantly amplified compared to the chloroform solution due to the aggregation of PLLA chains (formation of more number of helical chains of PLLA). This situation is labeled as an aggregate state, where no crystals of PLLA are formed.

---

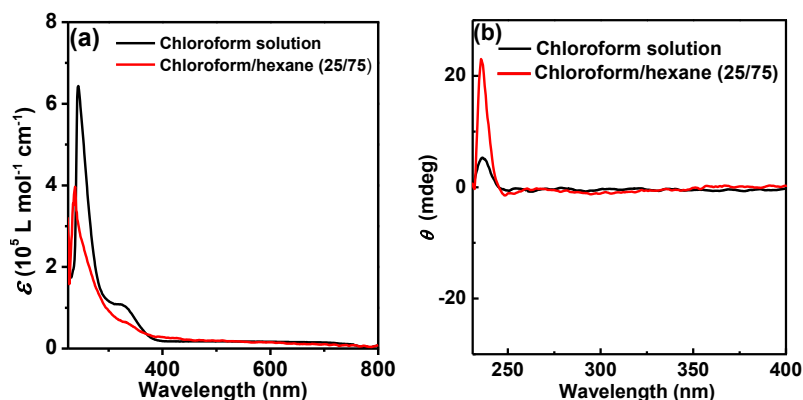


**Figure 2.6.** (a) UV-Vis absorption spectra (in solution and aggregate states) and (b) CD spectra (in solution and aggregate states) of SSPLLA with TPE core molecules.

For the purpose of comparison, the CD spectrum of SSPDLA was obtained under similar conditions as shown in Figure 2.7. It is obvious that the CD spectrum of SSPDLA showed a mirror-imaged Cotton effect compared to SSPLLA indicating the opposite handedness in the helical chains. On the basis of the coupled oscillator method, it was assigned that PLLA and PDLA adopt left- and right-handed helical chain conformations, respectively.<sup>70</sup> A similar observation was made in the cases of one-armed and two-armed PLLAs.

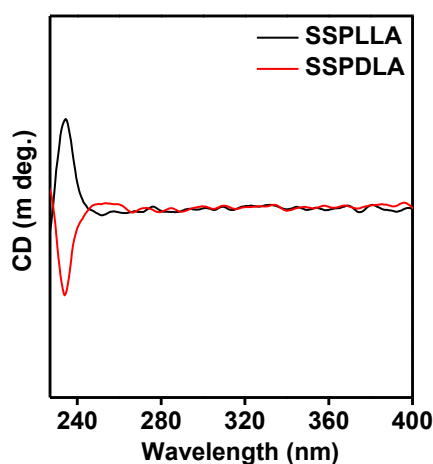


**Figure 2.7.** CD spectra of SSPLLA and SSPDLA in the aggregate states.

### 2.5.3. Aggregation-Induced Emission of One-armed PLLA, Two-armed PLLA and SSPLLA

Figure 2.8 shows the emission spectra of one-armed PLLA, two-armed PLLA and SSPLLA in different states. As seen, the PL spectra of all the PLLAs dissolved in chloroform (solution state) show almost flat lines (dashed lines in Figure 2.8a) indicating that the TPE incorporated polymer is non-emissive in the completely dissolved state where most of the PLLA chains adopt random coil conformation with less number of aggregated helical chains. Interestingly, the emission intensity increased gradually with the increase of poor solvent (hexane) content in all the three polymers (the PL emission spectra of SSPLLA is shown in Figure 2.8b as a representative) and the maximum emission was observed when the poor solvent content is around 75 % (chloroform/hexane:25/75 v/v) (aggregate state). However, the increase is quite significant in the case of SSPLLA. Similar to the aggregate state, SSPLLA emits strongly in the gel state (crystalline state) compared to the one-armed and two-armed PLLA gels (Figure 2.8c) and the corresponding photographs of gels under UV-light illumination (Figure 2.8d) further confirms the different emission behavior. In gel state, the physical networks are formed through crystallization of polymer chains and the fiber-like structures exist. It was shown that PLLA takes  $10_7$  helical conformation both in aggregate and gel states.<sup>56, 66</sup> It means that the change in the conformation of PLLA from random to helical chains has a significant influence on the TPE molecules and it is expected that the covalently linked PLLA chains alter the torsion angles of the peripheral phenyl rings and restrict their intramolecular rotation.<sup>1</sup> In the case of one-armed and two-armed PLLAs, the excited-state energy of TPE can be dissipated through the rotations of its free phenyl rings<sup>35</sup> (that are not covalently connected to PLLA) and that can result in the lower emission. In the gel state, the emission behavior of one-armed and two-armed PLLAs is almost similar because of the free rotations of phenyl rings of TPE in the solvated

---

amorphous phase (higher mobility of PLLA chains). On the other hand, in SSPLLA, all the phenyl rings are covalently connected to PLLA chains and these chains strongly restrict the intramolecular rotations of phenyl rings. Such a situation leads to the strong aggregation-induced emission of SSPLLA compared to one-armed and two-armed PLLAs with TPE molecules. Zhao et al. reported a similar behavior in TPE labeled star PLLA in THF/water mixture, where the PLLA chains are connected to core TPE through two ethylene glycol units.<sup>22</sup> In this way, we found that SSPLLA emits strongly both in aggregate and gel states and we have used this particular system for further studies.

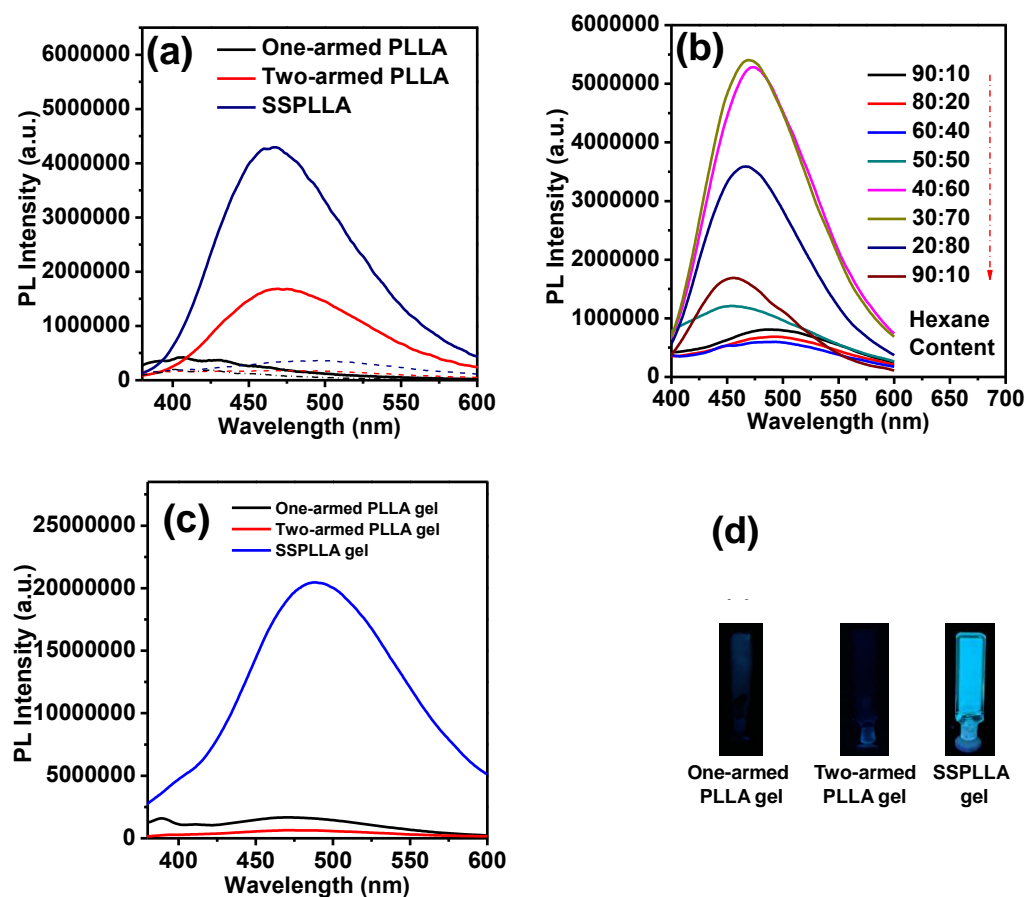


**Figure 2.8.** (a) PL spectra of one-armed PLLA, two-armed PLLA and SSPLLA in solution state (dashed lines), in the aggregate state (in the mixture of solvents chloroform/hexane 25/75 v/v) (thick lines), (b) PL spectra of SSPLLA in chloroform/hexane mixtures with different hexane content, (c) PL spectra of one-armed PLLA, two-armed PLLA and SSPLLA in gel state (excited at 330 nm) and (d) photographs of gels under UV light illumination.

The fluorescence lifetime-decay profiles of SSPLLA with TPE core in the aggregated state (in chloroform/hexane mixture) and gel state are shown in Figure 2.9 and Table 2.2. Both aggregated and gel states exhibited tri-exponential decay, with average lifetimes of 1.3 and 0.56 ns, respectively. A slight increase in the lifetime of the aggregated state than that of the gel state may be due to local environments caused by the restriction of intramolecular rotation of the peripheral phenyl rings with the branched polymer chains. To further get the insights on the role of PLLA helical chains on the emission behavior of core TPE, different crystalline forms of SSPLLA were prepared and systematically investigated using variable temperature UV-Vis, PL and WAXS measurements.

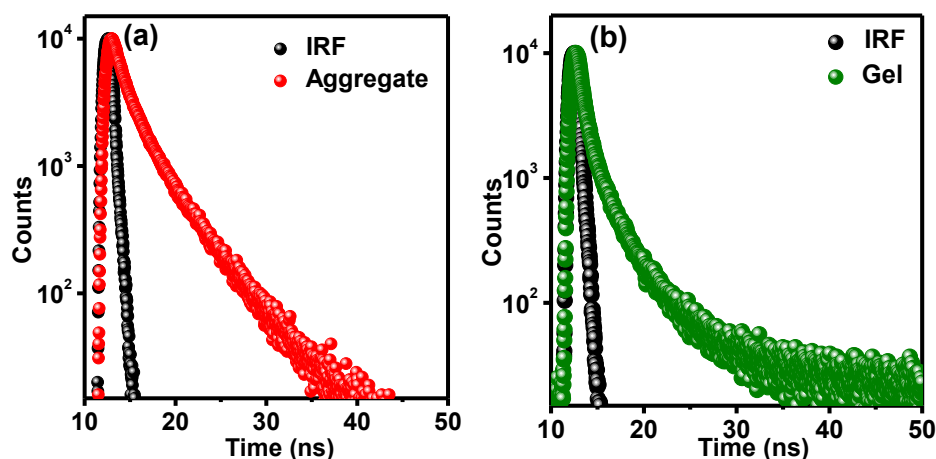


**Figure 2.9.** Fluorescence lifetime plot of SSPLLA in the (a) aggregated state (in chloroform/hexane mixture) and (b) gel state ( $\epsilon$  form).

**Table 2.2.** Fluorescence lifetime-decay of SSPLLA in aggregated and gel states.

Sample	$\tau_1$ (ns)	$\tau_2$ (ns)	$\tau_3$ (ns)
Aggregated state	1.88 (42.6%)	4.96 (40.6 %)	0.37 (16.8 %)
Gel state	1.57 (37.3 %)	5.19 (18.1%)	0.29 (44.6 %)

The gel formation of SSPLLA in DMF was further confirmed by performing the viscoelastic measurements. Figure 2.10a shows the dynamic frequency sweep tests

conducted at 20 °C. The observed storage modulus ( $G'$ ) is higher than the loss modulus ( $G''$ ) in the frequency range of 0.1-100 rad s<sup>-1</sup>, a typical feature of supramolecular gels. These results are in good agreement with the reported data on PLLA/DMF gels.<sup>66</sup>

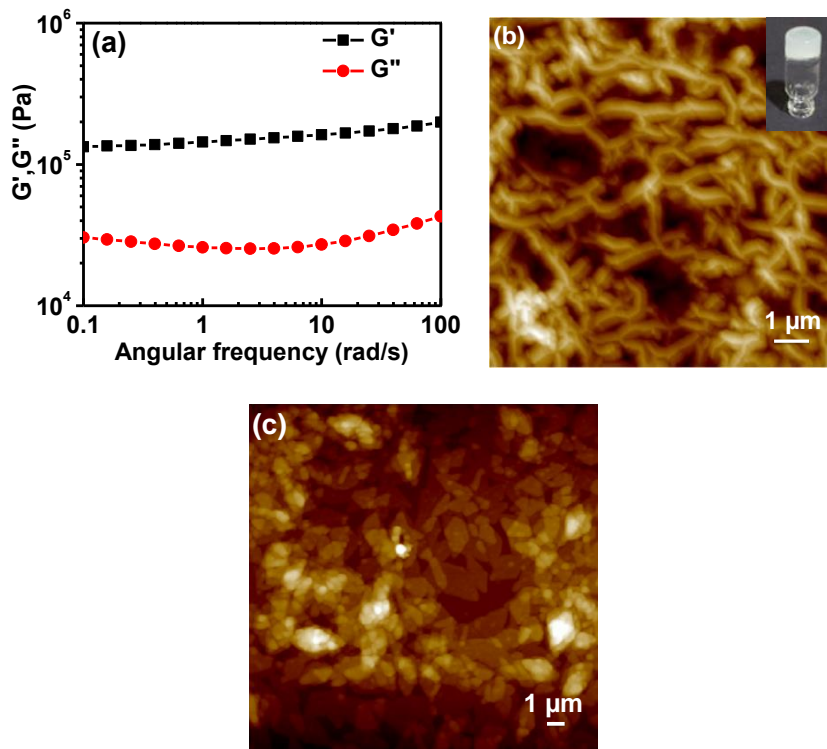


**Figure 2.10.** (a) Plot of angular frequency ( $\omega$ ) versus dynamic storage modulus ( $G'$ ) and loss modulus ( $G''$ ) for PLLA gel in DMF at 20 °C, AFM height images of (b) PLLA gel in DMF ( $\epsilon$  form) (inset shows the photograph of gel under room light) and (c) PLLA precipitate in DMA ( $\alpha$  form). The surface roughness of dried PLLA gel and PLLA precipitate are 10 and 8 nm, respectively.

Atomic force microscopy (AFM) image of SSPLLA/DMF gel shows the entangled fibrillar networks having a length of a few micrometers, as shown in Figure 2.10b. The formation of fibrillar morphology is mainly responsible for the SSPLLA gels in DMF. As discussed in the preceding section, PLLA crystallized into the  $\epsilon$  form in SSPLLA/DMF gels. On the other hand, as shown in Figure 2.10c, SSPLLA formed aggregate particle

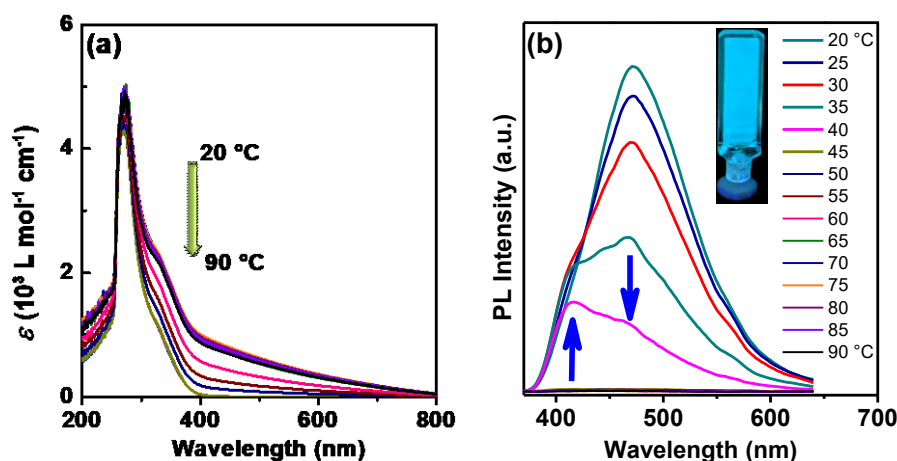
morphology in N,N-dimethylacetamide (DMA) and no gelation was observed in DMA, which might be due to the difference in the interactions between the polymer and solvent. In this case, SSPLLA leads to the formation of a precipitate and the WAXS pattern of this precipitate shows the typical  $\alpha$  form, as shown in a later section. In this way, solvents play a significant role in determining the crystal structure, morphology and the physical state of SSPLLA.

#### **2.5.4. Effect of Crystal-to-crystal Transition on Emission Behavior of SSPLLA**

To further understand the influence of PLLA chains on the aggregation properties of TPE, temperature-dependent UV-Vis absorption and PL emission studies of SSPLLA/DMF gels and SSPLLA/DMA precipitates were carried out. Figure 2.11 depicts the temperature-dependent UV-Vis absorption spectra and PL emission spectra of SSPLLA/DMF gel. At 20 °C, the absorption spectrum of SSPLLA/DMF gel (Figure 2.11a) shows two bands around 272 nm and 331 nm corresponding to the  $n \rightarrow \pi^*$  transition of the carbonyl groups in PLLA<sup>67</sup> and the  $\pi \rightarrow \pi^*$  transition of the TPE unit, respectively.<sup>34, 68</sup> The band corresponding to the carbonyl groups in PLLA is red-shifted from 244 nm to 272 nm compared to the SSPLLA/chloroform solution, which may be due to the change in the polarity of solvent used (DMF) and the interactions between PLLA and DMF. Marini et al. reported that the polarity of the solvent plays a role on the fluorescent properties of solvated molecular probes.<sup>71</sup> As DMF is a polar solvent, the absorption spectrum of SSPLLA/DMF gel is red-shifted compared to the SSPLLA/chloroform solution. Besides, the UV-Vis spectrum showed a Mie scattering effect for the gel, indicating the existence of nanofibers. Upon heating, no change in the absorption spectra is observed up to 35 °C and above this temperature, a slight decrease in the intensity of bands is observed. At higher temperatures, above 80 °C, the Mie scattering effect disappeared, indicating the formation of a homogeneous solution. Figure 2.11b shows temperature-dependent PL emission spectra of

---

SSPLLA/DMF gel. At low temperature, gel emits strongly at 472 nm and the PL intensity decreased with the increase in the temperature. At around 35 °C, the emission peaks blue-shifted to 415 nm. Around 45 °C, a sudden quenching in the PL emission is observed. To further understand the reason for these observations, we have carried out DSC and temperature-dependent WAXS studies of SSPLLA/DMF gels.



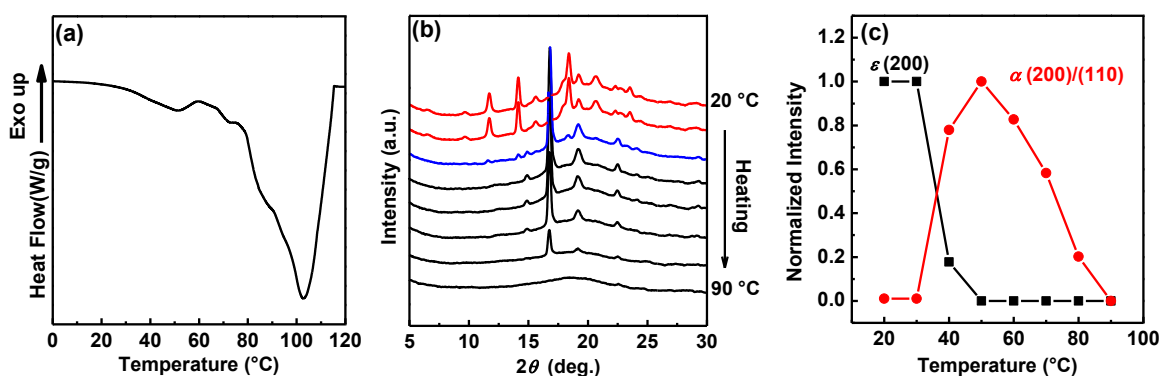
**Figure 2.11.** Temperature-dependent (a) absorption and (b) emission spectra of SSPLLA/DMF gel. The inset of (b) shows the photograph of gel under UV light illumination.

Figure 2.12 shows the DSC thermogram and temperature-dependent WAXS patterns of the SSPLLA/DMF gel in the heating process. As seen in Figure 2.12a, two transitions are observed in the temperature range of 30 - 120 °C. Matsuda et al. demonstrated the formation of  $\varepsilon$  gels using PLLA in DMF and showed that the  $\varepsilon$  to  $\alpha$  transition occurs over a broad temperature range of 27 - 42 °C.<sup>66</sup> The transition at 30 - 40 °C can be assigned to the crystal-to-crystal transition ( $\varepsilon$  to  $\alpha$  form) and the onset of the transition temperature is around 30 °C. On further heating, a broad endothermic peak is observed at 104 °C, corresponding to the melting of the  $\alpha$  form. As seen in Figure 2.12b, at 20 °C, several X-ray reflections corresponding to the  $\varepsilon$  form appeared at  $2\theta = 11.7^\circ$ ,  $14.1^\circ$ ,  $15.6^\circ$ ,  $18.3^\circ$ ,  $19.2^\circ$ ,  $20.6^\circ$ ,  $22.3^\circ$ ,  $23.5^\circ$ , and  $29.1^\circ$  similar to the PLLA. This



observation suggested that the presence of covalently linked TPE core molecules in SSPLLA has no influence on the formation of the  $\varepsilon$  form in the gel state. As TPE molecule is quite large in size, it is expected that these molecules will be excluded out of the crystalline lamellae and reside at the interface of crystalline and amorphous phases or in the amorphous phase. In the  $\varepsilon$  form (gel), DMF molecules are distributed both in the crystalline and amorphous phases. Upon heating, the intensity of the  $\varepsilon$  form reflections started to decrease from 30 °C and completely disappeared at 50 °C. It was demonstrated that the mobility in the amorphous region (i.e. glass transition temperature) triggers the  $\varepsilon$  to  $\alpha$  transition up on heating.<sup>55</sup> At this transition temperature, DMF molecules residing within the crystal lattice of the  $\varepsilon$  form are excluded into the amorphous state through the locally disordered helical chains and then the structure is transformed to the new crystalline form. Based on the X-ray reflections ( $2\theta = 14.8^\circ, 16.8^\circ, 19.1^\circ, 20.8^\circ, 22.4^\circ, 25.0^\circ$  and  $27.7^\circ$ ), the new form was assigned to the  $\alpha$  form and it started appearing from 40 °C. At around 90 °C, the reflections corresponding to the  $\alpha$  form disappeared, indicating the melting of  $\alpha$  crystals. Figure 2.12c shows the changes in the normalized intensities of representative reflection (200) of the  $\varepsilon$  form and (200/110) of the  $\alpha$  form against temperature. Both DSC and WAXS results indicated that the structural reorganization in the crystal lattice occurred in a broad temperature range from 30 – 45 °C and in this temperature range, conformational reorganization of helical chains ( $10_7$  (left-handed  $10_3$ )) occurred within the crystal lattice due to the exclusion of DMF molecules from the crystal lattice of the  $\varepsilon$  form to the amorphous phase of the  $\alpha$  form. In the case of gels, the solvent molecules reside in the polymer-poor phase or solvent phase (amorphous phase). It is also worth mentioning here that the  $\varepsilon$  to  $\alpha$  transition is irreversible as the obtained  $\alpha$  form is a stable form.

---



**Figure 2.12.** (a) DSC thermogram during heating at 10 °C/min, temperature-dependent (b) WAXS patterns and (c) normalized intensity of the reflections at  $2\theta = 11.2^\circ$  ( $\epsilon$ ), and  $16.6^\circ$  ( $\alpha$ ) evaluated from (b) during the heating process of SSPLLA/DMF gel.

Based on the insights from temperature-dependent UV-Vis spectroscopy, PL spectroscopy, WAXS and DSC, it is now possible to summarize the emission behavior of TPE in SSPLLA upon heating of the SSPLLA/DMF gel. Figure 2.13 depicts the schematic representation of structural changes occurring on heating of the SSPLLA/DMF gel. At 20 °C, SSPLLA/DMF gel forms the  $\epsilon$  form and DMF molecules are distributed both in the crystalline and amorphous phases (Figure 2.13a). In this case, polymer chains take  $10_7$  (left-handed  $10_3$ ) helical conformation. In the  $\epsilon$  form, covalently linked core TPE molecules are excluded from the crystal lattice due to their large size and stabilized at the interface of crystalline and amorphous phases or in the amorphous phase. As a result, all the covalently linked phenyl rings intramolecular rotations are restricted to give higher emission. When heated, as evident from the DSC and WAXS, crystal-to-crystal transition ( $\epsilon$  to  $\alpha$  transition) occurred in the broad temperature range 30 – 40 °C and as a result, the solvent molecules residing in the crystal lattice of the  $\epsilon$  form are excluded into the amorphous phase of the  $\alpha$  form (Figure 2.13b). Such a situation resulted in the change in torsion angles of peripheral

phenyl rings. At the same time, covalently linked PLLA chains still restrict the intramolecular rotation of the peripheral phenyl rings. As a result, PL emission blue-shifted due to the decrease in the conjugation length of TPE. Xu et al. reported a similar situation in the case of two-armed nylon labeled TPE.<sup>36</sup> It was also reported that the blue shift in TPEs occurred due to the change in the twist angle of the aromatic rings with respect to the ethylenic stator in the case of columnar liquid-crystalline materials based on TPEs and piezofluorochromic materials based on TPEs.<sup>72, 73</sup> Such a twist changes the torsion angle of phenyl rings; as a result, the conjugation length reduces, resulting in the blue emission. On further heating, just above the transition temperature, drastic quenching in the PL emission is observed (Figure 2.11b) even though the structure remained in the crystalline state ( $\alpha$  crystal) (Figure 2.13c). We might have two possibilities to explain the quenching behavior of TPE above the transition temperature. For example, the thickness of the solvated amorphous phase may increase due to the expulsion of solvents from the crystal lattice of the  $\varepsilon$  form above the  $\varepsilon$  to  $\alpha$  transition and this situation leads to the reduction of the concentration of TPE molecules in the solvated amorphous phase. Another possibility is the vigorous mobility of the amorphous chains at higher temperatures result in the free rotation of phenyl rings of TPE in the solvated amorphous phase to completely quench PL emission even though the PLLA is in the semicrystalline state ( $\alpha$  crystal). On further heating, around 90 °C, crystals are melted and a clear solution is formed where phenyl rings free rotation is possible (Figure 2.13d). Till today, solvents forming PLLA gels with  $\alpha$  crystals are not reported. To further prove that the PL emission quenching is happening mainly due to the mobility of the amorphous chains and not due to the arrangement of polymer chains in the  $\alpha$  form, further investigations were carried out using the  $\alpha$  form of SSPLLA.

---

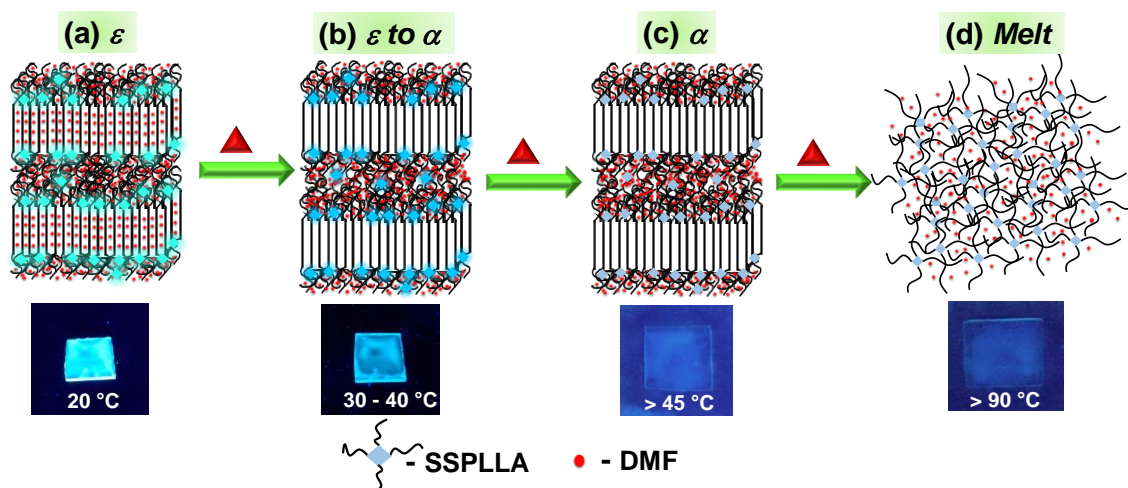


**Figure 2.13.** Schematic representation of structural changes and emission behavior of SSPLLA/DMF gel during the heating process.

Figure 2.14 shows the temperature-dependent UV-Vis absorption spectra, PL emission spectra and WAXS patterns of SSPLLA/DMA precipitate in the heating process. At 20 °C, the absorption spectrum of SSPLLA/DMA precipitate (Figure 2.14a) shows two bands at 264 nm and 330 nm corresponding to the carbonyl groups in PLLA and TPE unit, respectively. Upon heating, no change in the absorption spectra is observed in the entire temperature range. Unlike SSPLLA/DMF gel, in this case, no Mie scattering effect is observed due to the absence of the nanofibril structure (Figure 2.10c). Room temperature PL emission spectrum (Figure 2.14b) of SSPLLA/DMA precipitate shows strong emission at 472 nm and the PL intensity decreased gradually with the increase in the temperature. Unlike the SSPLLA/DMF gel ( $\epsilon$  form), the precipitate ( $\alpha$  form) shows emission peaks even at 70 °C. Similar to the observations made in the  $\epsilon$  gel case, the emission peak is blue-shifted to 415 nm (with lesser intensity), but at a higher temperature, i.e., 50 °C. This blue-shift is mainly due to the change in the torsion angle of phenyl rings and that resulted in the reduction of the conjugation length of TPE. On further heating, above 75 °C, complete quenching of PL emission was observed. Figure 2.14c shows the temperature-dependent

WAXS patterns of SSPLLA/DMA precipitate. As discussed in the preceding section, SSPLLA forms precipitate in DMA and shows aggregate particle morphology, as shown in Figure 2.10c. The room temperature WAXS pattern shows reflections corresponding to the typical  $\alpha$  form. Upon heating, the structure remained in the  $\alpha$  form until melting at 110 °C. Unlike SSPLLA/DMF gel, no crystal transition was observed in the case of SSPLLA/DMA precipitate. As observed in Figure 2.14b, the PL emission decreases gradually with temperature and a small shoulder at 417 nm was observed due to the change in the torsion angle of the phenyl rings in the temperature range of 50 – 70 °C. It means that even in the  $\alpha$  form (precipitate), at room temperature, the intramolecular rotations of phenyl rings of TPE are restricted to give higher emission similar to the SSPLLA/DMF gel ( $\varepsilon$  form). At the higher temperatures (above 50 °C), because of the higher mobility of amorphous chains, torsion angles of phenyl rings change, which resulted in the blue shift due to the change in the conjugation length of TPE molecules. The different emission behavior of  $\alpha$  form at the higher temperature in the case of SSPLLA/DMF and SSPLLA/DMA is mainly due to the difference in the polarity of the solvents and the interactions between PLLA and solvent molecules. On further heating, above 75 °C, complete quenching of PL emission was observed due to two possible reasons. For example, above 75 °C, partial melting of  $\alpha$  crystals and the segmental mobility of PLLA chains in the amorphous phase cause complete quenching. Another possibility is the conventional thermal-induced fluorescence decay at higher temperatures.

---

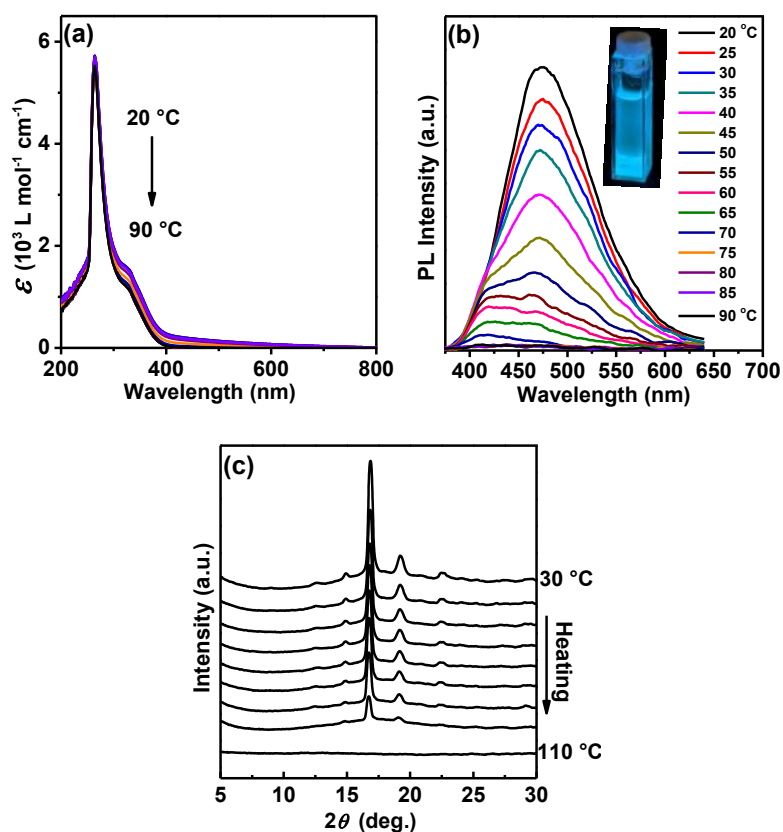


**Figure 2.14.** Temperature-dependent (a) absorption and (b) emission spectra and (c) WAXS patterns of SSPLLA/DMA precipitate. The inset of (b) shows the photograph of precipitate under UV light illumination.

### 2.5.5. Cytotoxicity and Antibacterial Properties of SSPLLA

To further evaluate the biocompatibility of SSPLLA, cytotoxicity assessment and antibacterial studies were carried out. Cytotoxicity of the SSPLLA was examined using human lung fibroblast cell line WI-38. The viability of WI-38 cell line was evaluated by 3-(4,5-dimethylthiazol-2-yl)-2,5-diphenyltetrazolium bromide (MTT) assay as reported by Maiti and co-workers.<sup>74</sup> WI-38 cells were incubated at various concentrations of SSPLLA (1, 5, 10, 50, 100  $\mu\text{g}/\text{mL}$ ) for 6, 12 and 24 h. The insoluble formazan crystals formed were solubilized by the addition of 100  $\mu\text{L}$  MTT lysis buffer followed by an incubation of 4 h and the absorbance was measured at 570 nm using a microplate spectrophotometer (BioTek, Power Wave XS). As shown in Figure 2.15, SSPLLA did not exhibit any

noticeable toxicity, whereas Dox-induced toxicity was observed. The bacterial growth on SSPLLA/DMF gel was tested against three species of pathogens: *E. Coli* DH5a, *E. Coli* and *S. aureus*, as shown in Figure 2.16. DMF was used as a control. After spreading the bacteria, the plates were sealed and incubated at 37 °C for 36 h. As seen in Figure 2.16, the uniform growth of bacteria was observed both on sample and control, suggesting that the SSPLLA possessed bacterial activity of both the Gram-negative and Gram-positive pathogens. These experiments further confirm the nontoxic nature of SSPLLA.

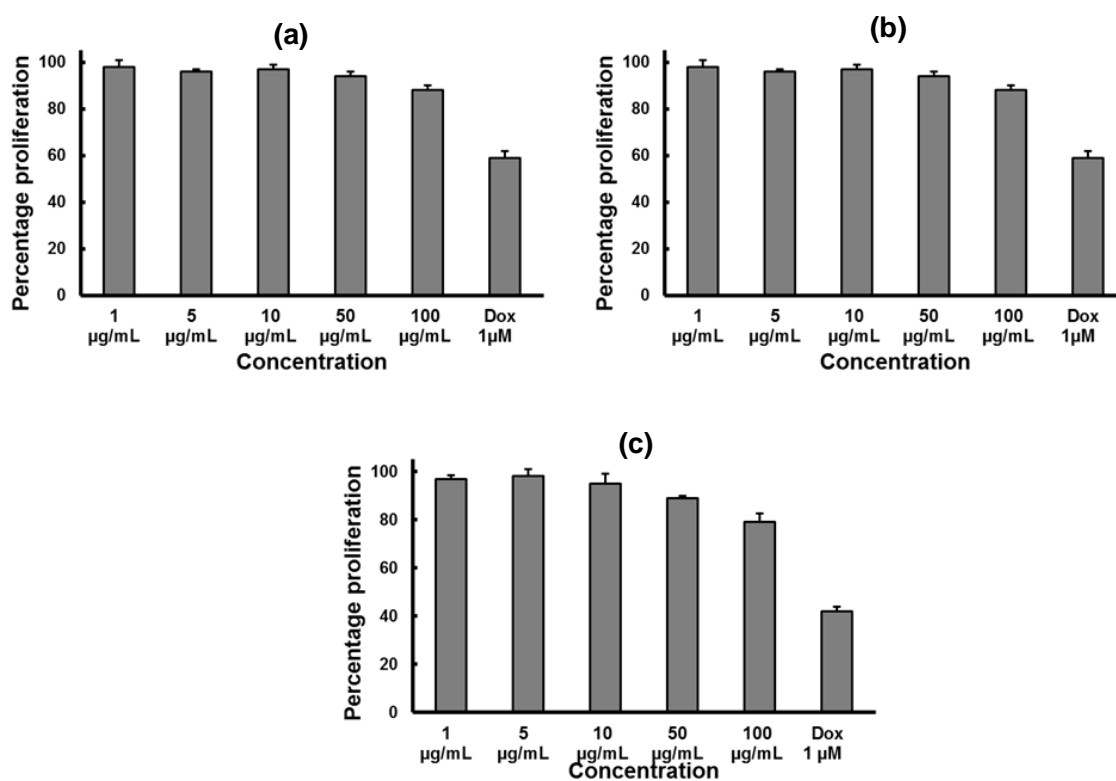


**Figure 2.15.** Evaluation of cytotoxicity by SSPLLA after (a) 6 h, (b) 12 h and (c) 24 h incubation with human lung fibroblast cell line (WI-38 cells) by MTT assay. Data represent mean  $\pm$  SD from three independent experiments.

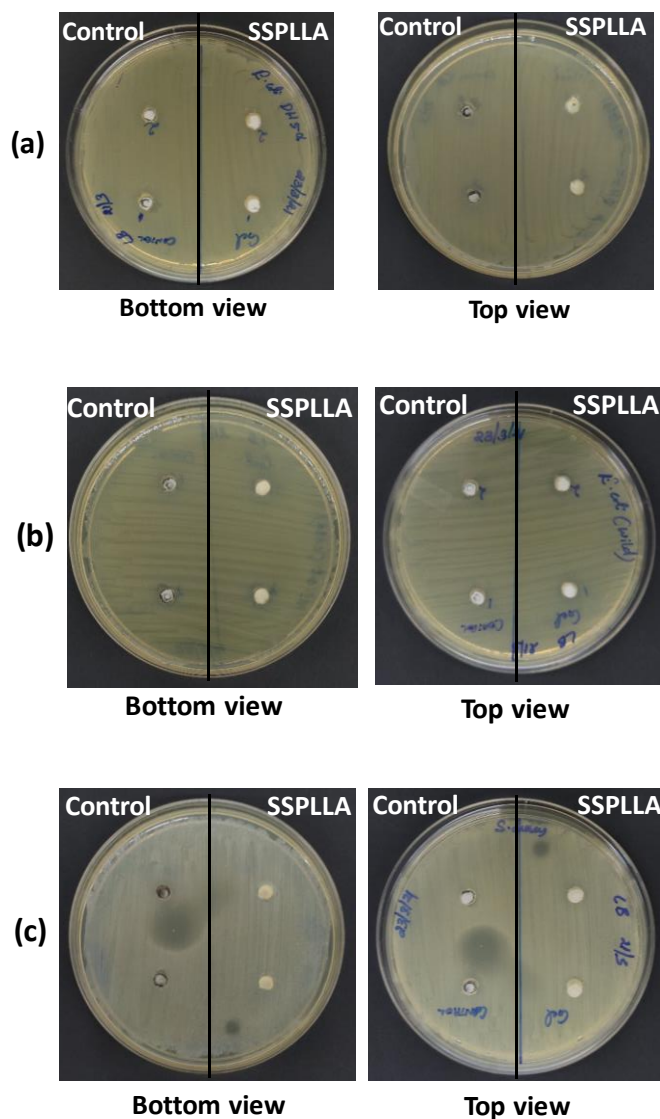


**Figure 2.16.** Growth of bacteria (a) *E. Coli* DH5 $\alpha$ , (b) *E. Coli* and (c) *S. aureus* on the agar plate at the incubation time of 36 h at 37 °C. 25  $\mu$ l of the SSPLLA gel in DMF (2 replicates) was loaded onto the agar plate well (right panel) and DMF without SSPLLA (2 replicates) was used as the control (left panel) in the experiment.

## 2.6. Conclusions

In summary, we have synthesized one-armed PLLA, two-armed PLLA and SSPLLA with a fluorophore TPE and investigated their AIE characteristics in the solution, aggregate and gel states. The synthesized polymers are non-emissive in good solvents and emit in the aggregated state. Compared to one-armed and two-armed PLLAs, SSPLLA



emits strongly in the aggregated and gel states. In SSPLLA, four arms of TPE molecules are held covalently with PLLA chains and therefore, the emission behavior of core TPE is sensitive to the conformational changes (structural changes) of PLLA. In the case of SSPLLA gels in DMF, PLLA crystallized into the  $\varepsilon$  form and the large TPE molecules are excluded out of the crystalline phase. These gels emitted cyan light at 20 °C because intramolecular rotations of covalently linked phenyl rings are restricted. Upon heating, over a broad temperature range (30 – 40 °C), a significant blue-shift in its fluorescence is observed. WAXS and DSC revealed that the structure of SSPLLA was transformed from the  $\varepsilon$  to  $\alpha$  form in this temperature range by the expulsion of solvents from the crystal lattice. The solvent expulsion and the segmental mobility of amorphous chains (above  $T_g$ ) induce the rotation of phenyl rings of TPE and are responsible for the blue shift of emission due to the change in the conjugation length of TPE. At higher temperatures, enhanced mobility of the amorphous chains leads to the complete quenching of emission due to the free rotation of phenyl rings of TPE. In the case of SSPLLA precipitate in DMA, PLLA was crystallized into the  $\alpha$  form at room temperature. The fluorescence emission decreased gradually with temperature and the blue shift was observed relatively at higher temperatures (above 50 °C) due to the vigorous mobility of amorphous chains. The combination of biocompatible and biodegradable polymers and AIE fluorophores is expected to open a new horizon in the biomedical area, such as medical and pharmaceutical fields and bio-imaging.

## 2.7. References

1. J. Mei, N. L. C. Leung, R. T. K. Kwok, J. W. Y. Lam and B. Z. Tang, *Chem. Rev.*, 2015, **115**, 11718-11940.
  2. Y. Yang, Q. Zhao, W. Feng and F. Li, *Chem. Rev.*, 2013, **113**, 192-270.
  3. J. Wu, W. Liu, J. Ge, H. Zhang and P. Wang, *Chem. Soc. Rev.*, 2011, **40**, 3483-3495.
  4. X. Feng, L. Liu, S. Wang and D. Zhu, *Chem. Soc. Rev.*, 2010, **39**, 2411-2419.
  5. F. Cicoira and C. Santato, *Adv. Funct. Mater.*, 2007, **17**, 3421-3434.
-

6. L. Tong, R. R. Gattass, J. B. Ashcom, S. He, J. Lou, M. Shen, I. Maxwell and E. Mazur, *Nature*, 2003, **426**, 816-819.
  7. J. Y. Zheng, Y. Yan, X. Wang, Y. S. Zhao, J. Huang and J. Yao, *J. Am. Chem. Soc.*, 2012, **134**, 2880-2883.
  8. M. Bredol, U. Kynast and C. Ronda, *Adv. Mater.*, 1991, **3**, 361-367.
  9. Y. Chen, A. J. H. Spiering, S. Karthikeyan, G. W. M. Peters, E. W. Meijer and R. P. Sijbesma, *Nat. Chem.*, 2012, **4**, 559-562.
  10. T. Jüstel, H. Nikol and C. Ronda, *Angew. Chem. Int. Ed.*, 1998, **37**, 3084-3103.
  11. S. S. Babu, V. K. Praveen and A. Ajayaghosh, *Chem. Rev.*, 2014, **114**, 1973-2129.
  12. A. P. de Silva, H. Q. N. Gunaratne, T. Gunnlaugsson, A. J. M. Huxley, C. P. McCoy, J. T. Rademacher and T. E. Rice, *Chem. Rev.*, 1997, **97**, 1515-1566.
  13. M. A. Baldo, D. F. O'Brien, Y. You, A. Shoustikov, S. Sibley, M. E. Thompson and S. R. Forrest, *Nature*, 1998, **395**, 151-154.
  14. J. B. Birks, *Photophysics of Aromatic Molecules*. Wiley: New York, 1970.
  15. T. M. Figueira-Duarte, P. G. Del Rosso, R. Trattnig, S. Sax, E. J. W. List and K. Müllen, *Adv. Mater.*, 2010, **22**, 990-993.
  16. S. W. Thomas, G. D. Joly and T. M. Swager, *Chem. Rev.*, 2007, **107**, 1339-1386.
  17. J. Mei, Y. Hong, J. W. Y. Lam, A. Qin, Y. Tang and B. Z. Tang, *Adv. Mater.*, 2014, **26**, 5429-5479.
  18. Y. Hong, J. W. Y. Lam and B. Z. Tang, *Chem. Commun.*, 2009, DOI: 10.1039/B904665H, 4332-4353.
  19. Y. Hong, J. W. Y. Lam and B. Z. Tang, *Chem. Soc. Rev.*, 2011, **40**, 5361-5388.
  20. R. Hu, N. L. C. Leung and B. Z. Tang, *Chem. Soc. Rev.*, 2014, **43**, 4494-4562.
  21. Q. Zeng, Z. Li, Y. Dong, C. a. Di, A. Qin, Y. Hong, L. Ji, Z. Zhu, C. K. W. Jim, G. Yu, Q. Li, Z. Li, Y. Liu, J. Qin and B. Z. Tang, *Chem. Commun.*, 2007, DOI: 10.1039/B613522F, 70-72.
  22. W. Zhao, C. Li, B. Liu, X. Wang, P. Li, Y. Wang, C. Wu, C. Yao, T. Tang, X. Liu and D. Cui, *Macromolecules*, 2014, **47**, 5586-5594.
  23. Y. Dong, J. W. Y. Lam, A. Qin, J. Liu, Z. Li, B. Z. Tang, J. Sun and H. S. Kwok, *Appl. Phys. Lett.*, 2007, **91**, 011111.
  24. A. Ajayaghosh and S. J. George, *J. Am. Chem. Soc.*, 2001, **123**, 5148-5149.
  25. Y. Jiang and N. Hadjichristidis, *Macromolecules*, 2019, **52**, 1955-1964.
  26. X.-H. Wang, N. Song, W. Hou, C.-Y. Wang, Y. Wang, J. Tang and Y.-W. Yang, *Adv. Mater.*, 2019, **31**, 1903962.
  27. Z. Zhang, P. Bilalis, H. Zhang, Y. Gnanou and N. Hadjichristidis, *Macromolecules*, 2017, **50**, 4217-4226.
  28. G. Das, R. Thirumalai, B. Vedhanarayanan, V. K. Praveen and A. Ajayaghosh, *Adv. Opt. Mater.*, 2020, **8**, 2000173.
  29. X. Qi, H. Li, J. W. Y. Lam, X. Yuan, J. Wei, B. Z. Tang and H. Zhang, *Adv. Mater.*, 2012, **24**, 4191-4195.
  30. G. Yu, S. Yin, Y. Liu, J. Chen, X. Xu, X. Sun, D. Ma, X. Zhan, Q. Peng, Z. Shuai, B. Tang, D. Zhu, W. Fang and Y. Luo, *J. Am. Chem. Soc.*, 2005, **127**, 6335-6346.
-

31. Q. Chen, D. Zhang, G. Zhang, X. Yang, Y. Feng, Q. Fan and D. Zhu, *Adv. Funct. Mater.*, 2010, **20**, 3244-3251.
  32. B.-K. An, J. Gierschner and S. Y. Park, *Acc. Chem. Res.*, 2012, **45**, 544-554.
  33. M. Martínez-Abadía, R. Giménez and M. B. Ros, *Adv. Mater.*, 2018, **30**, 1704161.
  34. R. Taniguchi, T. Yamada, K. Sada and K. Kokado, *Macromolecules*, 2014, **47**, 6382-6388.
  35. N. L. C. Leung, N. Xie, W. Yuan, Y. Liu, Q. Wu, Q. Peng, Q. Miao, J. W. Y. Lam and B. Z. Tang, *Chem. Eur. J.*, 2014, **20**, 15349-15353.
  36. J. Xu, W. Ji, C. Li, Y. Lv, Z. Qiu, L. Gao, E. Chen, J. W. Y. Lam, B. Tang and L. Jiang, *Adv. Opt. Mater.*, 2018, **6**, 1701149.
  37. Z. Qiu, X. Liu, J. W. Y. Lam and B. Z. Tang, *Macromol. Rapid Commun.*, 2019, **40**, 1800568.
  38. Y.-G. He, S.-Y. Shi, N. Liu, Y.-S. Ding, J. Yin and Z.-Q. Wu, *Macromolecules*, 2016, **49**, 48-58.
  39. X. Guan, D. Zhang, L. Meng, Y. Zhang, T. Jia, Q. Jin, Q. Wei, D. Lu and H. Ma, *Ind. Eng. Chem. Res.*, 2017, **56**, 680-686.
  40. J. Xue, W. Bai, H. Duan, J. Nie, B. Du, J. Z. Sun and B. Z. Tang, *Macromolecules*, 2018, **51**, 5762-5772.
  41. A. C. B. Rodrigues, J. Pina, W. Dong, M. Forster, U. Scherf and J. S. Seixas de Melo, *Macromolecules*, 2018, **51**, 8501-8512.
  42. Y.-D. Jiu, C.-F. Liu, J.-Y. Wang, W.-Y. Lai, Y. Jiang, W.-D. Xu, X.-W. Zhang and W. Huang, *Polym. Chem.*, 2015, **6**, 8019-8028.
  43. Y. Jiu, J. Wang, J. Yi, C.-F. Liu, X.-W. Zhang, W.-Y. Lai and W. Huang, *Polym. Chem.*, 2017, **8**, 851-859.
  44. C.-F. Liu, M. Sang, W.-Y. Lai, T. T. Lu, X. Liu and W. Huang, *Macromolecules*, 2018, **51**, 1325-1335.
  45. C.-F. Liu, Y. Jiu, J. Wang, J. Yi, X.-W. Zhang, W.-Y. Lai and W. Huang, *Macromolecules*, 2016, **49**, 2549-2558.
  46. W. Huang, M. Bender, K. Seehafer, I. Wacker, R. R. Schröder and U. H. F. Bunz, *Macromolecules*, 2018, **51**, 1345-1350.
  47. G. Liang, L.-T. Weng, J. W. Y. Lam, W. Qin and B. Z. Tang, *ACS Macro Lett*, 2014, **3**, 21-25.
  48. Z. Wang, S. Chen, J. W. Y. Lam, W. Qin, R. T. K. Kwok, N. Xie, Q. Hu and B. Z. Tang, *J. Am. Chem. Soc.*, 2013, **135**, 8238-8245.
  49. H. Wang, G. Liu, H. Gao and Y. Wang, *Polym. Chem.*, 2015, **6**, 4715-4718.
  50. S. Sasaki and T. Asakura, *Macromolecules*, 2003, **36**, 8385-8390.
  51. J. Zhang, Y. Duan, H. Sato, H. Tsuji, I. Noda, S. Yan and Y. Ozaki, *Macromolecules*, 2005, **38**, 8012-8021.
  52. H. Marubayashi, S. Akaishi, S. Akasaka, S. Asai and M. Sumita, *Macromolecules*, 2008, **41**, 9192-9203.
  53. H. Marubayashi, S. Asai and M. Sumita, *Macromolecules*, 2012, **45**, 1384-1397.
  54. D. Sawai, K. Takahashi, A. Sasashige, T. Kanamoto and S.-H. Hyon, *Macromolecules*, 2003, **36**, 3601-3605.
-

- 
55. P. Shaiju, N. S. Murthy and E. B. Gowd, *Macromolecules*, 2016, **49**, 224-233.
  56. S. Nagarajan and E. B. Gowd, *Macromolecules*, 2017, **50**, 5261-5270.
  57. T.-S. Hsiao, P.-C. Huang, L.-Y. Lin, D.-J. Yang and J.-L. Hong, *Polym. Chem.*, 2015, **6**, 2264-2273.
  58. S. K. Nisha and S. K. Asha, *ACS Appl. Mater. Interfaces*, 2014, **6**, 12457-12466.
  59. S. K. Nisha and S. K. Asha, *J. Mater. Chem. C*, 2014, **2**, 2051-2060.
  60. M.-C. Li, H.-F. Wang, C.-H. Chiang, Y.-D. Lee and R.-M. Ho, *Angew. Chem. Int. Ed.*, 2014, **53**, 4450-4455.
  61. K. Kan, M. Fujiki, M. Akashi and H. Ajiro, *ACS Macro Lett*, 2016, **5**, 1014-1018.
  62. N. M. Praveena, S. Nagarajan and E. B. Gowd, *CrystEngComm*, 2021, **23**, 2122-2132.
  63. Y. Sakamoto and H. Tsuji, *Macromolecular Chemistry and Physics*, 2013, **214**, 776-786.
  64. K. Wasanasuk, K. Tashiro, M. Hanesaka, T. Ohhara, K. Kurihara, R. Kuroki, T. Tamada, T. Ozeki and T. Kanamoto, *Macromolecules*, 2011, **44**, 6441-6452.
  65. Y. Sakamoto and H. Tsuji, *Polymer*, 2013, **54**, 2422-2434.
  66. Y. Matsuda, A. Fukatsu, Y. Wang, K. Miyamoto, J. W. Mays and S. Tasaka, *Polymer*, 2014, **55**, 4369-4378.
  67. R. W. Newberry and R. T. Raines, *Chem. Commun.*, 2013, **49**, 7699-7701.
  68. T. Mori and Y. Inoue, *Appl. Phys. Lett. A*, 2005, **109**, 2728-2740.
  69. H.-F. Wang, C.-H. Chiang, W.-C. Hsu, T. Wen, W.-T. Chuang, B. Lotz, M.-C. Li and R.-M. Ho, *Macromolecules*, 2017, **50**, 5466-5475.
  70. N. Berova, L. D. Bari and G. Pescitelli, *Chem. Soc. Rev.*, 2007, **36**, 914-931.
  71. A. Marini, A. Muñoz-Losa, A. Biancardi and B. Mennucci, *J. Phys. Chem. B*, 2010, **114**, 17128-17135.
  72. J. Kim, S. Cho and B.-K. Cho, *Chem. Eur. J.*, 2014, **20**, 12734-12739.
  73. X. Zhang, Z. Chi, H. Li, B. Xu, X. Li, W. Zhou, S. Liu, Y. Zhang and J. Xu, *Chem. Asian J.*, 2011, **6**, 808-811.
  74. M. M. Joseph, A. N. Ramya, V. M. Vijayan, J. B. Nair, B. T. Bastian, R. K. Pillai, S. T. Therakathinal and K. K. Maiti, *Small*, 2020, **16**, 2003309.
-

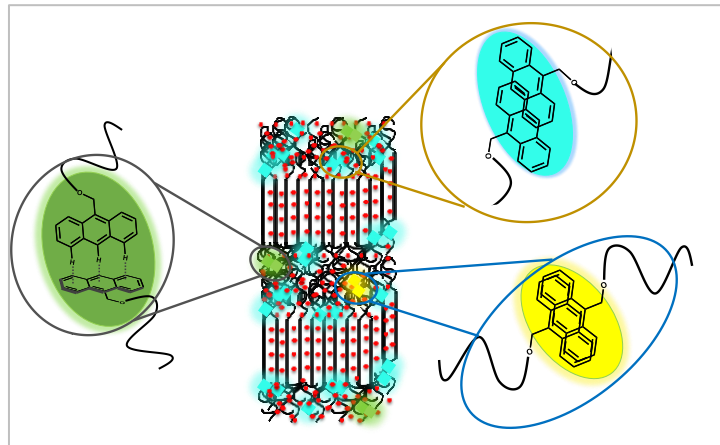
---

---

# Polymer Crystallization Enabled Excimer Emission in Anthracene-Appended Poly(L-lactide)s

---

---



### 3.1. Abstract

*The design and development of solid-state excimer-emitters bear great potential for attaining efficient solid-state luminescent materials. In this study, we have synthesized anthracene-appended poly(L-lactide)s (AAPs) to regulate the arrangement of anthracene moieties by controlling the crystallization and polymorphic form of covalently linked poly(L-lactide) (PLLA). In the high molecular weight AAP, the fluorescence intensity mainly arises from the monomeric anthracene moieties, whereas in the low molecular weight AAP, the excimer emission was observed depending on the structure and morphology of covalently-linked PLLA. The monomeric emission is predominantly observed in amorphous polymer due to the molecular level dispersion of covalently-linked anthracene moieties throughout the polymer matrix. When the polymer was crystallized under different conditions, covalently-linked anthracene moieties were excluded from polymer crystals or crystalline lamellae and are located on the surface or at the interface, which is advantageous for regulating the geometry of anthracene moieties. In the case of single crystals of PLLA, covalently-linked anthracene moieties assemble on the surface and emit mainly in their monomeric state due to the lack of  $\pi$ -stacking. In the melt-crystallized sample ( $\alpha$  form), covalently-linked anthracene moieties reside at the interface of crystalline and amorphous domains by either dipolar interactions or  $\pi$ -stacking and emit fluorescence arising from anthracene excimers and monomers. In the gel state ( $\epsilon$  form), only the excimer emission was observed due to the effective interactions between the anthracene moieties in the presence of excess solvent in the amorphous domains. In this way, polymer crystallization played a significant role in determining the arrangement of covalently-linked anthracene moieties in AAP. This study reveals the role of polymer crystallization on the excimer evolution in fluorophore-appended semicrystalline polymers and provides*

---

*new insight into the design and development of fluorophore-appended polymers for optoelectronic devices.*

### **3.2. Introduction**

The design and development of organic fluorophores that exhibits strong fluorescence properties in the solid state have attracted attention because of their potential applications in organic light-emitting diodes, photoelectronic devices, molecular sensors and bio-imaging.<sup>1-12</sup> The fluorescent properties of organic fluorophores have been explored widely in solution, but they lose the fluorescent property in the solid state because the intermolecular interactions influence the excited state in many ways.<sup>3, 13-18</sup> Many strategies have been developed for improving the solid-state emission of organic fluorophores in recent years. Among these, tuning of molecular packing and arrangements of fluorophores in the solid state attracts the attention of researchers because the packing arrangements strongly influence the solid-state fluorescence properties.<sup>19-21</sup> Various approaches have been developed to enhance the fluorescent properties of organic fluorophores by tuning the molecular arrangements including polymorphism, the introduction of substituents, the inclusion of guests, and the covalent incorporation of fluorophores into polymer chains at the molecular level.<sup>2, 18-20, 22-30</sup> Among these, fluorophore-appended polymers have recently become promising candidates from the application point of view because of their unparalleled advantages like processability, mechanical stability, and thermal stability. The fundamental understanding of the structure-property relationships of fluorophore-appended polymers at the molecular level is essential for optimizing the molecular arrangements of fluorophores and their fluorescent properties. So far, tuning the molecular arrangements of fluorophores in a well-ordered manner remains challenging.

Reported studies revealed that the crystallization of fluorophore-appended polymers plays a vital role in tuning the emission properties of fluorophores.<sup>29-33</sup>

---

Crystallization of polymers is associated with the hierarchical organization of polymer chains in different length scales, and it was proven to be an effective way to tune the properties of semicrystalline polymers.<sup>34</sup> The long chain nature of polymers never allows the chains to fully crystallize, where the intricate amorphous domains are accommodated in a crystalline material (termed semicrystalline). Polymers are known to form single crystals (chain-folded metastable state) similar to small molecules when crystallized from a dilute solution under appropriate conditions.<sup>35-37</sup> On the other hand, concentrated solutions of semicrystalline polymers resulted in thermoreversible gels, where physical crosslinks of the three-dimensional polymer networks are formed by tiny crystallites.<sup>38, 39</sup> The gel morphology is similar to bulk semicrystalline morphology, where the amorphous regions are filled with vast amounts of solvents. Furthermore, semicrystalline polymers are known to exhibit polymorphism and various crystalline phases show distinct packing structures and properties.<sup>40, 41</sup> The crystallization of the fluorophore-appended semicrystalline polymer in different forms (amorphous, semicrystalline, single crystal, and gel) offers a new opportunity for tuning the molecular arrangements of fluorophores. Although a few studies appeared on the polymer crystallization-induced emission properties of fluorophore-embedded polymers, polymer crystallization-enabled excimer emission in aromatic fluorophore-appended polymers is rarely studied to our knowledge. The fluorescence of an aromatic fluorophore (pyrene) in the solution state due to excimer formation was first reported by Förster and Kasper.<sup>42, 43</sup> Subsequently, excimer formation was widely investigated using diverse types of aromatic fluorophores both in the solution and solid states.<sup>15, 44-49</sup> Anthracene is a classical fluorophore and attracted the attention of researchers as it exhibits different photophysical properties in dilute solutions or polymer matrices (exists as a monomeric state) and close  $\pi$ - $\pi$  stacking states (in concentrated solutions, crystalline, and liquid crystalline states).<sup>15, 44, 46, 49-55</sup> The excimer emission of

---



anthracene is strongly dependent on the interplanar distance and degree of overlap of the  $\pi$ - $\pi$  dimer. Reported studies have suggested that the photophysical properties of anthracene can be efficiently modulated by tuning the degree of overlap of the  $\pi$ - $\pi$  dimers.<sup>15, 44, 46, 50, 53, 56-63</sup> However, it is difficult to understand the dimer geometry experimentally, which is a bottleneck for understanding excimers and their applications. Further, anthracene and its derivatives have the intrinsic issue of photodimerization.<sup>64</sup> To overcome this issue and to obtain intermolecular  $\pi$ - $\pi$  excimers in the solid state, various approaches have been developed, including incorporating anthracene into nanocapsules, polymers, and the attachment of anthracene to various derivatives.<sup>28, 44, 48, 62, 65</sup> Although a few studies appeared on the anthracene-appended polymeric systems, polymer crystallization-enabled excimer emission is unprecedented. Polymer crystallization can significantly change intermolecular interactions of fluorophores and effectively regulate their aggregation, which is suitable for investigating excimer formation under different conditions. Poly(L-lactide) (PLLA) is a popular synthetic biodegradable polymer and it is produced from renewable resources. Depending upon the conditions, PLLA crystallizes into different crystalline forms ( $\alpha$ ,  $\alpha'(\delta)$ ,  $\alpha'$ ,  $\beta$ ,  $\gamma$ , and  $\varepsilon$ ).<sup>66-71</sup> The PLLA chain adopts an intrinsic left-handed helical conformation in all the crystalline states and this helical chain conformation was found to influence the fluorescence properties of chromophore-embedded PLLA.

In this chapter, we synthesized two different molecular weight anthracene-appended PLLAs by ring-opening polymerization of L-lactide using 9-anthracenemethanol as a macroinitiator. Detailed experimental studies reveal that not only the molecular weight of the polymer but also the crystallization of polymers dictated the photophysical properties of the fluorescent hybrid systems. When these anthracene-appended polymers are allowed to crystallize under different conditions, anthracene molecules were excluded from polymer crystals or lamellae and are located close to one another, which is advantageous for

---

regulating the geometry of anthracene moieties. Furthermore, the molecular arrangement of anthracene moieties can be modulated by changing the structure and morphology of anthracene-appended PLLA in different forms (amorphous, semicrystalline, single crystals, and gels). In the case of low molecular weight polymers, it is possible to determine a reasonable arrangement that allows excimer emission in the semicrystalline and gel forms. The results reported herein elucidate factors involved in the modulation of the photophysical properties and provides new insight into the design and development of biodegradable and biocompatible polymeric fluorescent materials.

### **3.3. Experimental Section**

#### **3.3.1. Materials**

L-lactide, Sn(Oct)<sub>2</sub>, 9-anthracenemethanol, chloroform, toluene (anhydrous, 99.8%) and hexane were purchased from Sigma-Aldrich. Ethyl acetate, methanol and N, N-dimethylformamide (DMF) were purchased from Merck Chemicals and isopropyl alcohol (iPrOH) was purchased from Thermo Fisher Scientific. Before polymerization, the L-lactide monomer was recrystallized with ethyl acetate. The solvents used were carefully dried before use.

#### **3.3.2. Synthesis of Anthracene-Appended PLLA- 1 (AAP-1)**

AAP-1 was synthesized by ring-opening polymerization of L-lactide. Typically, for the synthesis of AAP-1, Sn(Oct)<sub>2</sub> (30  $\mu$ L) was added dropwise to a stirred toluene (15 mL) solution of a mixture of L-lactide (3 g) and 9-anthracenemethanol (50 mg) at 25 °C. Then, the solution was stirred under vacuum conditions for 1 h at room temperature to remove moisture and the reaction was carried out at 120 °C under an inert atmosphere. After 1 h, the reaction mixture was dissolved in chloroform and then slowly poured into methanol with stirring to obtain a solid precipitate, which was reprecipitated from

---

chloroform/methanol (1/10 v/v). The resulting precipitate was collected and dried at 40 °C for 12 h under reduced pressure. The chemical structure of AAP-1 was confirmed by <sup>1</sup>H NMR. The number-average molecular weight of AAP-1 was 2944 g mol<sup>-1</sup> from NMR and dispersity (Đ) of 1.25 was estimated by GPC.

### **3.3.3. Synthesis of Anthracene-Appended PLLA- 2 (AAP-2)**

AAP-2 was synthesized using the same procedure as mentioned for AAP-1 other than the amounts of 9-anthracenemethanol (30 mg), Sn(Oct)<sub>2</sub> (30 μL), reaction time and temperature (140 °C). The chemical structure of AAP-2 was confirmed by <sup>1</sup>H NMR. The number-average molecular weight of AAP-2 was 5320 g mol<sup>-1</sup> from NMR and dispersity (Đ) of 1.18 was estimated by GPC.

### **3.3.4. Sample Preparation**

#### **3.3.4.1. Preparation of Semicrystalline Sample of AAP-1**

AAP-1 was melted at 200 °C in a DSC pan and kept for 2 min to erase the thermal history. Then the sample was cooled rapidly (50 °C/min) to the required crystallization temperature and the sample was allowed to crystallize at that temperature.

#### **3.3.4.2. Preparation of Single Crystals of AAP-1**

AAP-1 (1mg/ml) was dissolved in iso-propyl alcohol by heating at 80 °C for about 2 min and the clear solution was gradually cooled to room temperature and kept for equilibration.

#### **3.3.4.3. Preparation of AAP-1 Gel**

AAP-1 (10 wt%) was dissolved in DMF by heating at 120 °C for about 2-3 min and the clear solution was gradually cooled to room temperature and kept overnight in a freezer

---

at -4 °C for gelation. Gel formation was confirmed by the failure of the solvent to flow while inverting the container.

### 3.4. Characterization

The molecular weight and dispersity ( $\mathcal{D}$ ) of the synthesized polymers were determined by gel permeation chromatography (GPC) using an Agilent Technologies-1260 instrument with RI detector, which is equipped with a PL-gel 20  $\mu\text{m}$  mixed bed column operated at 30 °C with THF as solvent (flow rate of 1 mL/min). Narrow disperse polystyrene standards were used for the calibration.  $^1\text{H}$  NMR spectra were recorded on a 500 MHz Bruker Advance DPX spectrometer using tetramethylsilane (TMS) as an internal reference. NMR samples were analyzed in  $\text{CDCl}_3$ . Differential scanning calorimetry (DSC) thermograms of polymers were recorded using a thermal analyzer (TA instrument Q2000) at a heating and cooling rate of 10 °C/min under the  $\text{N}_2$  atmosphere. Semicrystalline samples for UV and PL measurements were prepared using DSC. Amorphous samples were prepared by sudden quenching of melt in liquid nitrogen. Circular dichroism (CD) spectra were recorded on a JASCO-J- 810 spectropolarimeter with a Peltier thermostatic controller using a quartz cell of 1.0 cm path length and the sample concentration was fixed at 1 mg/ml for polymer in chloroform/hexane mixture. UV-vis absorption spectra were collected on a SHIMADZU UV-2600 spectrophotometer, and samples were analyzed at room temperature. Photoluminescence and excitation spectra were recorded on SPEX-Fluorolog-3 FL3-221 spectrofluorimeter at room temperature. Variable temperature photoluminescence spectra were recorded on the Spex-Fluoromax FL22 spectrofluorimeter with a double grating 0.22 m Spex 1680 monochromator, a 450 W Xe lamp as the excitation source, and a Hamamatsu R928P photomultiplier tube detector. All these measurements were carried out using a 1 cm or 1 mm quartz cuvette. The morphology of single crystals of polymers was investigated using JEOL 2010 transmission electron microscope (TEM)

---

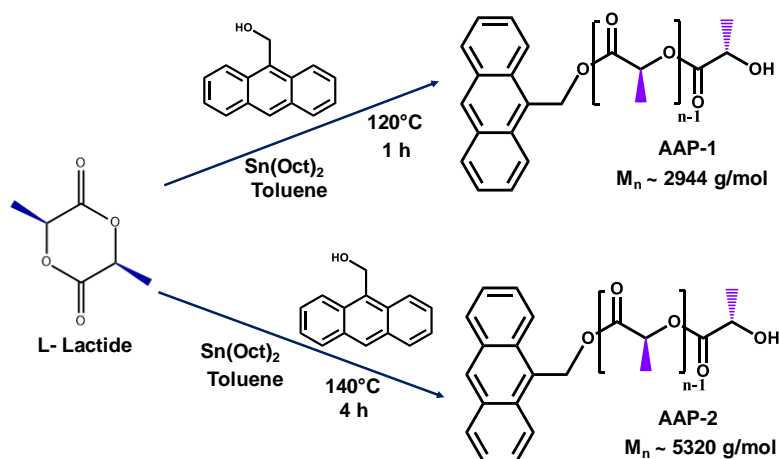
operating at 200 kV. For TEM measurements, the colloidal suspension of polymer in iPrOH was drop-casted on a carbon-coated copper grid and dried under dust free atmosphere. AFM images were probed in tapping mode using Multimode SPM (Bruker Nanoscope V). Antimony doped silicon cantilever with a resonant frequency of 300 kHz and spring constant of 40 Nm<sup>-1</sup> was used. Samples were prepared by drop-casting the colloidal suspension of AAP-1 in iPrOH on a cleaned silicon wafer surface and dried in the air for 2 days in a closed petri dish at room temperature. Wide-angle X-ray diffraction (WAXD) patterns were measured using a XEUSS SAXS/WAXS system (from Xenocs) operated at 50 kV and 0.60 mA using Cu K $\alpha$  radiation (wavelength,  $\lambda = 1.54 \text{ \AA}$ ). The fiber diffraction patterns were recorded on a Mar 345 image plate system (detector) and the data was processed using the Fit2D program. Silver behenate was used as a calibration standard for the precise measurement of the sample-to-detector distance. The variable temperature measurements of polymer gel were carried out using a Linkam THMS 600 hot stage fitted to the X-ray system.

### **3.5. Results and Discussion**

#### **3.5.1. Structural and Thermal Properties of Anthracene-Appended PLLAs**

Anthracene is a common fluorophore used for assembling an excimer. To understand the formation mechanism of excimers, anthracene-appended PLLA (AAP-1) was synthesized by ring-opening polymerization of L-lactide using 9-anthracenemethanol as the macroinitiator and tin(II) 2-ethylhexanoate (Sn(Oct)<sub>2</sub>) as the catalyst (Scheme 3.1).

---



**Scheme 3.1.** Synthesis of AAP-1 and AAP-2 with different PLLA chain lengths.

The chemical structure of AAP-1 was confirmed by <sup>1</sup>H NMR in CDCl<sub>3</sub> (Figure 3.1). As seen in Figure 3.1, the chemical shifts of PLLA were observed at 1.58 and 5.16 ppm. Chemical shift at 4.37 ppm corresponds to CH protons of the PLLA chain end. Further, the incorporation of anthracene molecules at the chain end was confirmed by the presence of peaks at 6.1 and 6.3 ppm which are corresponding to benzyl protons of anthracene, and chemical shift between 7.4 to 8.6 ppm corresponding to aromatic protons of anthracene molecule. The number average molecular weight ( $M_n$ ) of AAP-1 was estimated to be  $\approx 2944 \text{ g mol}^{-1}$  by <sup>1</sup>H NMR (integrating the anthracene protons with the PLLA backbone protons)<sup>72</sup> and  $\approx 3354 \text{ g mol}^{-1}$  by gel permeation chromatography (GPC) with molecular weight distribution ( $D$ ) of  $\approx 1.25$  (Figure 3.2). To further clarify the influence of the chain length of PLLA on the excimer formation, a higher molecular weight polymer (AAP-2) was prepared following a similar technique by changing the reaction conditions as shown in Scheme 3.1 ( $M_{n, NMR} \approx 5320 \text{ g mol}^{-1}$ , and  $M_{n, GPC} \approx 5482 \text{ g mol}^{-1}$  and  $D \approx 1.18$ ).

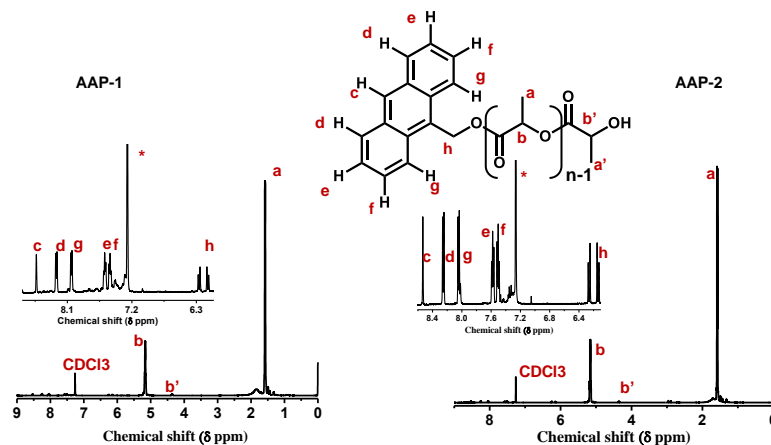


Figure 3.1.  $^1\text{H}$  NMR spectra of AAP-1 and AAP-2.

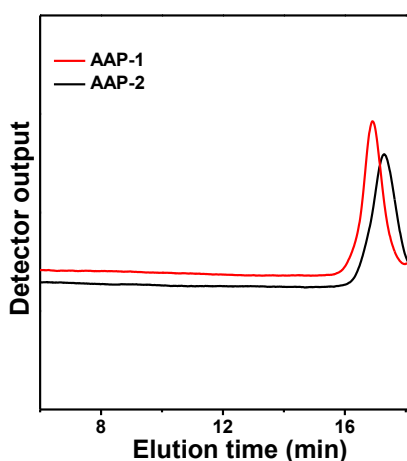
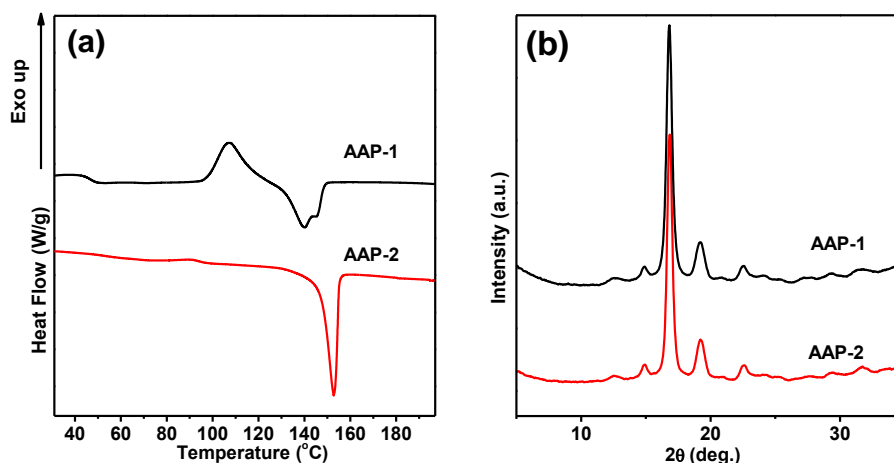


Figure 3.2. GPC traces of AAP-1 and AAP-2 polymers in THF.

DSC thermograms of AAP-1 and AAP-2 showed melting points of PLLA  $\approx 140$  °C and  $\approx 153$  °C, respectively. The difference in the melting points further confirmed the difference in the molecular weights of these polymers (Figure 3.3a). The wide-angle X-ray diffraction (WAXD) patterns (Figure 3.3b) of as-synthesized polymers show X-ray reflections corresponding to the  $\alpha$  form of PLLA at  $2\theta = 14.8^\circ$  (010),  $16.7^\circ$  (110/200),  $19.0^\circ$  (203),  $20.7^\circ$  (204),  $22.3^\circ$  (015), and  $27.3^\circ$  (207) irrespective of the molecular weight.<sup>66</sup> It was reported that due to the presence of an intrinsic chiral center along the main chain, left-handed  $10_7$  helical chains of PLLA are packed into the orthorhombic unit cell.<sup>66, 73</sup>



**Figure 3.3.** (a) DSC thermograms (heating at a rate of 10 °C/min.) and (b) WAXD patterns of AAP-1 and AAP-2 polymers.

### 3.5.2. Impact of Polymer Chain Length on Anthracene Excimer Formation

Further, we compared the optical properties of AAP-1 and AAP-2 in the solid state as shown in Figure 3.4. The UV-Vis absorption spectra of AAP-1 and AAP-2 reveal a structured absorption band in the range of 300 to 450 nm in the solid state (Figure 3.4a), which is assigned to the  $S_0 \rightarrow S_1$  absorption ( $\pi$ - $\pi^*$  transition) located on the anthracene. The absorption spectrum of AAP-2 (Figure 3.4a) shows a similar spectrum to the anthracene solution in a good solvent, indicating that the anthracene molecule exists in the monomeric state (non-aggregated state). On the other hand, an additional absorption band with  $\lambda_{\max} \approx 410$  nm was observed in the case of AAP-1. As reported in the literature, the appearance of a new absorption band in the long-wavelength region suggests the formation of aggregates.<sup>65, 74</sup> These results suggest that  $\pi$ - $\pi$  stacking of anthracene moieties was dependent on the PLLA chain length and the excimer-like emission can be observed in the low molecular weight polymer (AAP-1) in the solid state.



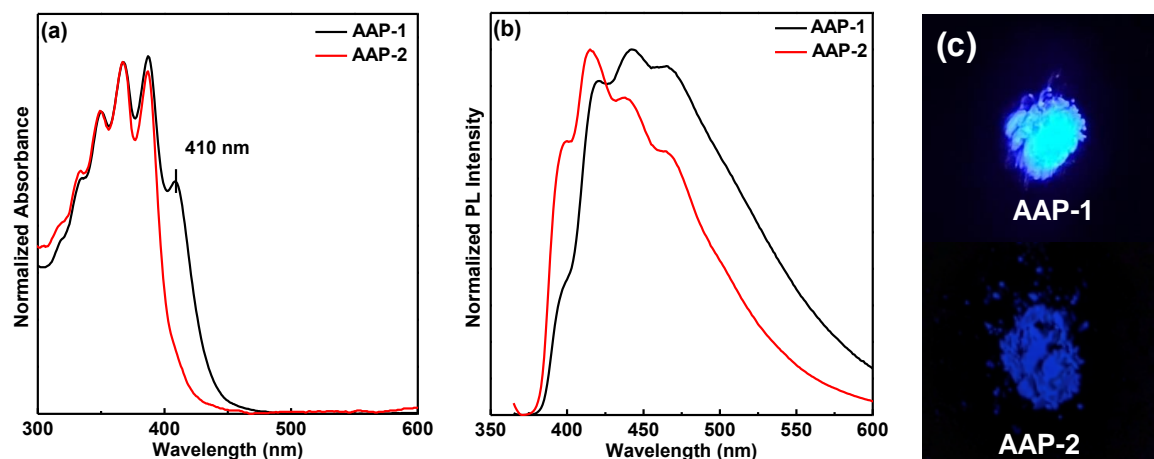


**Figure 3.4.** (a) Normalized absorption, (b) emission spectra ( $\lambda_{ex} \approx 355$  nm), and (c) photographs of AAP-1 and AAP-2 polymers in the solid state under UV illumination (solvent vapor crystallized samples).

The emission spectra of AAP-1 and AAP-2 in the solid state differ, with a vibronic emission from 370 to 600 nm (Figure 3.4b). AAP-2 exhibits a deep blue emission ( $\lambda_{max} \approx 415$  nm) in the solid state and resembles the 9-anthracenemethanol structure in the solution state (Figure 3.5a). This observation further confirms that the emission of AAP-2 originates from the monomeric form of the anthracene molecules. On the other hand, the emission spectrum of AAP-1 is broadened and red-shifted, emitting cyan color ( $\lambda_{max} \approx 442$  nm), which is characteristic of the excimer formation.<sup>15, 57, 62, 63, 65, 74</sup> All these pieces of evidence clarify that the chain length of PLLA is critical in determining the emission behavior of anthracene-appended PLLAs. In higher molecular weight polymers, the emission is dominated by the monomeric state as long polymer chains limit the aggregation of anthracene units. Whereas, in the case of low molecular weight polymers, shorter PLLA chains allow the intermolecular interactions ( $\pi$ - $\pi$  stacking) between the anthracene units to facilitate the excimer formation on excitation. To further investigate the influence of polymer crystallization on excimer formation, AAP-1 is exclusively used because of the possibility of excimer formation.

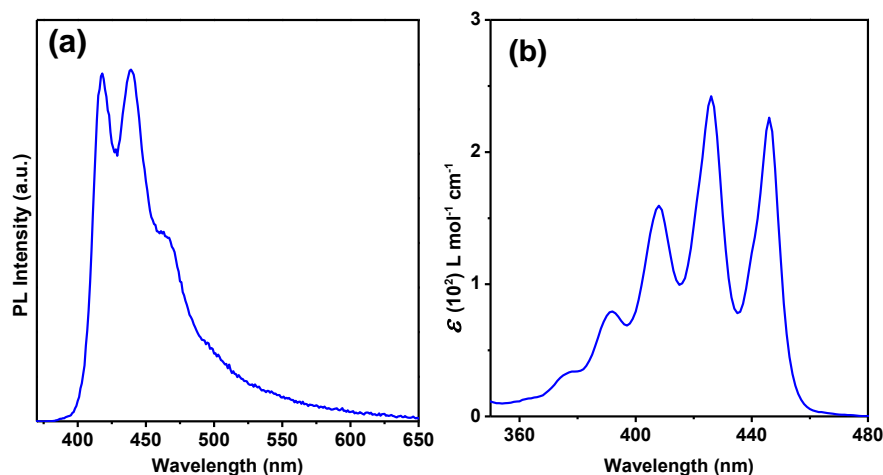


**Figure 3.5.** (a) Emission and (b) absorption spectra of 9-anthracenemethanol in chloroform.

### 3.5.3. Impact of Polymer Chain Packing on Anthracene Emission

We have investigated the optical properties of AAP-1 in chloroform solution and isopropanol (iPrOH) solution. Chloroform is a good solvent for AAP-1 and dissolves the polymer completely to form a clear solution at room temperature. The absorption spectrum of AAP-1 in chloroform (Figure 3.6a) shows a spectrum similar to the anthracene solution (Figure 3.5b), where the anthracene units are dispersed in the monomer state. No peak at 410 nm was observed indicating the absence of excimers. AAP-1 in chloroform shows dark blue emission and the emission spectrum shows several emission bands (Figure 3.6b) assignable to the vibrational structures of the anthracene (0-0, 0-1, 0-2, 0-3, and 0-4) at 396, 416, 440, 468 and 500 nm with an emission maximum at 416 nm.<sup>75</sup> As chloroform is a good solvent for PLLA, polymer chains adopt random coil conformation with less possibility for the aggregation of anthracene units and the emission spectrum matches well with the monomeric emission of anthracene units. On the other hand, AAP-1 is not readily soluble in iPrOH at room temperature. The AAP-1 in iPrOH was heated for 2 min at  $\approx 80$  °C and allowed to cool to room temperature gradually. As reported earlier, PLLA crystallized into well-ordered single crystals (diamond-shaped platelets) in iPrOH as

evident from transmission electron microscopy (TEM) and atomic force microscopy (AFM) (Figures 3.6c and 3.6d).<sup>76</sup> It has to be noted that the attachment of larger anthracene moieties did not influence the crystallization of PLLA into single crystals and they hang on the surface of single crystals (Figure 3.6e). The obtained single crystals show excellent colloidal stability even after aging for a few days. TEM images show thinner crystals where anthracene molecules reside on the surface of the crystals as shown in the schematic representation (Figure 3.6e). AFM image shows a relatively large-sized crystal because the solution was aged for a few days before casting on a silicon wafer. The ATR-FTIR spectrum (the presence of  $921\text{ cm}^{-1}$  band assigned to  $\nu(\text{C}-\text{C}) + r(\text{CH}_3)$  vibrational modes) and the WAXD pattern (Figure 3.7) of these suspensions confirm the presence of the  $\alpha$  crystals (orthorhombic unit cells).<sup>67</sup> The UV/Vis spectrum of AAP-1 in iPrOH (Figure 3.6a) exhibits an absorption spectrum almost similar to the spectrum of AAP-1 in chloroform solution in the range of 320 – 400 nm, however, a broad Mie scattering was observed at a higher wavelength in iPrOH due to the existence of nanometer-sized single crystals in the suspensions. A slight blue shift of  $\approx 2\text{ nm}$  was observed in the case of the iPrOH solution possibly due to the formation of a few dimers (excimers) on the surface of single crystals as depicted in Figure 3.6e, compared to the chloroform solution. AAP-1 single crystals in iPrOH also show a dark blue emission and the emission spectrum is slightly broader than the chloroform solution with an emission maximum of 414 nm. This suggests that the anthracene units that are terminated at the chain end of PLLA remain in the monomeric state on the surface of the single crystals with negligible excimers due to the  $\pi$ - $\pi$  interactions between AAP-1 crystals as seen in the AFM image. Rajak et al. demonstrated the possibility of assembly and disassembly of PLLA 2D crystals in pyrene-appended PLLA with respect to the temperature and also demonstrated the excimer formation in the pyrene-appended PLLA system.<sup>76</sup>

---

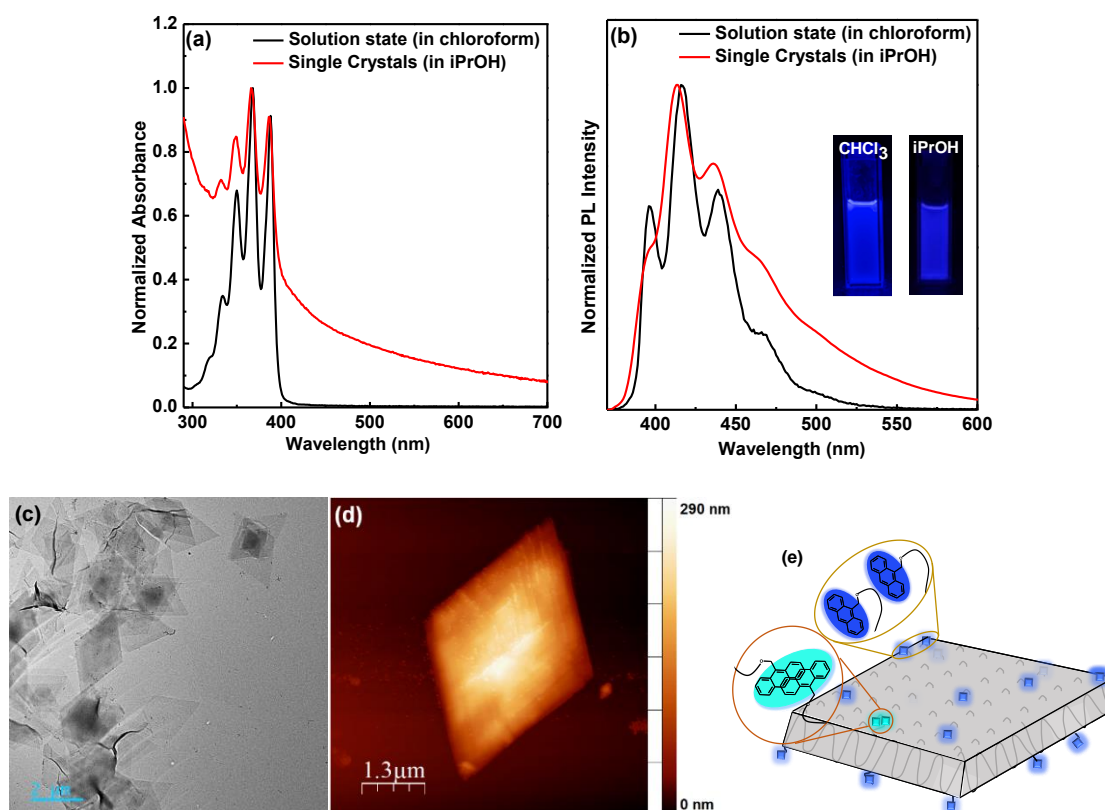


**Figure 3.6.** (a) Normalized absorption and (b) emission spectra ( $\lambda_{ex} \approx 355$  nm) of AAP-1 in chloroform and *iPrOH* (inset shows photographs of AAP-1 in chloroform and *iPrOH* solution under UV illumination). (c) TEM and (d) AFM images of single crystals of AAP-1 in *iPrOH*. (e) Schematic illustration of anthracene moieties arrangement on the surface of the single crystal and emission behavior of AAP-1.

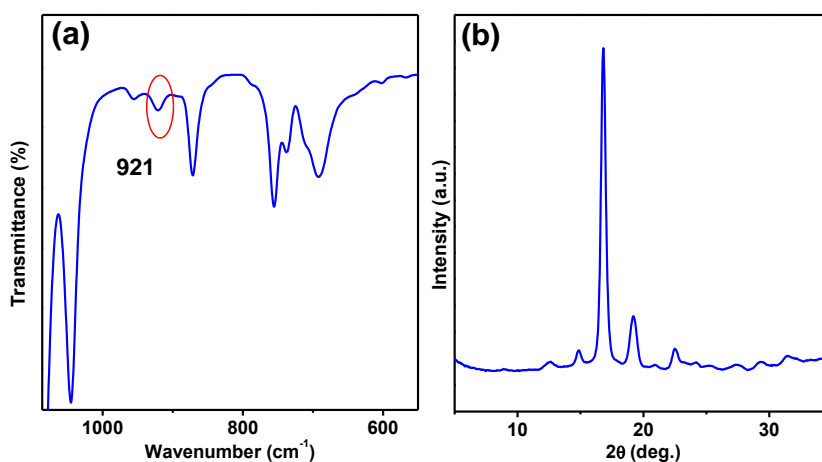


**Figure 3.7.** (a) ATR-FTIR spectrum and (b) WAXD pattern of AAP-1 suspensions in *iPrOH*.

### 3.5.4. Influence of Crystallization of AAP-1 on Anthracene Excimer Emission

Depending on the cooling rate of the polymer melt, polymers can arrange into semicrystalline or amorphous states. This section discusses the excimer formation in the anthracene-appended low molecular weight polymer (AAP-1) in semicrystalline and amorphous states. The amorphous film was prepared by melting and sudden quenching of AAP-1 in liquid nitrogen (Figure 3.8a). The absorption spectrum of melt-quenched amorphous AAP-1 film (Figure 3.8b) shows a broad absorption band. At the same time, its end absorption wavelength is longer than that in chloroform solution because of the organization of anthracene moieties in the amorphous phase. It has to be noted that the absorption maximum was observed at 396 nm and a weak shoulder is noticed at 416 nm. These results indicate that the anthracene moieties are mainly in the monomeric state in the amorphous films with a few excimers. The emission spectrum of the amorphous film preserves the entire vibrational structure that is assigned to the monomeric emission peak at 443 nm. In addition to this, an excimer emission peak appeared as a shoulder at 465 nm (Figure 3.8c). In the amorphous films, the polymer chains are randomly organized where the terminated anthracene moieties are dispersed throughout the polymer matrix with less possibility of agglomeration to form excimers as depicted in the schematic representation (Figure 3.8d). The excimer emission to monomer emission intensity ratio suggested that the excimer content is more in amorphous films compared to the single crystals of AAP-1 in *i*PrOH as discussed in the preceding section. On the other hand, when the polymer melt was allowed to cool slowly, PLLA crystallizes into the  $\alpha$  form. The WAXD pattern of the AAP-1 shows well-defined X-ray reflections characteristic of the ordered  $\alpha$  form at  $2\theta = 14.8^\circ$  (010),  $16.7^\circ$  (110/200),  $19.0^\circ$  (203),  $20.7^\circ$  (204),  $22.3^\circ$  (015), and  $27.3^\circ$  (207) (Figure 3.8a).<sup>66</sup> The WAXD pattern revealed that the polymer is partially crystalline (semicrystalline) with a degree of crystallinity of  $\approx 40\%$ . A clearly different absorption

---

spectrum was observed for the semicrystalline AAP-1 with the absorption maximum at 421 nm compared to the amorphous film. It is obvious that the absorbance corresponding to the anthracene monomer is reduced drastically compared to the amorphous film. It has been reported that the absorption at the long-wavelength region is due to the formation of excimers.

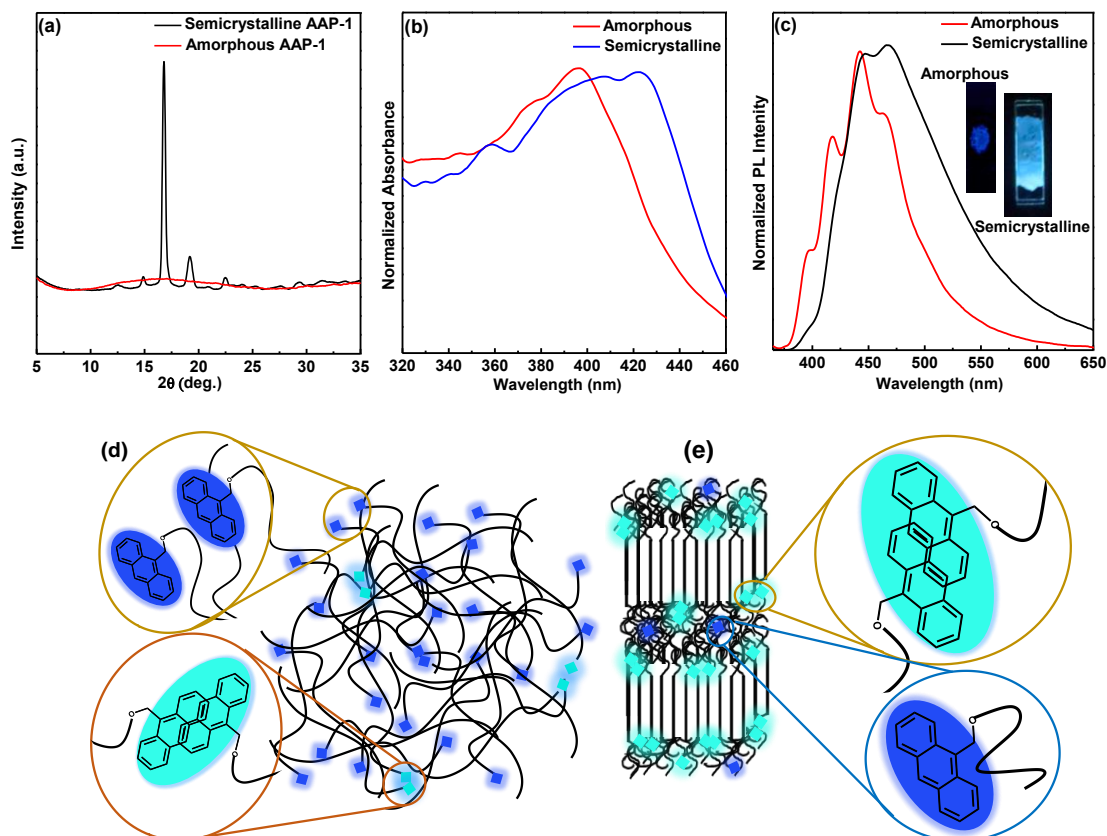


**Figure 3.8.** (a) WAXD patterns, (b) normalized absorption and (c) emission spectra ( $\lambda_{ex} \approx 355$  nm) of AAP-1 in amorphous and semicrystalline states (inset of (c) shows photographs of AAP-1 in amorphous and semicrystalline states under UV illumination). Schematic illustration of anthracene moieties arrangement and emission behavior in the (d) amorphous AAP-1 and (e) semicrystalline states.

The emission spectrum of the semicrystalline film shows a broadened and structureless spectrum with an emission maximum at 467 nm (cyan emission), which is the characteristic emission of excimers.<sup>53, 65</sup> A shoulder emission peak corresponding to the

monomer emission (blue emission) is also observed in semicrystalline films. Compared to amorphous films and single crystals, the emission spectrum of the semicrystalline film shifted to longer wavelengths resulting in a cyan emission (mix of blue and cyan) in the solid state. This supports that upon the crystallization of the polymer, the terminal anthracene molecules are excluded from the crystalline lamellae and occupy the interface of the crystalline and amorphous domains as shown schematically in Figure 3.8e. It is known that a decent overlap of anthracene moieties is essential for excimer formation. The rejection of anthracene moieties into the amorphous phase upon the crystallization of PLLA allows the  $\pi$ - $\pi$  interactions that lead to the bathochromic shift of the emission wavelength. It has to be noted that only a few reports appeared on the excimer formation of anthracene derivatives in the solid state.<sup>15, 49, 57, 62, 63</sup> The overlap area of anthracene moieties plays a major role in determining the bathochromic shift of the emission wavelengths. It was reported that the anthracene moieties can form two types of excimers based on their packing geometry in the excited state.<sup>77-79</sup> The excimer that emits close to 470 nm is relatively stable and it has two anthracene moieties overlapping at an angle of 55° to each other.<sup>48</sup> The second type of excimer emits at a higher wavelength of 560 nm is a sandwich-type excimer in which the anthracene moieties are symmetrically stacked with strong  $\pi$ - $\pi$  overlap.<sup>48</sup> Later, a third type of excimer (T-shaped) was reported and it emits at 510 nm.<sup>55</sup> Based on the literature, the anthracene excimers of the present study match with the first case, where a strong excimer emission was observed close to 470 nm. The present results suggest that in a semicrystalline state, both excimers and monomers are present at the interface of the crystalline and amorphous domains as well as in the amorphous domains, where the anthracene moieties are partially overlapping at an angle of 55° to each other to form excimers with cyan emission, and also the monomers with blue emission in the amorphous phase. The deconvolution of the emission spectrum of the semicrystalline polymer suggests

---

the presence of minor fractions of sandwich-type excimer and T-shaped excimers. To further understand the excimer formation in the semicrystalline state, we have prepared the co-crystal of AAP-1 in N, N-dimethylformamide (DMF) by forming a thermoreversible gel.

### 3.5.5. Role of Polymorphism of AAP-1 on Anthracene Excimer Emission

PLLA is known to form gels in solvents that are capable of forming co-crystals ( $\varepsilon$  form).<sup>30, 39, 80, 81</sup> In our earlier studies, we have reported that the physical networks in gels are constructed by crystalline domains of polymers and these gels exhibit fiber-like structures.<sup>30</sup> In the  $\varepsilon$  form, PLLA chains adopt  $10_7$  helical conformation.<sup>71</sup> In the gel form ( $\varepsilon$  form), terminal anthracene moieties are omitted from the crystal lattice due to their large size and stabilized at the interface of crystalline and amorphous phases or in the amorphous phase. AAP-1 gel was prepared in DMF as detailed in the experimental section. The absorption spectrum of AAP-1 gel (Figure 3.9a) shows a structured absorption band from 340 to 420 nm. As discussed in the preceding sections, the presence of the absorption band at 410 nm indicates the existence of excimer structures in gels. Temperature-dependent UV-Vis spectra show no changes upon heating up to 90 °C other than a slight reduction in the intensity of bands (Figure 3.9a). Figure 3.9b shows the temperature-dependent emission spectra of AAP-1 gel. The gel reveals structureless cyan emission at 473 nm at room temperature with shoulder bands at longer wavelengths at 505 and 560 nm. The emission spectrum of the gel is quite different from the emission spectra of AAP-1 in the solution, single crystals, amorphous and semicrystalline states as discussed in the preceding sections. No emission from the anthracene monomeric moieties was observed in the gel state indicating that the DMF present in the amorphous state of the gel facilitated the formation of anthracene excimers effectively. The anthracene moieties that are emitted from the

---



crystalline lamellae are residing at the interface or in the amorphous phase along with the excess of DMF molecules. The solvent-rich phase (amorphous phase) in gels is dynamic at room temperature and allowed the formation of excimers due to the strong  $\pi$ - $\pi$  interactions between anthracene moieties. The presence of emission bands at 473, 505 and 560 nm revealed the formation of three types of excimers, (i.e., anthracene moieties overlapping at an angle of  $55^\circ$  to each other, T-shaped excimers and sandwich-type excimers) in the gel state.<sup>48,55,77-79</sup> As shown schematically in Figure 3.9c, the major contribution of the excimer emission is mainly from the partial overlapping of the anthracene moieties, which emit in the cyan region (473 nm band) and a small fraction of the green emission is due to the formation of T-shaped anthracene excimers as evident from the 505 nm band. In the solvent-rich amorphous phase, a few anthracene units overlap in an edge-to-face dimeric conformation because of the random organization of PLLA chains leading to the formation of T-shaped anthracene excimers. The emission contribution from the strong  $\pi$ - $\pi$  overlap of anthracene moieties (sandwich-type excimers) is almost negligible (a very weak shoulder at 560 nm) because of the dynamic nature of amorphous PLLA chains that are covalently linked to anthracene moieties at the chain ends. Temperature-dependent photoluminescence (PL) emission spectra show drastic changes during heating (Figure 3.9b). The PL intensity decreased with the increase in the temperature and at around  $50^\circ\text{C}$ , quenching in the PL emission is observed (Figure 3.9e). To clarify the reason for such quenching behavior, temperature-dependent WAXD measurements were performed on AAP-1 gel. Figure 3.9d shows the temperature-dependent WAXD patterns of the AAP-1/DMF gel in the heating process. At room temperature, the WAXD pattern shows X-ray reflections at  $2\theta = 11.7^\circ, 14.1^\circ, 15.6^\circ, 18.3^\circ, 19.2^\circ, 20.6^\circ, 22.3^\circ, 23.5^\circ,$  and  $29.1^\circ$  corresponding to the reported  $\epsilon$  form of PLLA.<sup>69</sup> The X-ray pattern suggested that AAP-1 formed a thermoreversible gel in DMF and it formed a co-crystal form of PLLA/DMF

---

( $\varepsilon$  form).<sup>81</sup> The terminal anthracene molecules do not influence the formation of the co-crystal form ( $\varepsilon$  form) and the gelation process. As discussed in the preceding sections, anthracene molecules are excluded from the crystalline lamellae because of their large size and exist at the crystal-amorphous interface or in the amorphous phase. We have reported that the  $\varepsilon$  form transformed into the  $\alpha$  form ( $2\theta = 14.8^\circ, 16.8^\circ, 19.1^\circ, 20.8^\circ, 22.4^\circ, 25.0^\circ$  and  $27.7^\circ$ ) in a broad temperature range  $30 - 50^\circ\text{C}$  due to the segmental mobility of the amorphous PLLA chains and during this transition, the DMF molecules resided within the crystal lattice of the  $\varepsilon$  form expelled into the amorphous phase of the  $\alpha$  form.<sup>71, 81</sup> During this transition, conformational reorganization of helical chains ( $10_7$  (left-handed  $10_3$ )) occurred through locally disordered helical chains. The WAXD results suggested the local disorder in the crystal lattice and the enhanced mobility of PLLA chains in the amorphous phase above the transition temperature. Based on these observations, we might have several possibilities to explain the decrease of the PL intensity with increasing temperature and quenching of the PL intensity above the transition temperature. For example, the formation of aggregates above the  $T_g$  of PLLA resulting the aggregation-caused quenching effect of anthracene moieties via  $\pi$ - $\pi$  interactions. The solvent molecules present in the gel facilitated the formation of anthracene aggregates above the  $T_g$  of PLLA and it results in fluorescence quenching. Further, it was reported that dynamic quenching increases as the temperature increases because of the collisions between molecules and more intermolecular interactions.<sup>82</sup> Another possibility is the collision of anthracene moieties due to the vigorous motions of PLLA chains above the transition temperature that resulted in more intermolecular interactions. Shen et al. reported that the decrease in PL intensity with increasing temperature of anthracene derivative of 2-(anthracen-9-yl)thianthrene is due to the increase in vibrational deactivation.<sup>83</sup> Nevertheless, the reason for the quenching

---

process is not clear and it still remains to be revealed. Investigations in these directions are currently in progress in our laboratory.

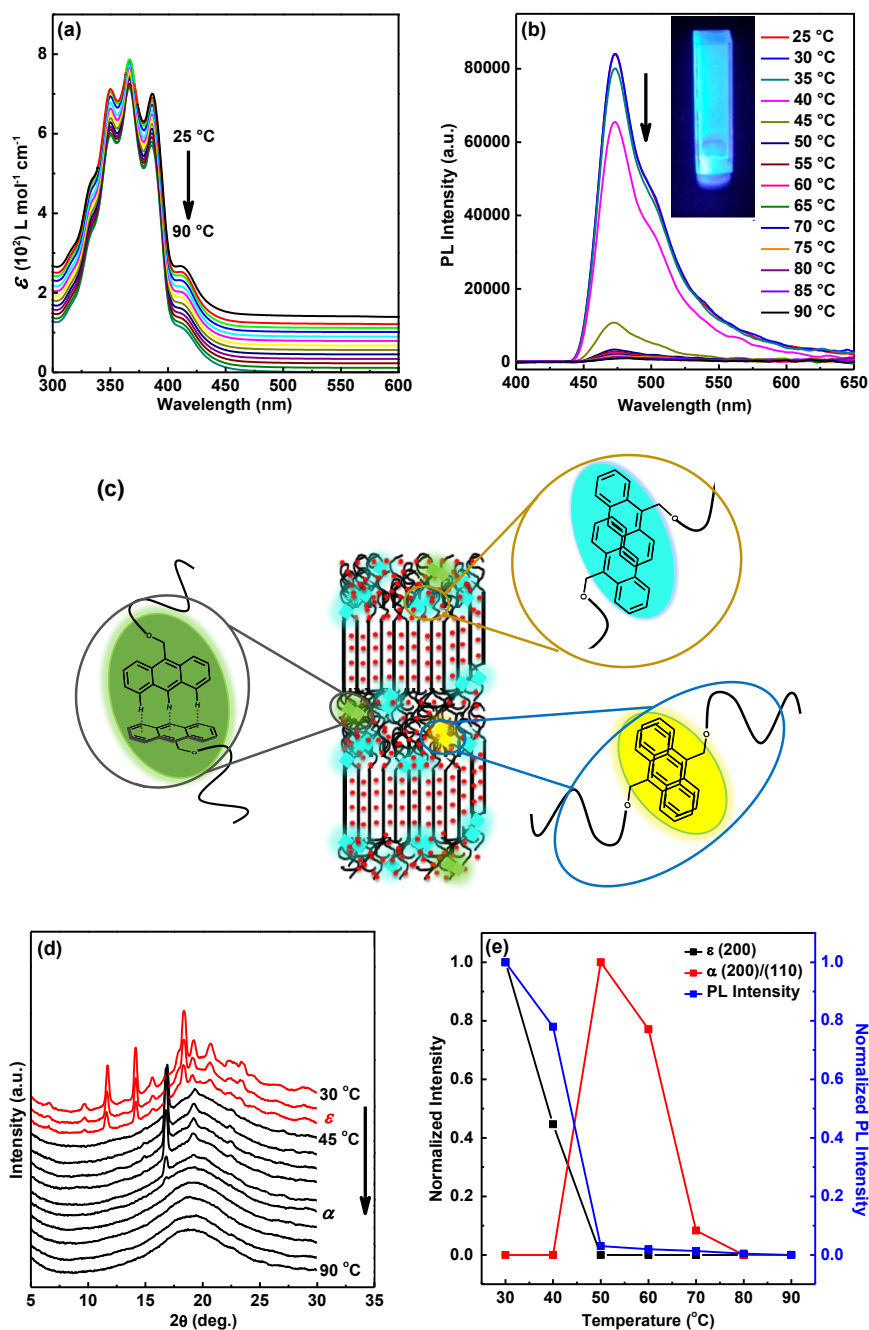


**Figure 3.9.** Temperature-dependent (a) absorption and (b) emission spectra of AAP-1/DMF gel (inset of (b) shows the photograph of AAP-1/DMF gel under UV illumination). (c) Schematic illustration of anthracene moieties arrangement and emission of AAP-1/DMF gel at room temperature (co-crystal of AAP-1/DMF ( $\epsilon$  form)). (d) WAXD patterns

and (e) normalized intensity of the reflections at  $2\theta = 11.2^\circ$  ( $\varepsilon$  (200)), and  $16.6^\circ$  ( $\alpha$  ((200)/(110)) evaluated from (d) and PL intensity evaluated from (b) during the heating process of AAP-1/DMF gel.

### 3.6. Conclusions

In summary, we synthesized anthracene-appended PLLAs and identified the suitable molecular weight polymer for investigating the excimer formation. For the first time, we successfully demonstrated that the crystallization and polymorphism of polymers dictated the photophysical properties of the anthracene-appended PLLAs. The amorphous (melt-quenched) polymer predominantly emits in the dark blue region mainly from its monomeric state due to the fine dispersion of anthracene moieties throughout the polymer matrix. Crystallization of the polymer expels the anthracene moieties into the amorphous region or on the surface of crystals (in the case of single crystals). Crystallization of the PLLA chains into diamond-shaped crystals regulates the anthracene moieties to locate on the surface of the crystals and no evidence of  $\pi$ - $\pi$  stacking of anthracene moieties was observed in this case resulting in the dark blue emission similar to the amorphous thin films. In the semicrystalline state (melt-crystallized  $\alpha$  form and gel state ( $\varepsilon$  form)), covalently-linked anthracene moieties reside at the interface of crystalline and amorphous domains by either dipolar interactions or  $\pi$ -stacking. The  $\alpha$  form emits fluorescence in the cyan region that is mainly arising from both anthracene excimers and monomers. But in the case of gels ( $\varepsilon$  form), exclusive excimer emission was observed where the emission bands are located at 473, 505, and 560 nm indicating the formation of three types of excimers (i.e., anthracene moieties overlapping at an angle of  $55^\circ$  to each other, T-shaped excimers and sandwich-type excimers). These results suggested that the molecular arrangement of anthracene moieties can be modulated by changing the structure and morphology of anthracene-appended PLLA in different forms (amorphous, semicrystalline, single crystals, and gels).

---

The results obtained here not only improve the understanding of excimer formation in hybrid materials but also provide new insights for designing processable fluorescent materials.

### 3.7. References

1. C. Löwe and C. Weder, *Adv. Mater.*, 2002, **14**, 1625-1629.
2. T. Mutai, H. Satou and K. Araki, *Nature Materials*, 2005, **4**, 685-687.
3. J. Mei, N. L. C. Leung, R. T. K. Kwok, J. W. Y. Lam and B. Z. Tang, *Chem. Rev.*, 2015, **115**, 11718-11940.
4. J. Wu, W. Liu, J. Ge, H. Zhang and P. Wang, *Chem. Soc. Rev.*, 2011, **40**, 3483-3495.
5. X. Feng, L. Liu, S. Wang and D. Zhu, *Chem. Soc. Rev.*, 2010, **39**, 2411-2419.
6. G. Niu, R. Zhang, J. P. C. Kwong, J. W. Y. Lam, C. Chen, J. Wang, Y. Chen, X. Feng, R. T. K. Kwok, H. H. Y. Sung, I. D. Williams, M. R. J. Elsegood, J. Qu, C. Ma, K. S. Wong, X. Yu and B. Z. Tang, *Chem. Mater.*, 2018, **30**, 4778-4787.
7. M. A. Baldo, D. F. O'Brien, Y. You, A. Shoustikov, S. Sibley, M. E. Thompson and S. R. Forrest, *Nature*, 1998, **395**, 151-154.
8. A. P. de Silva, H. Q. N. Gunaratne, T. Gunnlaugsson, A. J. M. Huxley, C. P. McCoy, J. T. Rademacher and T. E. Rice, *Chem. Rev.*, 1997, **97**, 1515-1566.
9. Y. Chen, A. J. H. Spiering, S. Karthikeyan, G. W. M. Peters, E. W. Meijer and R. P. Sijbesma, *Nature Chemistry*, 2012, **4**, 559-562.
10. F. Cicoira and C. Santato, *Adv. Funct. Mater.*, 2007, **17**, 3421-3434.
11. F. Würthner, T. E. Kaiser and C. R. Saha-Möllner, *Angew. Chem. Int. Ed.*, 2011, **50**, 3376-3410.
12. S. Srinivasan, P. A. Babu, S. Mahesh and A. Ajayaghosh, *J. Am. Chem. Soc.*, 2009, **131**, 15122-15123.
13. H. Langhals, T. Potrawa, H. Nöth and G. Linti, *Angewandte Chemie International Edition in English*, 1989, **28**, 478-480.
14. R. Schmidt, S. Göttling, D. Leusser, D. Stalke, A.-M. Krause and F. Würthner, *J. Mater. Chem.*, 2006, **16**, 3708-3714.
15. T. Schillmöller, R. Herbst-Irmer and D. Stalke, *Advanced Optical Materials*, 2021, **9**, 2001814.
16. Y. Hong, J. W. Y. Lam and B. Z. Tang, *Chem. Commun.*, 2009, DOI: 10.1039/B904665H, 4332-4353.
17. R. Hu, N. L. C. Leung and B. Z. Tang, *Chem. Soc. Rev.*, 2014, **43**, 4494-4562.
18. Z. Qiu, X. Liu, J. W. Y. Lam and B. Z. Tang, *Macromol. Rapid Commun.*, 2019, **40**, 1800568.
19. H. Y. Zhang, Z. L. Zhang, K. Q. Ye, J. Y. Zhang and Y. Wang, *Adv. Mater.*, 2006, **18**, 2369-2372.
20. K. Wang, H. Zhang, S. Chen, G. Yang, J. Zhang, W. Tian, Z. Su and Y. Wang, *Adv. Mater.*, 2014, **26**, 6168-6173.
21. C. Wang and Z. Li, *Materials Chemistry Frontiers*, 2017, **1**, 2174-2194.

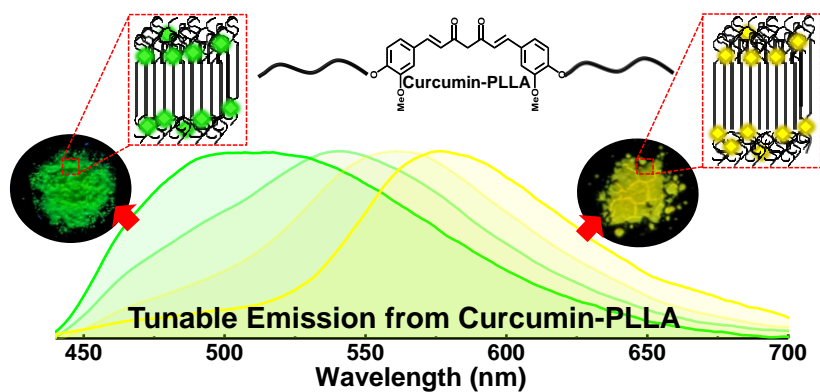
22. M. K. Bera, C. Chakraborty and S. Malik, *J. Mater. Chem. C*, 2017, **5**, 6872-6879.
23. J. Dai, L. Yao, C. Wang, Y. Wang, F. Liu, X. Yan, P. Sun, H. Zhang, Y. Wang, J. Zhou and G. Lu, *The Journal of Physical Chemistry Letters*, 2022, **13**, 4754-4761.
24. W. Z. Yuan, Y. Tan, Y. Gong, P. Lu, J. W. Y. Lam, X. Y. Shen, C. Feng, H. H.-Y. Sung, Y. Lu, I. D. Williams, J. Z. Sun, Y. Zhang and B. Z. Tang, *Adv. Mater.*, 2013, **25**, 2837-2843.
25. Y. Sagara and T. Kato, *Angew. Chem. Int. Ed.*, 2011, **50**, 9128-9132.
26. W. Zhao, C. Li, B. Liu, X. Wang, P. Li, Y. Wang, C. Wu, C. Yao, T. Tang, X. Liu and D. Cui, *Macromolecules*, 2014, **47**, 5586-5594.
27. Y. Jiang and N. Hadjichristidis, *Macromolecules*, 2019, **52**, 1955-1964.
28. X.-H. Wang, N. Song, W. Hou, C.-Y. Wang, Y. Wang, J. Tang and Y.-W. Yang, *Adv. Mater.*, 2019, **31**, 1903962.
29. S. Nagarajan and E. B. Gowd, *Macromolecules*, 2017, **50**, 5261-5270.
30. G. Virat and E. B. Gowd, *Polym. Chem.*, 2022, **13**, 838-849.
31. M.-C. Li, H.-F. Wang, C.-H. Chiang, Y.-D. Lee and R.-M. Ho, *Angew. Chem. Int. Ed.*, 2014, **53**, 4450-4455.
32. T.-S. Hsiao, P.-C. Huang, L.-Y. Lin, D.-J. Yang and J.-L. Hong, *Polym. Chem.*, 2015, **6**, 2264-2273.
33. G. Liang, L.-T. Weng, J. W. Y. Lam, W. Qin and B. Z. Tang, *ACS Macro Lett*, 2014, **3**, 21-25.
34. B. Lotz, T. Miyoshi and S. Z. D. Cheng, *Macromolecules*, 2017, **50**, 5995-6025.
35. A. Keller, *The Philosophical Magazine: A Journal of Theoretical Experimental and Applied Physics*, 1957, **2**, 1171-1175.
36. P. H. Till Jr., *Journal of Polymer Science*, 1957, **24**, 301-306.
37. E. W. Fischer, *Zeitschrift für Naturforschung A*, 1957, **12**, 753-754.
38. J. Guenet, 1992.
39. V. G. Krishnan, N. M. Praveena, R. B. A. Raj, K. Mohan and E. B. Gowd, *ACS Applied Polymer Materials*, 2023, **5**, 1556-1564.
40. E. B. Gowd, K. Tashiro and C. Ramesh, *Prog. Polym. Sci.*, 2009, **34**, 280-315.
41. P. Pan and Y. Inoue, *Prog. Polym. Sci.*, 2009, **34**, 605-640.
42. T. Förster, *Angewandte Chemie International Edition in English*, 1969, **8**, 333-343.
43. T. Förster and K. Kasper, *Zeitschrift für Elektrochemie, Berichte der Bunsengesellschaft für physikalische Chemie*, 1955, **59**, 976-980.
44. A. Das, A. Danao, S. Banerjee, A. M. Raj, G. Sharma, R. Prabhakar, V. Srinivasan, V. Ramamurthy and P. Sen, *J. Am. Chem. Soc.*, 2021, **143**, 2025-2036.
45. F. M. Winnik, *Chem. Rev.*, 1993, **93**, 587-614.
46. Y. Mizobe, M. Miyata, I. Hisaki, Y. Hasegawa and N. Tohnai, *Organic Letters*, 2006, **8**, 4295-4298.
47. J. Chen, A. Neels and K. M. Fromm, *Chem. Commun.*, 2010, **46**, 8282-8284.
48. L. S. Kaanumalle, C. L. D. Gibb, B. C. Gibb and V. Ramamurthy, *J. Am. Chem. Soc.*, 2005, **127**, 3674-3675.
49. Y. Shen, H. Liu, S. Zhang, Y. Gao, B. Li, Y. Yan, Y. Hu, L. Zhao and B. Yang, *J. Mater. Chem. C*, 2017, **5**, 10061-10067.

50. M. Sugino, Y. Araki, K. Hatanaka, I. Hisaki, M. Miyata and N. Tohnai, *Cryst. Growth Des.*, 2013, **13**, 4986-4992.
  51. M. Lehmann, S. Gloza and S. Roth, *Chem. Mater.*, 2015, **27**, 8181-8184.
  52. Z. Chen, A. Lohr, C. R. Saha-Möller and F. Würthner, *Chem. Soc. Rev.*, 2009, **38**, 564-584.
  53. S. Hisamatsu, H. Masu, M. Takahashi, K. Kishikawa and S. Kohmoto, *Cryst. Growth Des.*, 2015, **15**, 2291-2302.
  54. H. Osaki, C.-M. Chou, M. Taki, K. Welke, D. Yokogawa, S. Irle, Y. Sato, T. Higashiyama, S. Saito, A. Fukazawa and S. Yamaguchi, *Angew. Chem. Int. Ed.*, 2016, **55**, 7131-7135.
  55. G. Zhang, G. Yang, S. Wang, Q. Chen and J. S. Ma, *Chemistry – A European Journal*, 2007, **13**, 3630-3635.
  56. Z. Zhang, Y. Zhang, D. Yao, H. Bi, I. Javed, Y. Fan, H. Zhang and Y. Wang, *Cryst. Growth Des.*, 2009, **9**, 5069-5076.
  57. J. Lee, H. Jung, H. Shin, J. Kim, D. Yokoyama, H. Nishimura, A. Wakamiya and J. Park, *J. Mater. Chem. C*, 2016, **4**, 2784-2792.
  58. B. M. Chapin, P. Metola, S. L. Vankayala, H. L. Woodcock, T. J. Mooibroek, V. M. Lynch, J. D. Larkin and E. V. Anslyn, *J. Am. Chem. Soc.*, 2017, **139**, 5568-5578.
  59. K. Nagarajan, S. K. Rajagopal and M. Hariharan, *CrystEngComm*, 2014, **16**, 8946-8949.
  60. J.-Y. Hu, Y.-J. Pu, Y. Yamashita, F. Satoh, S. Kawata, H. Katagiri, H. Sasabe and J. Kido, *J. Mater. Chem. C*, 2013, **1**, 3871-3878.
  61. H. Liu, Y. Dai, Y. Gao, H. Gao, L. Yao, S. Zhang, Z. Xie, K. Wang, B. Zou, B. Yang and Y. Ma, *Advanced Optical Materials*, 2018, **6**, 1800085.
  62. Y. Dai, H. Liu, T. Geng, R. Duan, X. Li, Y. Liu, W. Liu, B.-G. He, L. Sui, K. Wang, B. Zou, B. Yang and Y. Qi, *J. Mater. Chem. C*, 2023, **11**, 4892-4898.
  63. Y. Dai, H. Liu, T. Geng, F. Ke, S. Niu, K. Wang, Y. Qi, B. Zou, B. Yang, W. L. Mao and Y. Lin, *J. Mater. Chem. C*, 2021, **9**, 934-938.
  64. H. Bouas-Laurent, A. Castellan, J.-P. Desvergne and R. Lapouyade, *Chem. Soc. Rev.*, 2000, **29**, 43-55.
  65. P. K. Lekha and E. Prasad, *Chemistry – A European Journal*, 2010, **16**, 3699-3706.
  66. S. Sasaki and T. Asakura, *Macromolecules*, 2003, **36**, 8385-8390.
  67. J. Zhang, Y. Duan, H. Sato, H. Tsuji, I. Noda, S. Yan and Y. Ozaki, *Macromolecules*, 2005, **38**, 8012-8021.
  68. H. Marubayashi, S. Akaishi, S. Akasaka, S. Asai and M. Sumita, *Macromolecules*, 2008, **41**, 9192-9203.
  69. H. Marubayashi, S. Asai and M. Sumita, *Macromolecules*, 2012, **45**, 1384-1397.
  70. D. Sawai, K. Takahashi, A. Sasashige, T. Kanamoto and S.-H. Hyon, *Macromolecules*, 2003, **36**, 3601-3605.
  71. P. Shaiju, N. S. Murthy and E. B. Gowd, *Macromolecules*, 2016, **49**, 224-233.
  72. Y. Sakamoto and H. Tsuji, *Macromolecular Chemistry and Physics*, 2013, **214**, 776-786.
-

73. K. Wasanasuk, K. Tashiro, M. Hanesaka, T. Ohhara, K. Kurihara, R. Kuroki, T. Tamada, T. Ozeki and T. Kanamoto, *Macromolecules*, 2011, **44**, 6441-6452.
  74. T. Schillmöller, P. N. Ruth, R. Herbst-Irmer and D. Stalke, *Chem. Commun.*, 2020, **56**, 7479-7482.
  75. Y. Mizobe, T. Hinoue, A. Yamamoto, I. Hisaki, M. Miyata, Y. Hasegawa and N. Tohnai, *Chemistry – A European Journal*, 2009, **15**, 8175-8184.
  76. A. Rajak and A. Das, *Angew. Chem. Int. Ed.*, 2022, **61**, e202116572.
  77. T. Kobayashi, S. Nagakura and M. Szwarc, *Chemical Physics*, 1979, **39**, 105-110.
  78. S. Hashimoto, N. Fukazawa, H. Fukumura and H. Masuhara, *Chemical Physics Letters*, 1994, **219**, 445-451.
  79. S. Hashimoto, S. Ikuta, T. Asahi and H. Masuhara, *Langmuir*, 1998, **14**, 4284-4291.
  80. Y. Matsuda, A. Fukatsu, Y. Wang, K. Miyamoto, J. W. Mays and S. Tasaka, *Polymer*, 2014, **55**, 4369-4378.
  81. N. M. Praveena, G. Virat, V. G. Krishnan and E. B. Gowd, *Polymer*, 2022, **241**, 124530.
  82. A. Kastrati, F. Oswald, A. Scalabre and K. M. Fromm, *Journal*, 2023, **3**, 227-273.
  83. Y. Shen, H. Liu, J. Cao, S. Zhang, W. Li and B. Yang, *Phys. Chem. Chem. Phys.*, 2019, **21**, 14511-14515.
-



## Impact of Polymer Chain Packing and Crystallization on Emission Behavior of Curcumin-Embedded Poly(L-lactide)s



#### 4.1. Abstract

*The development of biodegradable and biocompatible fluorescent materials with tunable emission in the solid state has become increasingly relevant for smart packaging and biomedical applications. The photophysical characteristics of fluorescent materials can be significantly tuned by manipulating their molecular packing and conformations. Molecular packing and conformations play a significant role in tuning the photophysical properties of fluorescent materials. In this chapter, tunable emission of bioactive curcumin was attained by tuning the crystallization conditions and polymorphic form of covalently linked poly(L-lactide) in the curcumin-embedded poly(L-lactide) (curcumin-PLLA). In the melt-crystallized curcumin-PLLA, when crystallization temperature increases, a bathochromic shift in the fluorescence of curcumin-PLLA was observed due to the change in the intramolecular conjugation length of curcumin. The differences in the isothermal crystallization temperature of curcumin-PLLA leads to the different twisting behavior of terminal phenyl rings of curcumin with respect to the central keto-enol group due to the covalently linked helical PLLA chains. In addition, solvent-induced single crystals and gels of curcumin-PLLA were prepared, and studied the impact of the polymorphic form of PLLA on the emission behavior of curcumin-PLLA. The results indicate that the polymer chain packing, crystallization conditions, morphology, and polymorphic form could play an influential role in dictating the fluorescent properties of fluorophore-embedded polymers.*

#### 4.2. Introduction

Bioactive fluorescent materials have attracted a great deal of interest because of their prospective applications in bio-imaging, fluorescent biosensors, drug delivery and biomedical devices.<sup>1-8</sup> Fluorescent materials usually exhibit different emission behavior in the solution state, crystalline (aggregate) and amorphous states, which restricts the applications of these materials. For most practical applications, solid state fluorescent

---

materials with the high efficiency are essential. Tang et al. initiated aggregation-induced emission (AIE) upon crystallization/self-assembly or aggregation of organic molecules.<sup>1, 9-14</sup> Even in the aggregated state, the molecular conformations and molecular packing modes have a major role in controlling the emission behavior of fluorescent materials.<sup>15-20</sup> Although several attempts were made to understand the emission behavior of small organic molecules, their processability, solubility, mechanical stability, and thermal stability are some of the major issues from the application point of view. To overcome these challenges, fluorophores have been covalently fixed to polymer chains at the molecular level. Varieties of fluorophores were incorporated into polymers having different architectures to obtain room-temperature stable solid-state fluorescent materials.<sup>21-31</sup> The fluorescence behavior of these hybrid materials was tuned by controlling the aggregation of fluorescent molecules within the polymer. However, limited studies are available on the impact of polymer chain packing (conformation and crystallization) on the fluorescence properties of fluorophores-embedded polymers.

The crystallization process is associated with the packing of polymer chains in hierarchical length scales of polymers and it serves an important role in determining the polymer properties. Our previous studies demonstrated that the polymer crystallization controls the fluorescence properties of fluorophores after the chemical incorporation into the polymer's backbone.<sup>29, 30</sup> In one case, dipyridamole was used as a core molecule in a four-arm star-shaped poly(L-lactide) (SSPLLA) that enhanced the emission of dipyridamole due to the helicity transfer from the PLLA polymer chains to the dipyridamole and also the molecular level dispersion of dipyridamole in the amorphous regions of the semicrystalline PLLA.<sup>29</sup> In another case, it was demonstrated that the variation in the conformation and crystalline structure of PLLA influence the emission properties of the tetraphenylethylene (TPE) core in SSPLLA due to the change in the

---

intramolecular conjugation length of TPE.<sup>30</sup> Hsiao et al. showed that the AIE behavior of 1,2-bis (2,4-dihydroxybenzylidene)hydrazine could be tuned by the polymer crystallization after the successful incorporation of this fluorophore into the backbone of PLLA.<sup>32</sup> Li et al. investigated the transfer of molecular chirality into hierarchical chirality in fluorophore-appended PLLA by lamellar twisting caused by the helical chains of PLLA.<sup>31</sup> Inspired by these studies, we envisioned replacing the fluorophore molecule with a naturally occurring bioactive compound, curcumin, and investigated the impact of PLLA crystallization on the photophysical properties of curcumin-embedded PLLA.

Curcumin is a principal active ingredient of turmeric and it is widely exploited by researchers to investigate the chemistry behind its diverse pharmaceutical applications and biological importance.<sup>33-38</sup> This has been used as antioxidant, anticancer, antiviral, and anti-inflammatory molecule, as well as for other crucial physicochemical and pharmacological activities.<sup>36, 39-42</sup> Poor aqueous solubility and degradability at higher pH are the major factors that limit the applications of curcumin.<sup>43, 44</sup> It was demonstrated that the loading of curcumin into polymeric micelles stabilizes this compound and the rate of degradation is greatly suppressed in micellar nanocavity.<sup>45</sup> Curcumin is also used as a chemical indicator in polymer packaging films where it is physically entrapped inside the polymer matrix.<sup>46</sup> This compound is incorporated into various polymers by blending and tested for food packaging and wound healing applications.<sup>47, 48</sup> Curcumin exhibits photosensitizing and photobiological activity and it has been reported that the photochemical properties of this compound depend on the environment.<sup>49</sup> Very limited studies are available on the chemical incorporation of curcumin into the backbone of polymer chains. PLLA is synthetic semicrystalline biodegradable polymer, approved by a Food and Drug Administration (FDA). This polymer is made from sustainable resources and it shows biocompatible behavior. PLLA chains adopt a helical conformation because of the existence of an

---

asymmetric carbon in the main chain. Being a semicrystalline polymer, PLLA exhibits different crystalline forms ( $\alpha$ ,  $\alpha'(\delta)$ ,  $\alpha''$ ,  $\beta$ ,  $\gamma$ , and  $\varepsilon$  forms) depending on the crystallization conditions.<sup>50-55</sup>

Curcumin exists in a various polymorphic form due to the twisting in its molecular conformation.<sup>38,56</sup> Thus, it is feasible to change the conformation of curcumin by covalently linking it to the helical polymer chains. Herein, curcumin-embedded PLLA (Curcumin-PLLA) was synthesized by ring-opening polymerization of L-lactide using curcumin as a macroinitiator. As molecular packing and molecular conformations significantly impact the emission properties, the conformation of the covalently linked curcumin was tuned by changing the crystallization conditions and polymorphic form of the polymer. The twisting caused by the helical PLLA chains in the spherulite has a significant role in changing the conformation of curcumin. As a consequence, tunable emission behavior of curcumin-PLLA was achieved in the solid state and this behavior is mainly due to the twisting of two benzene rings with respect to the central keto-enol group induced by the covalently linked helical PLLA chains. To verify the suggested mechanism, the photophysical properties of curcumin-PLLA were investigated in amorphous and isothermally crystallized samples (solid-state) and solvent-crystallized (single crystals and gel) samples.

### **4.3. Experimental Section**

#### **4.3.1. Materials**

L-lactide, Sn(Oct)<sub>2</sub>, curcumin, chloroform, toluene (anhydrous, 99.8%) and hexane were acquired from Sigma-Aldrich. Methanol, N, N-dimethylformamide (DMF) and ethyl acetate were acquired from Merck Chemicals and N, N-dimethylacetamide (DMA) was purchased from Alfa Aesar. The L-lactide monomer was recrystallized in ethyl acetate before polymerization.

---

### 4.3.2. Synthesis of Curcumin-PLLA

L-Lactide (3.0 g), curcumin (5.0 mg) and Sn(Oct)<sub>2</sub> (20  $\mu$ L) were taken in a dried round bottom flask and the mixture was dissolved in dry toluene (30 ml). The solution was mechanically stirred in under vacuum conditions for 1 h at room temperature to remove moisture. The reaction was conducted at 120 °C for 6 h under an inert atmosphere. Such obtained reaction mixture was dissolved in chloroform and re-precipitated twice in cold methanol. The collected precipitate was filtered and dried in a vacuum oven at 40 °C for 24 h. The chemical structure of Curcumin-PLLA was analysed by <sup>1</sup>H NMR. The molecular weight ( $M_n$ ) of Curcumin-PLLA was 29 kDa and dispersity ( $\mathcal{D}$ ) of 1.25 was estimated by GPC.

### 4.3.3. Preparation of Isothermally Melt-crystallized Samples

Curcumin-PLLA was melted at 200 °C in a DSC pan and kept for 2 min to erase the thermal history. Then the sample was cooled rapidly (50 °C/min) to the required isothermal crystallization temperature and the samples were allowed to crystallize at that temperature.

### 4.3.4. Preparation of Single Crystals of Curcumin-PLLA

Curcumin-PLLA (10 wt%) was dissolved in DMA by heating at 100 °C for about 2-3 min and the clear solution was gradually cooled to ambient temperature and kept overnight in a freezer at -4 °C for equilibration.

### 4.3.5. Preparation of Curcumin-PLLA Gel

Curcumin-PLLA (10 wt%) was dissolved in DMF by heating at 120 °C for about 2-3 min and the clear solution was gradually cooled to room temperature and kept overnight in a freezer at -4 °C for gelation. Gel formation was confirmed by the failure of the solvent to flow while inverting the container.

---

#### 4.4. Characterization and Measurements

The morphology of single crystals of curcumin-PLLA was investigated using Zeiss EVO 18 cryo-SEM (scanning electron microscopy (SEM)) with an accelerating voltage of 20 kV and JEOL 2010 transmission electron microscope (TEM) operating at 200 kV. The colloidal solution of curcumin-PLLA in DMA was casted onto a copper grid and dried in a vacuum condition for TEM observations. The morphology of the spherulites was examined using a Leica DFC 490 Polarised optical microscope (POM) fitted with a Mettler Toledo FP82HT heating stage under isothermal crystallisation conditions. For other characterizations see chapter 2.

#### 4.5. Results and Discussion

##### 4.5.1. Structural and Thermal Properties of Curcumin-PLLA

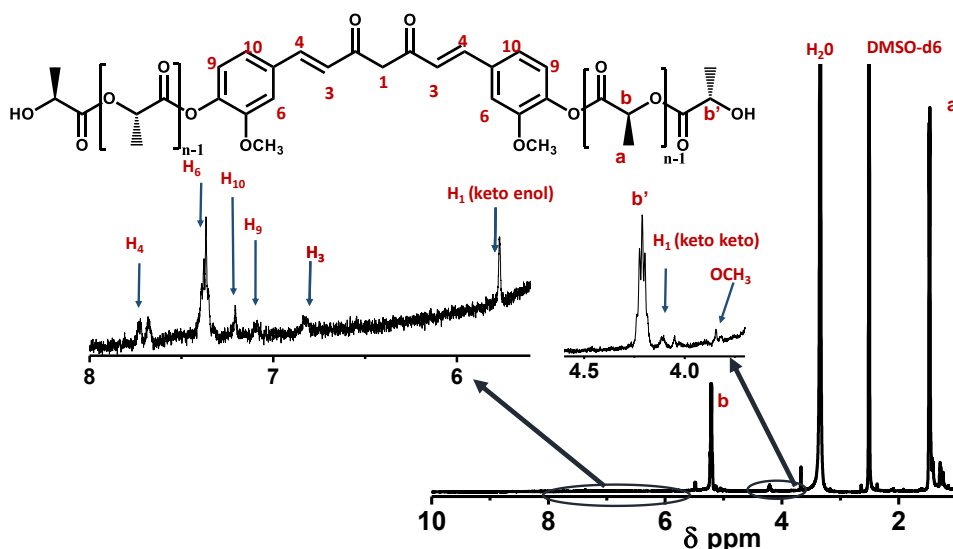
As illustrated in Scheme 4.1, curcumin-PLLA was synthesized by ring-opening polymerization of L-lactide using tin(II) 2-ethylhexanoate ( $\text{Sn}(\text{Oct})_2$ ) as the catalyst and curcumin as a macroinitiator. Curcumin exists as keto-enol and  $\beta$ -diketone tautomer forms.<sup>33, 38, 43, 56</sup> At the polymerization temperature, two phenolic groups in curcumin react with L-lactide resulting in the curcumin-embedded linear polymer, as depicted in Scheme 4.1.



**Scheme 4.1.** Synthesis of curcumin-embedded PLLA.

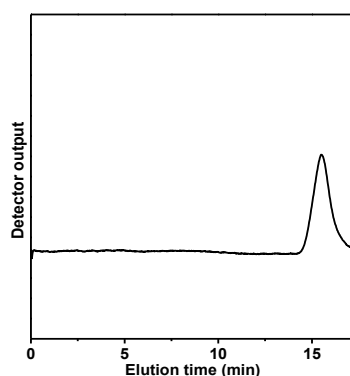
The reactivity of enolic hydroxyl group is limited due to the keto-enol-enolate equilibrium state.<sup>44</sup> The presence of curcumin in the obtained polymer was confirmed by

$^1\text{H}$  NMR (Figure 4.1). The protons resonate at  $\delta = 7.70, 7.36, 7.20, 7.08, 6.82$  and  $5.76$  ppm in the  $^1\text{H}$  NMR spectrum indicated that the curcumin moiety was incorporated within the PLLA chains and remained intact during the polymerization. The protons resonate at  $\delta = 5.21, 4.21$  and  $1.47$  ppm correspond to the CH, terminal CH and  $\text{CH}_3$  protons of PLLA, respectively.



**Figure 4.1.**  $^1\text{H}$  NMR spectrum of curcumin-PLLA in  $d_6$ -DMSO.

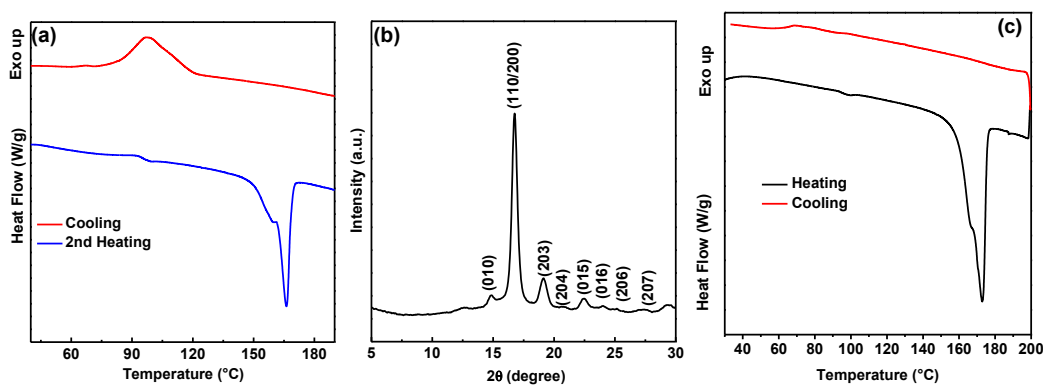
The molecular weight of the curcumin-PLLA was measured using gel permeation chromatography (GPC) (Figure 4.2) and the number average molecular weight ( $M_n$ ) of curcumin-PLLA is  $\sim 29$  kDa and molecular weight distribution ( $\text{Đ}$ ) is  $\sim 1.25$ .



**Figure 4.2.** GPC trace of curcumin-PLLA in THF.



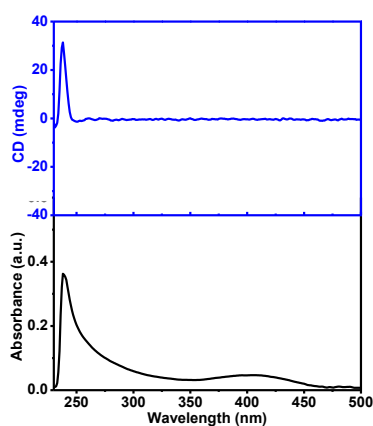
Figure 4.3a shows the differential scanning calorimetry (DSC) thermograms of synthesized curcumin-PLLA during the cooling and reheating process. Upon cooling, a broad exotherm was noticed at  $\sim 97^\circ\text{C}$ , confirming the melt-crystallization of PLLA. The melt-cooled sample collected from the DSC pan was analyzed using wide-angle X-ray scattering (WAXS). The X-ray reflections (Figure 4.3b) corresponding to the  $\alpha$ -form (with a minor fraction of the  $\alpha'$ -form) of PLLA were observed at  $2\theta = 14.8^\circ$  (010),  $16.8^\circ$  (110/200),  $19.1^\circ$  (203),  $20.8^\circ$  (204),  $22.4^\circ$  (015),  $24.0^\circ$  (016),  $25.2^\circ$  (206) and  $27.7^\circ$  (207).<sup>50</sup> No traces of crystalline reflections related to the curcumin were noticed in the X-ray pattern, confirming that the curcumin molecules are molecularly dispersed in PLLA without any agglomeration. Upon reheating the sample, DSC shows the melting temperature of curcumin-PLLA at  $\sim 166^\circ\text{C}$ , which is slightly lower than the melting temperature of pristine curcumin ( $175^\circ\text{C}$ ) (Figure 4.3c), further confirming the fine dispersion of curcumin molecules without the formation of aggregates.



**Figure 4.3.** (a) DSC thermograms (with a rate of  $10^\circ\text{C}/\text{min}$ ) and (b) WAXS data of curcumin-PLLA, and (c) DSC data of pristine curcumin while heating and cooling (with a rate of  $10^\circ\text{C}/\text{min}$ ).

Figure 4.4 shows the UV–Visible spectrum and the corresponding circular dichroism (CD) spectrum of curcumin-PLLA in the solution state determined in a mixture

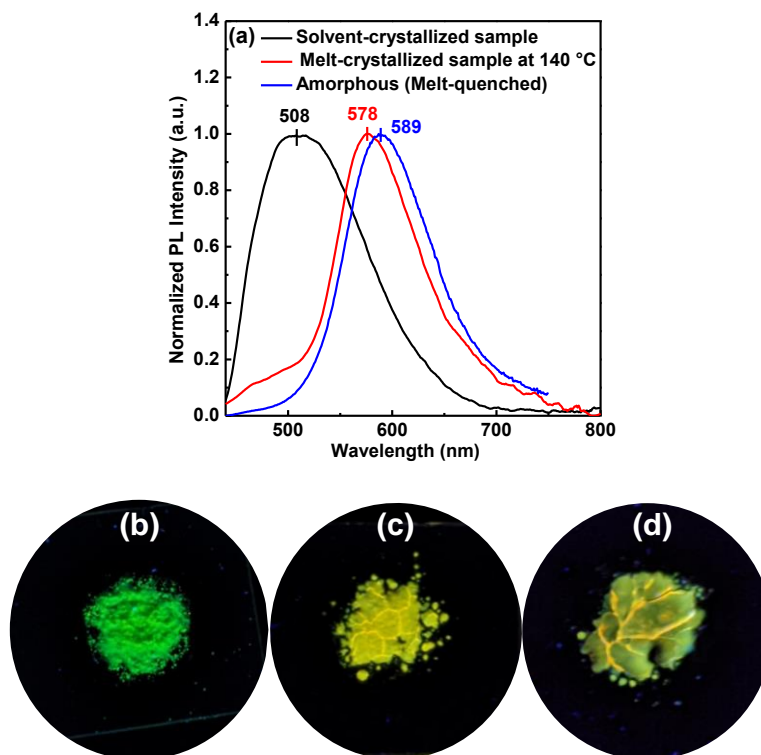
of chloroform and hexane (50:50 v/v). The absorption spectrum of curcumin-PLLA shows two bands around 236 nm and 410 nm corresponding to the  $n \rightarrow \pi^*$  transition of the carbonyl groups in PLLA and the low-energy  $\pi \rightarrow \pi^*$  transition of the curcumin, respectively.<sup>44, 57</sup> Shen et al. assigned the broad absorption peak at around 410-420 nm to the enol form of curcumin using time-dependent density functional theory and a similar experimental value was reported for the enol form of curcumin in the solution state.<sup>58</sup> This observation further confirms that the enolic hydroxyl groups of curcumin were not reacted effectively with L-lactide monomer during the polymerization. In our earlier works, we reported that PLLA absorbs at 244 nm in a good solvent (chloroform) in the molecularly dissolved state and a blue shift of the carbonyl absorption band (236 nm) occurred upon the addition of a non-solvent (hexane) due to the aggregation or crystallization of PLLA chains.<sup>29, 30</sup> A similar shift in the absorption band of curcumin-PLLA is observed (244 nm to 236 nm) in the presence of a mixture of chloroform and hexane (50:50 v/v). The CD spectrum shows a large positive Cotton effect at 236 nm with respect to the  $n \rightarrow \pi^*$  transition of the carbonyl groups in PLLA indicating that the PLLA polymer chains takes helical chain conformation.<sup>57</sup> No additional bands were noticed in the CD spectrum of curcumin-PLLA and this indicates that the transfer of chirality/helicity did not occur from chiral PLLA chains to achiral curcumin molecules.



**Figure 4.4.** UV-Vis and CD spectra of curcumin-PLLA.

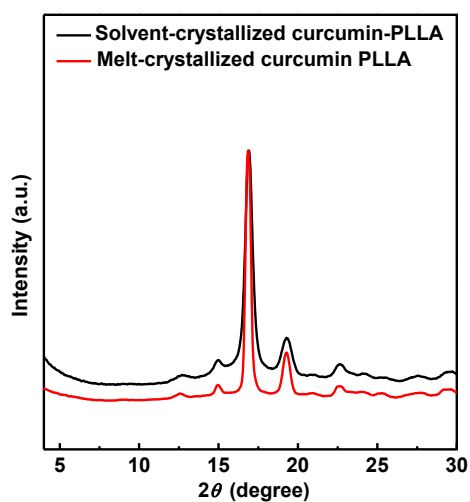
#### 4.5.2. Influence of Polymer Chain Conformation and Crystallization on Curcumin Emission

Figure 4.5a shows normalized photoluminescence (PL) emission spectra of solvent-crystallized (precipitated in methanol from chloroform solution), melt-crystallized (at isothermal crystallization temperature  $\sim 140$  °C) and melt-quenched (amorphous) curcumin-PLLA. The solvent-crystallized curcumin-PLLA shows a broad emission spectrum at 508 nm and this peak red-shifts to 578 nm (spectrum shift up to 70 nm) when the sample is isothermally melt-crystallized at 140 °C. The melt-quenched amorphous curcumin-PLLA shows a broad emission spectrum at 589 nm, which is higher than the crystallized samples. The solvent-crystallized sample appeared greenish yellow (Figure 4.5b) under UV light, whereas the melt-crystallized and amorphous curcumin-PLLA appeared yellow (Figure 4.5c and 4.5d).



**Figure 4.5.** (a) PL emission spectra and (b, c & d) fluorescent microscopy images of solvent-crystallized, melt-crystallized and melt-quenched (amorphous) curcumin-PLLA.

The WAXS patterns of both the crystallized samples show typical  $\alpha$  form structures with almost similar degrees of crystallinity ( $\sim 40\%$ ) (Figure 4.6). It has to be noted that the emission behavior of organic luminescent solids is strongly dependent on the molecular packings.<sup>18, 20</sup> Sanphui et al. reported the conformational polymorphs of curcumin based on the torsional flexibility of outermost benzene groups and the position of hydroxyl and methoxy groups with respect to the central keto-enol group.<sup>38, 56</sup> We speculate here that the polymer chain conformation and crystallization conditions of curcumin-PLLA have a strong influence on the conformations of the curcumin molecules that are covalently linked to the helical PLLA chains and the change in conformations of the curcumin molecules are responsible for the different emission behavior of solvent-crystallized, melt-crystallized and melt-quenched (amorphous) curcumin-PLLA. To decipher the origin of the different emission behavior in crystallized samples, we systematically investigated the effect of isothermal crystallization of curcumin-PLLA at various temperatures from the melt state on the emission behavior of curcumin-PLLA.



**Figure 4.6.** WAXS patterns of solvent-crystallized and melt-crystallized curcumin-PLLA.

### 4.5.3. Effect of Isothermal Crystallization of Curcumin-PLLA on the Emission of Curcumin

DSC was further employed to determine the overall crystallization rate at different isothermal crystallization temperatures ranging from 80 to 140 °C (Figure 4.7a). The period at which 50% of the crystallinity develops is known as the crystallization half-time ( $T_{1/2}$ ). The overall crystallization rate is measured by the inverse of  $T_{1/2}$ , which includes both nucleation and growth.<sup>59</sup> Figure 4.7b shows the overall crystallization rate of curcumin-PLLA as a function of isothermal crystallization temperatures. Crystallization kinetics of curcumin-PLLA displays the characteristic bell-shaped pattern, switching from diffusion control at lower temperatures to the nucleation control at higher temperatures.

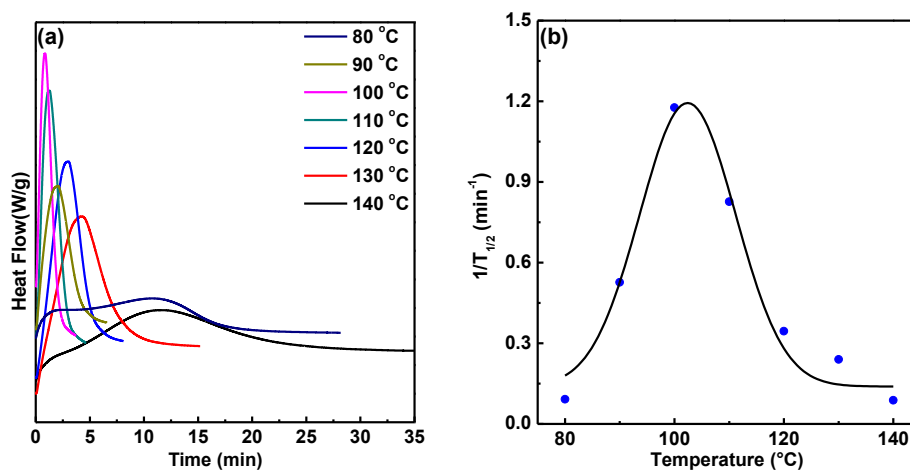


**Figure 4.7.** (a) DSC isotherms and (b) temperature dependence of crystallization rate ( $G = 1/T_{1/2}$ ) of curcumin-PLLA crystallized at various isothermal crystallization temperatures.

Figure 4.8a shows the WAXS patterns of isothermally crystallized curcumin-PLLA films at various crystallization temperatures. At lower crystallization temperatures ( $\leq 110$  °C), curcumin-PLLA samples crystallized into the mixture of  $\alpha'$  and  $\alpha$  forms, and at higher crystallization temperatures ( $\geq 120$  °C), the samples crystallized into the  $\alpha$  form. These results are in good agreement with the reported literature.<sup>51, 60</sup> Figure 4.8b shows SAXS patterns of isothermally crystallized curcumin-PLLA films at various crystallization

temperatures. Curcumin-PLLA samples crystallized  $\leq 100$  °C shows SAXS peaks indicating the formation of stacked lamellar structure (Figure 4.8c) and these scattering peaks correspond to the long period (total thickness of crystalline ( $l_c$ ) and amorphous ( $l_a$ ) domains). It has to be noted that large sized curcumin molecules will be resided mainly at the crystal-amorphous interface or in the amorphous phase. The long period values ( $L=2\pi/q$ ) estimated for these samples increased with the increase in the crystallization temperature and the long periods of 80, 90 and 100 °C crystallized samples were estimated to be 17.9, 20.2, and 22.4 nm, respectively. The curcumin-PLLA samples crystallized at or above 110 °C did not show SAXS peaks even though the corresponding WAXS patterns show the semicrystalline patterns of these samples. These results suggest that the electron density contrast among amorphous and crystalline domains in these samples is negligible.

To further get insights into the role of overall crystallization rate and isothermal crystallization temperature, absorption and PL measurements of the isothermally annealed samples were systematically collected. Figures 4.8d and 4.8e depict the absorption and PL spectra of curcumin-PLLA, respectively after isothermally crystallized at the specified temperatures. The absorption spectra of isothermally crystallized curcumin-PLLA show three bands around 236 nm, 323 nm and 406 nm. The band at 236 nm is corresponding to the  $n \rightarrow \pi^*$  transition of the carbonyl groups in PLLA and the bands at 323 nm and 406 nm are corresponding to the  $\pi \rightarrow \pi^*$  transitions of the curcumin. It has to be noted that the  $n \rightarrow \pi^*$  transition of the curcumin also overlaps with the  $n \rightarrow \pi^*$  transition of PLLA at 236 nm. The observation of the band at 323 nm is due to the fine dispersion of curcumin (in monomeric state) in PLLA as well as the twisting of the curcumin. Jagannathan et al. reported the presence of an additional peak at 345 nm for the  $\pi \rightarrow \pi^*$  transitions of curcumin in water at a higher temperature (90 °C) where the curcumin exists in the deagglomerated form (monomeric form) due to the breakage of hydrogen bonding at a higher temperature

---

and it was assigned to the variation in the curcumin's tautomeric form (keto-enol-enolate group) of.<sup>44</sup>

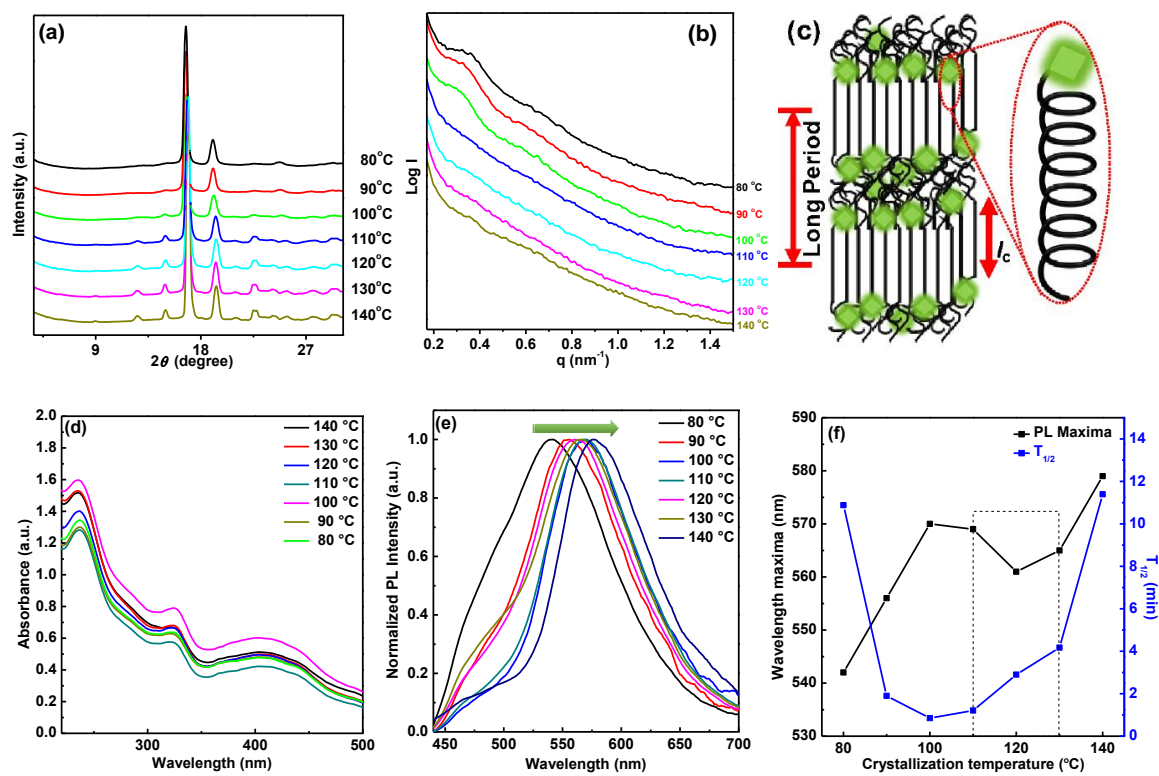


**Figure 4.8.** (a) WAXS patterns, (b) SAXS patterns, (c) Lamellar morphology of curcumin-PLLA where PLLA chains adopt helical conformation, (d) UV-Vis spectra, (e) PL spectra and (f) temperature dependence of PL wavelength maxima and crystallization half-time of curcumin-PLLA crystallized at various isothermal crystallization temperatures.

Based on the time-dependent density functional theory, Shen et al. assigned the absorption band in the wavelength range of 375 nm to the diketo form and the structure of curcumin is twisted in this form.<sup>58</sup> As discussed in the later section, covalently linked helical PLLA chains might induce the twisting in the curcumin structure due to the rotation of terminal phenyl rings and such type of twisting causes for the appearance of the absorption band at 323 nm. The intensities of the absorption peaks at 236 nm, 323 nm and 406 nm varied slightly with respect to the isothermal crystallization temperatures due to the change in the Boltzmann distribution of the populations at the ground state. The absorption

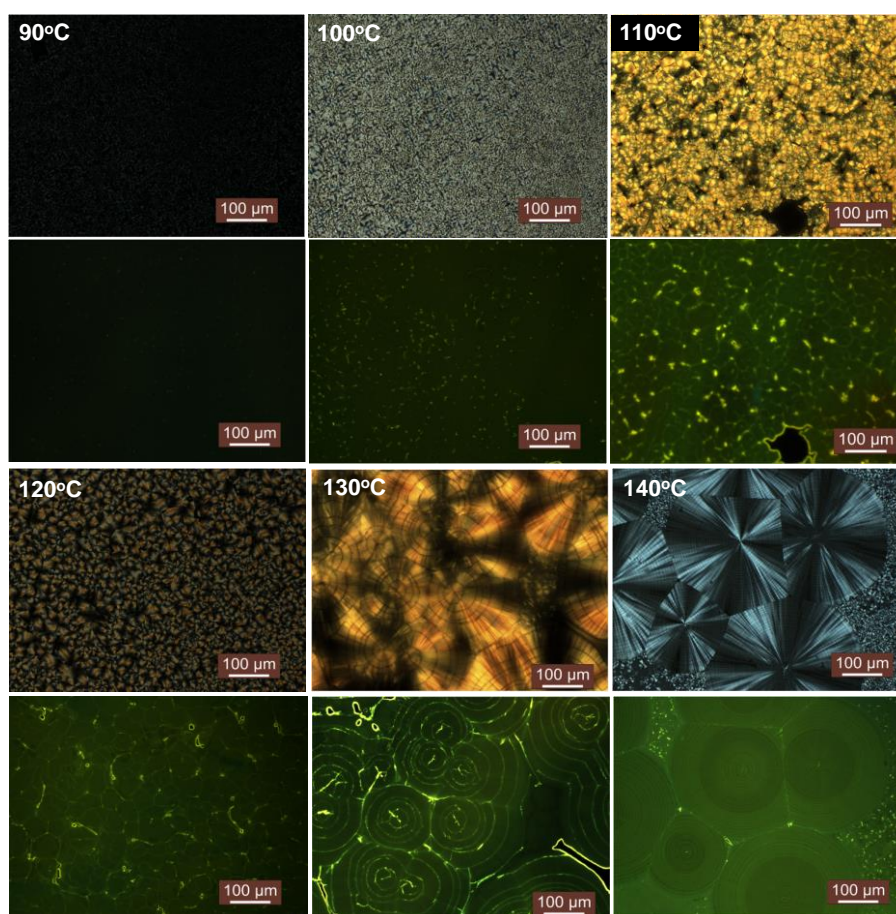
peaks at 323 nm and 406 nm are slightly red or blue shifted depending on the isothermal crystallization temperatures and it is mainly due to the twisting (distortions) of the curcumin molecules caused by the helical PLLA chains. On the other hand, PL emission spectra show a significant dependence on the isothermal crystallization temperature. Figures 4.8e and 4.8f present the PL emission spectra and PL emission maxima of curcumin-PLLA crystallized at various isothermal crystallization temperatures, respectively. The PL maxima show a red shift with the increase of isothermal crystallization temperature; however, a slight decrease in the PL emission maxima was observed in the crystallization temperature range of 110 to 130 °C. To provide insights into the underlying reasons for this dependence of emission behavior on the isothermal crystallization temperatures, fluorescent microscopy images of isothermally crystallized curcumin-PLLA were captured.

Figure 4.9 shows the microscopy images obtained at room temperature under polarized light and UV light (below the corresponding polarized optical microscopy (POM) images) of curcumin-PLLA crystallized at various isothermal crystallization temperatures. Typical spherulitic morphologies were observed at different crystallization temperatures and the spherulite sizes increased with the isothermal crystallization temperature (from 90 °C to 140 °C). At lower crystallization temperatures (< 100 °C), tiny spherulites were observed because the nucleation dominates the crystallization process (where the crystal growth is limited). Instead, larger spherulites were observed at higher temperatures (> 100 °C) because the nucleation process is limited and the crystal growth process is prominent at these temperatures. As PLLA exhibits a chiral molecular structure, ring-banded spherulites were reported in the literature, but no such ring-banded spherulites were observed in the case of curcumin-PLLA.<sup>31, 61</sup> Though the origin of lamellar twisting in semicrystalline polymers is still controversial, Li et al. demonstrated the induced circular

---



dichroism (ICD) to the achiral pyrene during the crystallization of polylactides (PLLA and PDLA) in the pyrene-appended polylactides.<sup>31</sup> They also reported the chirality transfer from helical polymer chains to the lamellar twisting in banded spherulites in isothermally crystallized pyrene-appended polylactides. The band spacing in the banded spherulites reflected the twisting power of the crystalline lamellae and this twisting power reduces with the increase in the crystallization temperature.



**Figure 4.9.** POM images of isothermally crystallized curcumin-PLLA films at various crystallization temperatures under polarized light (top row) and UV light (bottom row).

At higher isothermal crystallization temperatures ( $\geq 120$  °C), concentric rings (formation of the cracks) were observed within the spherulites. A similar observation was made in star-shaped PLLA with a dipyrindamole core.<sup>29</sup> In star-shaped PLLA, the conformation chirality of PLLA is transferred to the dipyrindamole core in the solid state

upon crystallization of PLLA at various isothermal crystallization temperatures. Based on these observations, we speculate that the unbalanced surface stresses between the irregular folding surfaces during the lamellar growth are responsible for the lamellar twisting, leading to the formation of cracks instead of banded spherulites. At lower crystallization temperatures, where the spherulite sizes are too small, such cracks are not observed, indicating that a critical spherulite size is essential for forming cracks, as reported.<sup>62</sup> These results indicated that the spherulite sizes and lamellar twisting are strongly dependent on the isothermal crystallization temperature. It has to be noted that in crystallized curcumin-PLLA, the covalently linked curcumin molecules are expected to be expelled from the crystalline lamellae and reside at the lamellar interface or the amorphous phase due to their large size.

Unlike pyrene-appended polylactides and dipyrindamole-embedded star-shaped PLLA, no ICD in the achiral curcumin was observed in the case of isothermally crystallized curcumin-PLLA.<sup>29, 31</sup> As seen in Figure 4.4, no additional CD signals were observed other than a large positive Cotton effect at 236 nm corresponding to the  $n \rightarrow \pi^*$  transition of the carbonyl groups in PLLA in the aggregated curcumin-PLLA. These results differ from the pyrene-appended PLLA or dipyrindamole-embedded PLLA, where the lamellar twisting in the crystalline spherulites caused the ICD to achiral molecules.<sup>29, 31</sup> Sanphui et al. reported the torsional flexibility between two terminal phenyl rings with respect to the central keto-enol group in curcumin.<sup>38</sup> We believe that the chirality of PLLA chains influences the conformation of the covalently linked curcumin in curcumin-PLLA due to the difference in the twisting power of the helical chains with respect to the crystallization temperature. Curcumin is reported to be a good example of the conformational polymorph based on flexible terminal phenyl rings. Based on this, we may conclude here that the lamellar twisting caused by the helical PLLA in the spherulites caused the rotation of the terminal

---

phenyl rings in curcumin, and such a situation changes the dihedral angle between the least-squares planes passing through C<sub>4</sub>/C<sub>7</sub>/C<sub>8</sub>/C<sub>9</sub>/C<sub>10</sub>/C<sub>11</sub> and C<sub>12</sub>/C<sub>13</sub>/C<sub>14</sub> (Figure 4.10).<sup>38</sup> The change in the dihedral angle between two phenyl rings in isothermally crystallized curcumin-PLLAs depends upon the spherulite sizes and the twisting power of the crystalline lamellae with respect to the isothermal crystallization temperature.<sup>63</sup> This conformational change in curcumin resulted in the different emission behavior of isothermally crystallized curcumin-PLLA. Recently, it was demonstrated that polymorphic manipulation of fluorescent molecules due to conformational flexibility plays an acute role in tuning the solid-state emission properties of crystalline materials.<sup>64</sup> The present study revealed that polymer crystallization plays a vital role in determining the solid-state emission properties of fluorophore-embedded semicrystalline polymers.

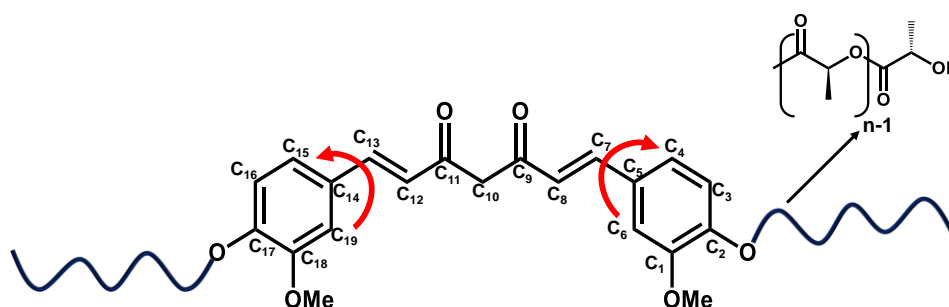


**Figure 4.10.** Torsional flexibility of terminal phenyl rings in curcumin-PLLA.

#### 4.5.4. Emission Behavior of Curcumin-PLLA Single Crystals

Further, colloidal dispersions of single crystals of curcumin-PLLA were prepared in N,N-dimethylacetamide (DMA) by dissolving the curcumin-PLLA at around 120 °C for 2-3 min. The transmission electron microscopy (TEM) studies revealed the formation of diamond-shaped single crystals (Figure 4.11a). PLLA helical chains are packed into the orthorhombic unit cell in single crystals, as reported earlier and the corresponding WAXS pattern shows the  $\alpha$  form.<sup>50</sup> These results suggested that the polymer crystallization is

unaffected by the covalently linked curcumin and upon the polymer crystallization, the curcumin molecules are expelled to the surface of the single crystals in the monomeric state (nonaggregated state). Single crystals formation of PLLA was established in other fluorophore-embedded PLLA systems irrespective of the polymer architecture.<sup>30, 65</sup> Similar to the solvent-crystallized samples, single crystals of curcumin-PLLA emitted greenish yellow color under the UV light illumination (inset of Figure 4.11b).

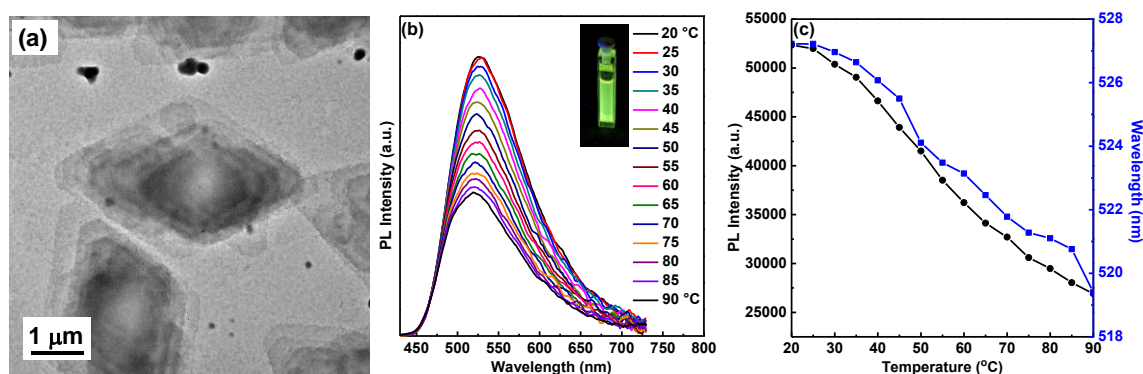


**Figure 4.11.** (a) TEM image, (b) temperature-dependent emission spectra and (c) temperature-dependent PL intensity and wavelength of curcumin-PLLA single crystals in DMA. (inset shows the photograph under the UV light illumination).

The PL emission spectra showed a broad band with an emission maximum of 527 nm (Figure 4.11b). The maximum of the PL spectra of single crystals in DMA is red-shifted compared to the solvent-crystallized curcumin-PLLA (508 nm) and blue-shifted compared to the melt-crystallized samples, as discussed in the preceding section. These results further confirm that polymer crystallization plays a significant role in determining the emission properties of the curcumin-PLLA. Temperature-dependent PL studies showed that the emission intensity decreased slightly with increasing temperature up to 90 °C and the emission maxima reduced slightly from 527 nm to 520 nm (Figure 4.11c). The difference in the emission intensity with respect to the temperature is mainly due to the thermal induced fluorescence decay at higher temperatures. On the other hand, the change in the

emission maxima is due to the change in the dihedral angle between two phenyl rings in curcumin. A slight reduction of the emission maxima up to 90 °C indicates that the single crystals of curcumin-PLLA are quite stable and no major conformational changes occurred both in PLLA chains and curcumin up to the melting of single crystals (90 °C).

#### 4.5.5. Emission Behavior of Curcumin-PLLA Gel

To further understand the influence of the polymorphic form of PLLA and the solvent on the emission properties of curcumin-PLLA, gels were prepared in N,N-dimethylformamide (DMF). PLLA is known to form gels in particular solvents that favor the formation of co-crystals or crystalline complexes ( $\epsilon$  form).<sup>30, 66-68</sup> Figure 4.12a shows the photograph of curcumin-PLLA gel in DMF solvent under UV light, along with the POM image. Curcumin-PLLA gel appeared greenish yellow under UV light. Our earlier studies reported that in PLLA, the formation of the gel is mainly caused by the fibrillar morphology.<sup>30</sup> The POM image shows the dendritic spherulites with numerous branches without any periodically ringed structures.

Figure 4.12b depicts the temperature-dependent WAXS data of the curcumin-PLLA gel during the heating. The room temperature WAXS pattern showed various X-ray reflections which are corresponding to the  $\epsilon$  crystalline form of PLLA at  $2\theta = 11.7^\circ, 14.1^\circ, 15.6^\circ, 18.3^\circ, 19.2^\circ, 20.6^\circ, 22.3^\circ, 23.5^\circ,$  and  $29.1^\circ$ , where DMF solvent molecules are trapped within the crystal lattice of PLLA.<sup>53</sup> It suggests that the covalent linkage of curcumin to PLLA has no influence on the gel formation as well as the formation of the  $\epsilon$  crystalline form. Similar to PLLA gels, upon heating, the  $\epsilon$  form transformed into the  $\alpha$  form ( $2\theta = 14.8^\circ, 16.8^\circ, 19.1^\circ, 20.8^\circ, 22.4^\circ, 25.0^\circ$  and  $27.7^\circ$ ) close to the glass transition temperature of PLLA in the gel state due to the segmental mobility of the polymer chains in amorphous region. As reported, the conformational reorganization of PLLA helical

---

chains occurred during this crystal-to-crystal transition by excluding the DMF solvent molecules from the  $\epsilon$  crystal lattice to the amorphous phase.<sup>30, 55</sup> On further heating, the  $\alpha$  crystals melt to obtain a homogeneous solution at 90 °C. The information garnered from the temperature-dependent WAXS results is helpful for understanding the temperature-dependent fluorescence behavior of curcumin-PLLA gels.

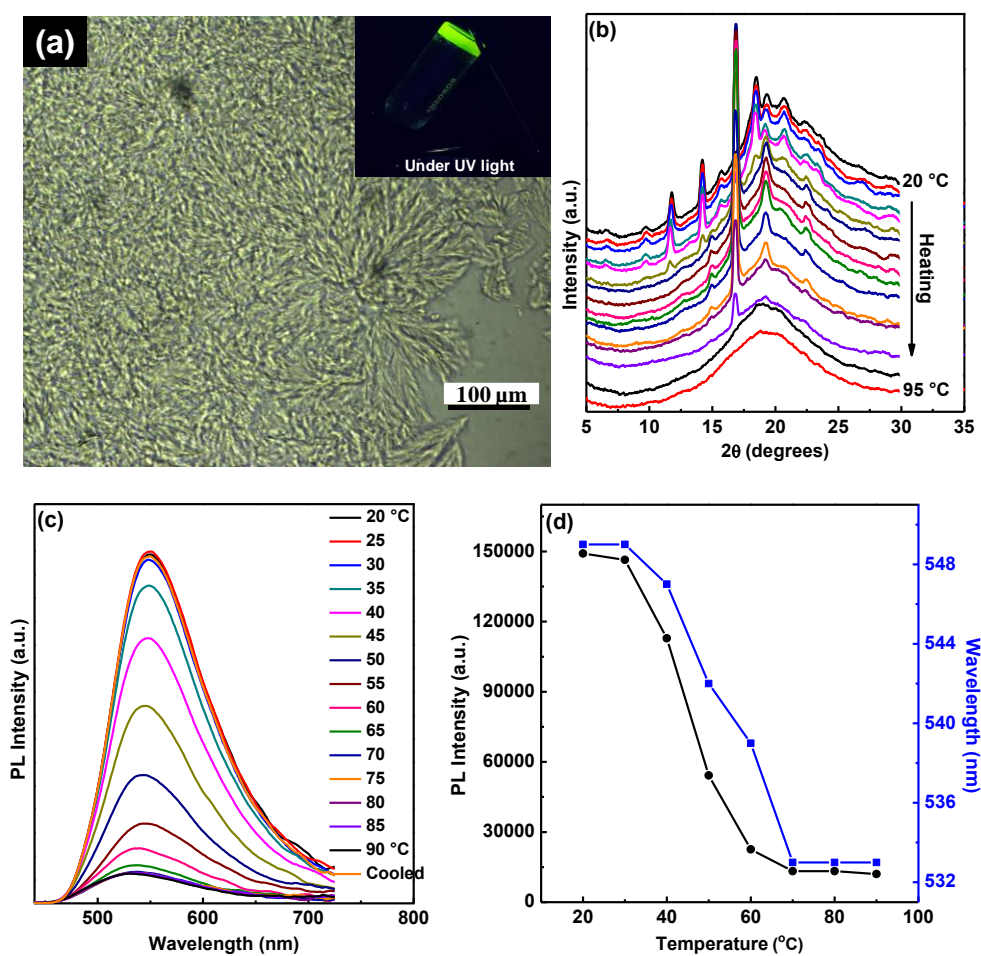


**Figure 4.12.** (a) Photographs of curcumin-PLLA gel under UV light, and POM image curcumin-PLLA gel under polarized light. Temperature-dependent (b) WAXS patterns, (c) emission spectra and (d) PL intensity and wavelength of curcumin-PLLA gel during the heating process.

Figure 4.12c shows the temperature-dependent PL spectra of curcumin-PLLA gel. At room temperature, the PL spectrum of curcumin-PLLA gel showed a broad peak with an emission maximum of 549 nm, different from the curcumin-PLLA single crystals in DMA (527 nm). Khopde et al. reported that the polarity and dielectric constant of the solvent plays a vital role in tuning the emission behavior of curcumin.<sup>69</sup> Figure 4.13 illustrates the schematic representation of  $\epsilon$  to  $\alpha$  transition of curcumin-PLLA gel upon heating. As evident from WAXS, curcumin-PLLA forms the crystal complex ( $\epsilon$ -form) in the gel state at 20 °C, where DMF solvent molecules are settled within in the crystal lattice (crystalline lamellae) as well as in the amorphous phase of PLLA (Figure 4.13a). In the crystal complex, covalently linked curcumin molecules are settled at the interface of the crystalline lamellae and amorphous phase or in the amorphous phase. At room temperature, curcumin-PLLA emits strongly and upon heating, the PL intensity reduced drastically in the temperature range of 40 – 60 °C, where the structural change from the  $\epsilon$  form to the  $\alpha$  form occurred, as evident from the WAXS results (Figure 4.12d). At the same time, the emission maxima blue-shifted with the increase in the temperature and stabilized at 533 nm after the crystal-to-crystal transition ( $\epsilon$ -to- $\alpha$ ). During the transition, the  $10_7$  left-handed helical PLLA chains of the  $\epsilon$  form momentarily pass through a disordered state before the formation of the stable  $\alpha$  form with  $10_7$  left-handed helical PLLA chains. At the same time, the DMF molecules which are residing within the crystal lattice of the  $\epsilon$  form are excluded into the amorphous phase of the  $\alpha$  form during the  $\epsilon$ -to- $\alpha$  transition (Figure 4.13b). Such a conformational change of PLLA chains resulted in the intramolecular rotations of the covalently linked phenyl rings (dihedral angle between two phenyl rings), and is responsible for the change in the emission behavior due to the change in the intramolecular conjugation length of curcumin. At higher temperatures, the dynamic nature of polymer chains in amorphous region leads to the reduction of PL intensity even in the

---

semicrystalline state ( $\alpha$  phase). In the melt state (clear solution), curcumin-PLLA emits weakly as seen in Figure 4.13c. These results are different from the curcumin-PLLA single crystals in DMA, where such a drastic change in the emission behavior was not observed during the heating process. In this way, we found that polymer crystallization and polymorphic form of PLLA play significant role in determining the emission properties of covalently linked curcumin. The emission color contrast is quite significant; thus such stimuli-responsive emitters can be used as smart packaging materials.

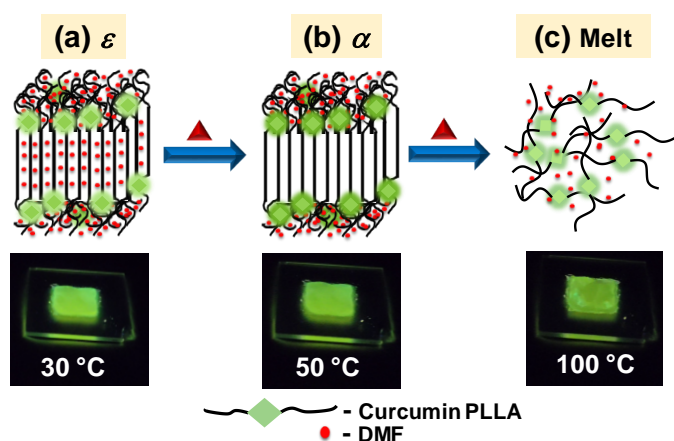


**Figure 4.13.** Schematic illustration of crystal-to-crystal transition and emission behavior of curcumin-PLLA gel during the heating process.

#### 4.6. Conclusions

In summary, curcumin-PLLA was synthesized and the role of PLLA crystallization, morphology and polymorphic form on the photophysical properties of curcumin was investigated. The solvent-crystallized curcumin-PLLA shows emission at 508 nm and it red-shifts to 578 nm and 589 nm for the melt-crystallized sample at 140 °C and melt-quenched (amorphous) sample, respectively. These results prompted us to systematically investigate the impact of isothermal crystallization temperature on the fluorescence



behavior of curcumin-PLLA. It was found that the increase of isothermal crystallization temperature resulted in the bathochromic shift in the fluorescence of curcumin-PLLA. Detailed crystallization studies revealed that different lamellar twisting in the polymeric spherulites was developed depending on the temperatures used for isothermal crystallization, which is mainly because of the chirality transfer from the chiral PLLA chains to the macroscopic level and it caused the twisting of the terminal benzene groups in curcumin. The intramolecular rotations of the covalently linked phenyl rings (dihedral angle between two phenyl rings) are responsible for the change in the fluorescence behavior due to the change in the intramolecular conjugation length of curcumin. Further, single crystals and gels of curcumin-PLLA were prepared using DMA and DMF as solvents, respectively, and investigated the temperature-dependent WAXS and PL studies to understand the role of solvents and crystal-to-crystal transition on the emission behavior of curcumin-PLLA. Both single crystals and gels of curcumin-PLLAs emit greenish yellow color. PLLA crystallized into the  $\alpha$  form in DMA and curcumin-PLLA is quite stable up to 90 °C. Only a slight change in the emission behavior is noticed while the heating of single crystals mainly due to the thermal induced fluorescence decay at higher temperatures. On the other hand, PLLA crystallized into the  $\epsilon$  form in curcumin-PLLA gels. WAXS studies revealed that the  $\epsilon$  crystalline form transformed to the  $\alpha$  crystalline form in a wide temperature range. During this crystal-to-crystal transition, PLLA helical chains momentarily pass through the disordered state by the expulsion of solvents from the crystal lattice which leads to the intramolecular rotations of the terminal benzene groups of curcumin and is responsible for the blue shift of emission due to the change in the conjugation length of curcumin. These findings demonstrate that the morphology and the crystallization of polymers could be crucial in defining the solid-state optical characteristics of fluorophores in fluorophore-embedded polymers.

---

#### 4.7. References

1. J. Mei, N. L. C. Leung, R. T. K. Kwok, J. W. Y. Lam and B. Z. Tang, *Chem. Rev.*, 2015, **115**, 11718-11940.
2. J. Wu, W. Liu, J. Ge, H. Zhang and P. Wang, *Chem. Soc. Rev.*, 2011, **40**, 3483-3495.
3. X. Feng, L. Liu, S. Wang and D. Zhu, *Chem. Soc. Rev.*, 2010, **39**, 2411-2419.
4. F. Cicoira and C. Santato, *Adv. Funct. Mater.*, 2007, **17**, 3421-3434.
5. Y. Chen, A. J. H. Spiering, S. Karthikeyan, G. W. M. Peters, E. W. Meijer and R. P. Sijbesma, *Nat. Chem.*, 2012, **4**, 559-562.
6. A. P. de Silva, H. Q. N. Gunaratne, T. Gunnlaugsson, A. J. M. Huxley, C. P. McCoy, J. T. Rademacher and T. E. Rice, *Chem. Rev.*, 1997, **97**, 1515-1566.
7. M. A. Baldo, D. F. O'Brien, Y. You, A. Shoustikov, S. Sibley, M. E. Thompson and S. R. Forrest, *Nature*, 1998, **395**, 151-154.
8. G. Niu, R. Zhang, J. P. C. Kwong, J. W. Y. Lam, C. Chen, J. Wang, Y. Chen, X. Feng, R. T. K. Kwok, H. H. Y. Sung, I. D. Williams, M. R. J. Elsegood, J. Qu, C. Ma, K. S. Wong, X. Yu and B. Z. Tang, *Chem. Mater.*, 2018, **30**, 4778-4787.
9. J. Luo, Z. Xie, J. W. Y. Lam, L. Cheng, H. Chen, C. Qiu, H. S. Kwok, X. Zhan, Y. Liu, D. Zhu and B. Z. Tang, *Chem. Commun.*, 2001, DOI: 10.1039/B105159H, 1740-1741.
10. J. Mei, Y. Hong, J. W. Y. Lam, A. Qin, Y. Tang and B. Z. Tang, *Adv. Mater.*, 2014, **26**, 5429-5479.
11. Y. Hong, J. W. Y. Lam and B. Z. Tang, *Chem. Commun.*, 2009, DOI: 10.1039/B904665H, 4332-4353.
12. Y. Hong, J. W. Y. Lam and B. Z. Tang, *Chem. Soc. Rev.*, 2011, **40**, 5361-5388.
13. R. Hu, N. L. C. Leung and B. Z. Tang, *Chem. Soc. Rev.*, 2014, **43**, 4494-4562.
14. Y. Dong, J. W. Y. Lam, A. Qin, J. Liu, Z. Li, B. Z. Tang, J. Sun and H. S. Kwok, *Appl. Phys. Lett.*, 2007, **91**, 011111.
15. C. Wang and Z. Li, *Mater. Chem. Front.*, 2017, **1**, 2174-2194.
16. J. Dai, L. Yao, C. Wang, Y. Wang, F. Liu, X. Yan, P. Sun, H. Zhang, Y. Wang, J. Zhou and G. Lu, *J. Phys. Chem. Lett.*, 2022, **13**, 4754-4761.
17. K. Wang, H. Zhang, S. Chen, G. Yang, J. Zhang, W. Tian, Z. Su and Y. Wang, *Adv. Mater.*, 2014, **26**, 6168-6173.
18. H. Y. Zhang, Z. L. Zhang, K. Q. Ye, J. Y. Zhang and Y. Wang, *Adv. Mater.*, 2006, **18**, 2369-2372.
19. W. Z. Yuan, Y. Tan, Y. Gong, P. Lu, J. W. Y. Lam, X. Y. Shen, C. Feng, H. H.-Y. Sung, Y. Lu, I. D. Williams, J. Z. Sun, Y. Zhang and B. Z. Tang, *Adv. Mater.*, 2013, **25**, 2837-2843.
20. Y. Sagara and T. Kato, *Angew. Chem. Int. Ed.*, 2011, **50**, 9128-9132.
21. W. Zhao, C. Li, B. Liu, X. Wang, P. Li, Y. Wang, C. Wu, C. Yao, T. Tang, X. Liu and D. Cui, *Macromolecules*, 2014, **47**, 5586-5594.
22. Y. Jiang and N. Hadjichristidis, *Macromolecules*, 2019, **52**, 1955-1964.
23. X.-H. Wang, N. Song, W. Hou, C.-Y. Wang, Y. Wang, J. Tang and Y.-W. Yang, *Adv. Mater.*, 2019, **31**, 1903962.
24. Z. Zhang, P. Bilalis, H. Zhang, Y. Gnanou and N. Hadjichristidis, *Macromolecules*, 2017, **50**, 4217-4226.

25. R. Taniguchi, T. Yamada, K. Sada and K. Kokado, *Macromolecules*, 2014, **47**, 6382-6388.
  26. J. Xu, W. Ji, C. Li, Y. Lv, Z. Qiu, L. Gao, E. Chen, J. W. Y. Lam, B. Tang and L. Jiang, *Adv. Opt. Mater.*, 2018, **6**, 1701149.
  27. Z. Qiu, X. Liu, J. W. Y. Lam and B. Z. Tang, *Macromol. Rapid Commun.*, 2019, **40**, 1800568.
  28. G. Liang, L.-T. Weng, J. W. Y. Lam, W. Qin and B. Z. Tang, *ACS Macro Lett*, 2014, **3**, 21-25.
  29. S. Nagarajan and E. B. Gowd, *Macromolecules*, 2017, **50**, 5261-5270.
  30. G. Virat and E. B. Gowd, *Polym. Chem.*, 2022, **13**, 838-849.
  31. M.-C. Li, H.-F. Wang, C.-H. Chiang, Y.-D. Lee and R.-M. Ho, *Angew. Chem. Int. Ed.*, 2014, **53**, 4450-4455.
  32. T.-S. Hsiao, P.-C. Huang, L.-Y. Lin, D.-J. Yang and J.-L. Hong, *Polym. Chem.*, 2015, **6**, 2264-2273.
  33. P. Anand, A. B. Kunnumakkara, R. A. Newman and B. B. Aggarwal, *Mol. Pharmaceutics*, 2007, **4**, 807-818.
  34. S. J. Hewlings and D. S. Kalman, *Foods*, 2017, **6**, 92.
  35. K. M. Nelson, J. L. Dahlin, J. Bisson, J. Graham, G. F. Pauli and M. A. Walters, *J. Med. Chem.*, 2017, **60**, 1620-1637.
  36. S. Zorofchian Moghadamtousi, H. Abdul Kadir, P. Hassandarvish, H. Tajik, S. Abubakar and K. Zandi, *Biomed Res. Int.*, 2014, **2014**, 186864.
  37. A. Goel, A. B. Kunnumakkara and B. B. Aggarwal, *Biochem. Pharmacol.*, 2008, **75**, 787-809.
  38. P. Sanphui and G. Bolla, *Cryst. Growth Des.*, 2018, **18**, 5690-5711.
  39. H. Hatcher, R. Planalp, J. Cho, F. M. Torti and S. V. Torti, *Cell. Mol. Life Sci.*, 2008, **65**, 1631-1652.
  40. R. K. Maheshwari, A. K. Singh, J. Gaddipati and R. C. Srimal, *Life Sci.*, 2006, **78**, 2081-2087.
  41. T. Ak and İ. Gülçin, *Chem. Biol. Interact.*, 2008, **174**, 27-37.
  42. A. J. Ruby, G. Kuttan, K. Dinesh Babu, K. N. Rajasekharan and R. Kuttan, *Cancer Lett.*, 1995, **94**, 79-83.
  43. Y.-J. Wang, M.-H. Pan, A.-L. Cheng, L.-I. Lin, Y.-S. Ho, C.-Y. Hsieh and J.-K. Lin, *J. Pharm. Biomed. Anal.*, 1997, **15**, 1867-1876.
  44. R. Jagannathan, P. M. Abraham and P. Poddar, *J. Phys. Chem. B*, 2012, **116**, 14533-14540.
  45. C. Banerjee, S. Maiti, M. Mustafi, J. Kuchlyan, D. Banik, N. Kundu, D. Dhara and N. Sarkar, *Langmuir*, 2014, **30**, 10834-10844.
  46. M. Cvek, U. C. Paul, J. Zia, G. Mancini, V. Sedlarik and A. Athanassiou, *ACS Appl. Mater. Interfaces*, 2022, **14**, 14654-14667.
  47. J. Zia, U. C. Paul, J. A. Heredia-Guerrero, A. Athanassiou and D. Fragouli, *Polymer*, 2019, **175**, 137-145.
  48. N. Luo, K. Varaprasad, G. V. S. Reddy, A. V. Rajulu and J. Zhang, *RSC Adv.*, 2012, **2**, 8483-8488.
-

49. L. D. Dias, K. C. Blanco, I. S. Mfouo-Tynga, N. M. Inada and V. S. Bagnato, *J. Photochem. Photobiol. C: Photochem. Rev.*, 2020, **45**, 100384.
  50. S. Sasaki and T. Asakura, *Macromolecules*, 2003, **36**, 8385-8390.
  51. J. Zhang, Y. Duan, H. Sato, H. Tsuji, I. Noda, S. Yan and Y. Ozaki, *Macromolecules*, 2005, **38**, 8012-8021.
  52. H. Marubayashi, S. Akaishi, S. Akasaka, S. Asai and M. Sumita, *Macromolecules*, 2008, **41**, 9192-9203.
  53. H. Marubayashi, S. Asai and M. Sumita, *Macromolecules*, 2012, **45**, 1384-1397.
  54. D. Sawai, K. Takahashi, A. Sasashige, T. Kanamoto and S.-H. Hyon, *Macromolecules*, 2003, **36**, 3601-3605.
  55. P. Shaiju, N. S. Murthy and E. B. Gowd, *Macromolecules*, 2016, **49**, 224-233.
  56. P. Sanphui, N. R. Goud, U. B. R. Khandavilli, S. Bhanoth and A. Nangia, *Chem. Commun.*, 2011, **47**, 5013-5015.
  57. R. W. Newberry and R. T. Raines, *Chem. Commun.*, 2013, **49**, 7699-7701.
  58. L. Shen, H.-Y. Zhang and H.-F. Ji, *Org. Lett.*, 2005, **7**, 243-246.
  59. B. Nagendra, C. V. S. Rosely, A. Leuteritz, U. Reuter and E. B. Gowd, *ACS Omega*, 2017, **2**, 20-31.
  60. J. Zhang, K. Tashiro, H. Tsuji and A. J. Domb, *Macromolecules*, 2008, **41**, 1352-1357.
  61. K. L. Singfield, J. K. Hobbs and A. Keller, *J. Crystal. Growth.*, 1998, **183**, 683-689.
  62. S. Nurkhamidah and E. M. Woo, *Colloid. Polym. Sci.*, 2012, **290**, 275-288.
  63. G. Solladié and R. G. Zimmermann, *Angew. Chem., Int. Ed.*, 1984, **23**, 348-362.
  64. X. Zhang, J. Wang, Y. Liu, Y. Hao, F. Yu, D. Li, X. Huang, L. Yu, T. Wang and H. Hao, *J. Phys. Chem. C*, 2021, **125**, 6189-6199.
  65. A. Rajak and A. Das, *Angew. Chem. Int. Ed.*, 2022, **61**, e202116572.
  66. N. M. Praveena, G. Virat, V. G. Krishnan and E. B. Gowd, *Polymer*, 2022, **241**, 124530.
  67. Y. Matsuda, A. Fukatsu, Y. Wang, K. Miyamoto, J. W. Mays and S. Tasaka, *Polymer*, 2014, **55**, 4369-4378.
  68. V. G. Krishnan, N. M. Praveena, R. B. A. Raj, K. Mohan and E. B. Gowd, *ACS Appl. Polym. Mater.*, 2023, **5**, 1556-1564.
  69. S. M. Khopde, K. Indira Priyadarsini, D. K. Palit\* and T. Mukherjee, *Photochem. Photobiol.*, 2000, **72**, 625-631.
-

## Chapter 5

---

---

### Overall Summary and Future Perspectives

---

---

### 5.1. Overall Summary

Fluorescent materials have attracted immense interest in recent decades due to their enormous applications in biosensors, bio-imaging, mechanochromism, optoelectronic devices, optical waveguides and organic light-emitting diodes. Incorporating fluorescent molecules into the polymers is expected to expand the application scope of fluorescent materials. The covalent incorporation of fluorescent molecules into polymers has several advantages, such as processability, solubility, mechanical stability, thermal stability and structural diversity. Currently, the development of biocompatible and biodegradable fluorescent polymers and understanding their fluorescent characteristics are highly desirable. The properties and performance of these materials are intrinsically linked to their molecular and hierarchical structures. Therefore, understanding the structure-property relationship is of great importance for the rational design of hybrid materials with optimized fluorescent properties and to promote their potential applications. The overall concept of the thesis is to develop color-tuneable semicrystalline polymers by incorporating suitable chromophores by covalent bonding into the backbone of polymers or the terminals of the polymers. Chromophore-embedded systems were prepared by ring-opening polymerization of L-lactide using chromophores as macroinitiators. The present thesis mainly focuses on understanding (i) the role of the number of substituted polymer chains on the aggregation-induced emission properties of fluorescent molecules, (ii) the effect of polymer chain length, crystallization and chain packing (polymorphism) on the photophysical properties of chromophores, and (iii) the influence of crystallization conditions and crystallization kinetics on the morphological and photophysical properties.

The first chapter provided a brief introduction on the importance of fluorescent-based systems and recent developments in the field of fluorescent-based polymers. This chapter also explains polymer crystallization highlighting the polymorphism and

---

cocrystals, and its role in controlling the photophysical properties of chromophore-embedded polymers.

In the second chapter, we have synthesized one-armed PLLA, two-armed PLLA and SSPLLA with a fluorophore TPE and investigated their AIE characteristics in the solution, aggregate and gel states. The synthesized polymers are non-emissive in good solvents and emit in the aggregated state. Compared to one-armed and two-armed PLLAs, SSPLLA emits strongly in the aggregated and gel states. In SSPLLA, four arms of TPE molecules are held covalently with PLLA chains and therefore, the emission behavior of core TPE is sensitive to the conformational changes (structural changes) of PLLA. In the case of SSPLLA gels in DMF, PLLA crystallized into the  $\varepsilon$  form and the large TPE molecules are excluded out of the crystalline phase. These gels emitted cyan light at 20 °C because intramolecular rotations of covalently linked phenyl rings are restricted. Upon heating, over a broad temperature range (30 – 40 °C), a significant blue-shift in its fluorescence is observed due to the crystal-to-crystal transition. The solvent expulsion during the crystal transition and the segmental mobility of amorphous chains (above  $T_g$ ) induce the rotation of phenyl rings of TPE, and are responsible for the blue shift of emission due to the change in the conjugation length of TPE. At higher temperatures, enhanced mobility of the amorphous chains leads to the complete quenching of emission due to the free rotation of phenyl rings of TPE. In the case of SSPLLA precipitate in DMA, PLLA was crystallized into the  $\alpha$  form at room temperature. The fluorescence emission decreased gradually with temperature and the blue shift was observed relatively at higher temperatures (above 50 °C) due to the vigorous mobility of amorphous chains.

In the third chapter, we synthesized anthracene-appended PLLAs and identified the suitable molecular weight polymer for investigating the excimer formation. For the first time, we successfully demonstrated that the crystallization and polymorphism of polymers

---

dictated the photophysical properties of the anthracene-appended PLLAs. The amorphous (melt-quenched) polymer predominantly emits in the dark blue region mainly from its monomeric state due to the fine dispersion of anthracene moieties throughout the polymer matrix. Crystallization of the polymer expels the anthracene moieties into the amorphous region or on the surface of crystals (in the case of single crystals). Crystallization of the PLLA chains into diamond-shaped crystals regulates the anthracene moieties to locate on the surface of the crystals and no evidence of  $\pi$ - $\pi$  stacking of anthracene moieties was observed in this case resulting in the dark blue emission similar to the amorphous thin films. In the semicrystalline state (melt-crystallized  $\alpha$  form and gel state ( $\varepsilon$  form)), covalently-linked anthracene moieties reside at the interface of crystalline and amorphous domains by either dipolar interactions or  $\pi$ -stacking. The  $\alpha$  form emits fluorescence in the cyan region that is mainly arising from both anthracene excimers and monomers. But in the case of gels ( $\varepsilon$  form), exclusive excimer emission was observed where the emission bands are located at 473, 505, and 560 nm indicating the formation of three types of excimers (i.e., anthracene moieties overlapping at an angle of  $55^\circ$  to each other, T-shaped excimers and sandwich-type excimers). These results suggested that the molecular arrangement of anthracene moieties can be modulated by changing the structure and morphology of anthracene-appended PLLA in different forms (amorphous, semicrystalline, single crystals, and gels).

In the fourth chapter, curcumin-PLLA was synthesized and the role of PLLA crystallization, morphology and polymorphic form on the photophysical properties of curcumin was investigated. The solvent-crystallized curcumin-PLLA shows emission at 508 nm and it red-shifts to 578 nm and 589 nm for the melt-crystallized sample at  $140^\circ\text{C}$  and melt-quenched (amorphous) sample, respectively. These results prompted us to systematically investigate the influence of isothermal crystallization temperature on the emission behavior of curcumin-PLLA. It was found that the increase in the isothermal

---



crystallization temperature resulted in the bathochromic shift in the fluorescence of curcumin-PLLA. Detailed crystallization studies revealed that different lamellar twisting in the spherulite was developed depending on the isothermal crystallization temperature because of the chirality transfer from the chiral PLLA chains to the macroscopic level and it caused the rotation of the terminal phenyl rings in curcumin. The intramolecular rotations of the covalently linked phenyl rings (dihedral angle between two phenyl rings) are responsible for the change in the emission behavior due to the change in the intramolecular conjugation length of curcumin. Both single crystals and gel of curcumin-PLLAs emit greenish-yellow color. The results obtained in this thesis work suggested that the polymer crystallization plays a significant role in controlling the photophysical properties of chromophore-embedded polymers. Further, the combination of biocompatible and biodegradable polymers and fluorophores is expected to open a new horizon in the biomedical area, such as medical and pharmaceutical fields and bio-imaging.

## 5.2. Future Perspectives

The results obtained in the present thesis provide an excellent scope for further studies, as discussed below.

- The present thesis revealed that the molecular weight of the polymer plays a significant role in the self-assembly of chromophores in chromophore-embedded polymer systems. The studies can be extended to new excimer-forming systems with optimized molecular weights of the polymers to obtain hybrid systems with high fluorescence efficiency.
  - Though the chiral polymer was used in this study to prepare the chromophore-embedded polymers, no focus was given to the influence of polymer chirality transfer on the chromophore organization. Therefore, it will be interesting to study
-

the chirality transfer from the polymer chains to the chromophores using vibrational circular dichroism and circularly polarized luminescence spectroscopy.

- The current thesis work mainly focused on single chromophore systems. It will be interesting to focus on the donor and acceptor systems using covalently linked enantiomers. The charge transfer complex formation can be evaluated systematically by using the stereocomplex formation approach.
-

## ABSTRACT

<b>Name of the Student:</b> <i>Gandu Virat</i>	<b>Registration No:</b> <i>10CC17A39006</i>
<b>Faculty of Study:</b> <i>Chemical Sciences</i>	<b>Year of Submission:</b> <i>2023</i>
<b>CSIR Lab:</b> <i>National Institute for Interdisciplinary Science &amp; Technology (CSIR-NIIST), TVM, Kerala</i>	<b>Name of the Supervisor:</b> <i>Dr. E. Bhoje Gowd</i>
<b>Title of the thesis:</b> <i>Structural and Photophysical Properties of Chromophores-Embedded Poly(Lactide)s</i>	

The present thesis focuses on the development of biodegradable and biocompatible fluorescent materials with color-tunable properties achieved via the incorporation of suitable chromophores by covalent bonding into the polymer backbone. The work carried out in the present thesis has been originated by conceiving the gradual development in the field of crystallization and photophysical properties of chromophore-embedded poly(L-lactide)s (PLLA). In the first working chapter, we synthesized 1-arm, 2-arm, SSPLLA polymers using tetraphenylethylene as a core molecule and studied the role of polymer chain packing on the emission properties and the effect crystal-to-crystal transition on the aggregation-induced emission behavior of tetraphenylethylene. In the second working chapter, excimer formation between the anthracene molecules explored in the anthracene-appended PLLAs in different states and the role of polymer crystallization on excimer emission is studied in detail. In the final working chapter, the influence of crystallization conditions on the morphological and photophysical properties of curcumin-embedded PLLA is studied. Overall studies reveal that the photophysical properties of these hybrid materials can be greatly influenced by their polymer chain packing and microstructure, which could find numerous applications in cutting-edge technological and biomedical fields and these results are summarized in the last chapter along with the future perspectives.

---

---

## LIST OF PUBLICATIONS

### Emanating from thesis work

1. Poly(L-lactide)s with Tetraphenylethylene: Role of Polymer Chain Packing in Aggregation-Induced Emission Behavior of Tetraphenylethylene.  
**G. Virat** and E. Bhoje Gowd\*  
*Polym. Chem.*, 2022,13, 838-849.
2. Impact of Polymer Chain Packing and Crystallization on Emission Behavior of Curcumin-Embedded Poly(L-lactide)s.  
**G. Virat**, K. K. Maiti, Amal Raj R B, and E. Bhoje Gowd\*  
Manuscript communicated to *Soft Matter*.
3. Polymer Crystallization Enabled Excimer Emission in Anthracene-Appended Poly(L-lactide)s.  
**G. Virat**, Mumthaz Salim, Jefin Parukoor Thomas and E. Bhoje Gowd\* -  
Manuscript communicated.

### Not Related to thesis

1. Stereocomplex Formation and Hierarchical Structural Changes During Heating of Supramolecular Gels Obtained by Polylactide Racemic Blends.  
N.M. Praveena, **G. Virat**, Vipin G. Krishnan and E. Bhoje Gowd  
*Polymer*, 2022, 241, 124530.
-

**LIST OF CONFERENCE PRESENTATIONS**


1. **G. Virat** and E. Bhoje Gowd, Role of Polymer Chain Packing on Photophysical Properties of Poly (L-lactide) Substituted Tetraphenylethylene, 2<sup>nd</sup> International Conference on Advanced Materials and Technology (ICMAT-20), held on January 16-18, 2020 at JSS Science and Technology University, Mysuru, India (**Best Poster Presentation Award**).
  2. **G. Virat** and E. Bhoje Gowd, Role of Polymer Chain Packing on Photophysical Properties of Poly (L-lactide) Substituted Tetraphenylethylene, 14<sup>th</sup> International Conference on Ecomaterials, 5-7, 2020, CSIR-NIIST, Thiruvananthapuram, India (Poster presentation).
  3. **G. Virat**, Amal Raj R. B., K.K. Maiti and E. Bhoje Gowd, Polymer Crystallization-Induced Emission Behavior in Curcumin-Appended Poly(L-lactide), International Conference on Chemistry and Applications of Soft Materials (CASM 2022), held on July 25-27, 2022 at CSIR-National Institute for Interdisciplinary Science and Technology, Thiruvananthapuram (Poster presentation).
  4. **G. Virat**, Amal Raj R. B., Kaustabh Kumar Maiti and E. Bhoje Gowd, Polymer Crystallization-Induced Emission Behavior in Curcumin-Appended Poly(L-lactide), 3<sup>rd</sup> International Conference on Crystal Engineering: From Molecule to Crystal (CE:FMC2022) held on 31 August- 02 September, 2022 at Pahalgam, Kashmir, India (Poster presentation).
  5. **G. Virat**, Amal Raj R. B., K. K. Maiti and E. Bhoje Gowd, Polymer Crystallization-Induced Emission Behavior in Curcumin-Appended Poly(L-lactide), SPSI MACRO 2022 - International Conference on Science and Technology of Polymers and Advanced Materials through Innovation, Entrepreneurship and Industry held on November 2-4, 2022 at Pune, India (Poster presentation).
  6. **G. Virat**, Mumthaz Salim, Jefin Parukoor Thomas and E. Bhoje Gowd, Polymer Crystallization Controlled Anthracene Excimer Emission in Anthracene Appended Poly (L-lactide)s, National Conference on New Developments in Polymeric Materials (DPM-2023) held on March 2-3, 2023, Thiruvananthapuram (Poster Presentation).
-

PAPER



Cite this: *Polym. Chem.*, 2022, **13**, 838

## Poly(L-lactide)s with tetraphenylethylene: role of polymer chain packing in aggregation-induced emission behavior of tetraphenylethylene†

G. Virat<sup>a,b</sup> and E. Bhoje Gowd  <sup>a,b</sup>

Development of biocompatible and biodegradable fluorescent polymers and understanding their fluorescent characteristics are highly desirable. In this work, we synthesized one-armed, two-armed and four-armed poly(L-lactide)s by ring-opening polymerization of L-lactide using hydroxyl functionalized tetraphenylethylenes (TPE) as a macroinitiator. PLLA with TPE is non-emissive in good solvents and it emits differently in the aggregate and gel states. Star-shaped poly(L-lactide) (SSPLLA) emits strongly compared to the one-armed and two-armed PLLAs in the gel state. Gels of SSPLLA in *N,N*-dimethylformamide (DMF) crystallized into the  $\epsilon$  form and emitted cyan light under UV illumination at room temperature. Temperature-dependent UV-vis spectroscopy, photoluminescence spectroscopy, X-ray diffraction and differential scanning calorimetry of SSPLLA/DMF gel in the heating process revealed that the emission behavior is sensitive to the structural changes of PLLA. Upon heating, the crystal structure of the SSPLLA gel transforms from the  $\epsilon$  to  $\alpha$  form over a broad temperature range. Such crystal-to-crystal transition of PLLA resulted in the rotation of phenyl rings of TPE and leads to a significant blue-shift in the fluorescence of SSPLLA due to the shorter intramolecular conjugation length. On further heating, even in the semicrystalline state ( $\alpha$  form), enhanced mobility of the amorphous chains leads to the complete quenching of emission due to the free rotation of phenyl rings of TPE. On the other hand, the precipitate of SSPLLA prepared using *N,N*-dimethylacetamide (DMA) crystallized into the  $\alpha$  form. Unlike gel, the fluorescence emission decreased gradually with temperature and the blue shift was observed relatively at higher temperatures due to the vigorous mobility of amorphous chains. We believe that bio-based polymers with aggregation-induced emission (AIE) characteristics can find applications in bio-imaging and medical/pharmaceutical fields.

Received 15th November 2021.

Accepted 3rd January 2022

DOI: 10.1039/d1py01539g

rsc.li/polymers

## Introduction

Fluorescent materials have attracted immense interest in recent decades due to their enormous applications in biosensors, bio-imaging, mechanochromism, optoelectronic devices, optical waveguides and organic light-emitting diodes.<sup>1–13</sup> Most of the fluorescent molecules exhibit reduced emission or are completely non-emissive in the aggregated or solid state due to self-quenching associated with the strong noncovalent interactions.<sup>14–16</sup> In contrast, some fluorescent

molecules are non-emissive in dilute solution and the fluorescence increases upon crystallization/self-assembly or aggregation.<sup>1,17–19</sup> The restricted rotation of chromophores in the aggregate or crystalline state is mainly responsible for aggregation-induced emission (AIE) due to the radiative decay of excitation.<sup>17,18,20–23</sup> This unusual phenomenon has been extensively studied in recent years using many AIE molecules such as tetraphenylethylenes, silole, stilbenes, distyrylanthracene, phenyleneethylenes, *etc.*<sup>1,23–34</sup> Among these, tetraphenylethylene (TPE) and its derivatives have been widely used to understand the fundamental emissive mechanism. The free rotation of the phenyl rings and partial twisting of the C=C bond in TPE lead to the fast nonradiative decay and quench the fluorescence emission in dilute solutions. On the other hand, the restriction of intramolecular rotation of the peripheral phenyl rings hinders the path of nonradiative transitions and enhances the fluorescence emission through radiative transitions.<sup>18,19,23,35</sup> Therefore, several strategies have been adopted to address the issue of restriction of intramolecular

<sup>a</sup>Materials Science and Technology Division, CSIR-National Institute for Interdisciplinary Science and Technology, Trivandrum 695 019, Kerala, India.  
E-mail: bhojegowd@niist.res.in; Fax: +91-471-2491712; Tel: +91-471-2515474

<sup>b</sup>Academy of Scientific and Innovative Research (AcSIR), Ghaziabad 201 002, India

†Electronic supplementary information (ESI) available: <sup>1</sup>H NMR, <sup>13</sup>C NMR, FTIR, GPC, PL spectra, fluorescence lifetime (aggregated and gel states), and TGA data of SSPLLA. Biocompatibility studies of SSPLLA. See DOI: 10.1039/d1py01539g

motions in TPEs to date and among them, covalent bond fixation of peripheral phenyl rings is one of the sensible strategies. The incorporation of AIE molecules into polymers is expected to expand the application scope of AIE materials.

The covalent incorporation of AIE molecules into polymers has several advantages such as processability, solubility, mechanical stability, thermal stability and structural diversity. Several synthetic strategies have been developed to synthesize AIE molecule incorporated polymers with different architectures such as linear, block, star, hyperbranched, dendritic, comb and cross-linked.<sup>20,22,25,34,36–40</sup> Owing to the structural diversity, the AIE properties of chromophores in these hybrid systems can be tuned in response to external stimuli such as light, heat, pH, solvents, *etc.*<sup>11,24,28,34,36,37,41</sup> The emission properties of these hybrid materials are sensitive to the packing structure and aggregation of fluorescent molecules. For example, the importance of molecular design in controlling the photophysical and optoelectronic behaviors is investigated in several star-shaped polymers for various applications.<sup>42–45</sup> Therefore, understanding the structure–property relationship is of great importance for the rational design of hybrid materials with optimized fluorescent properties and to promote their potential applications.

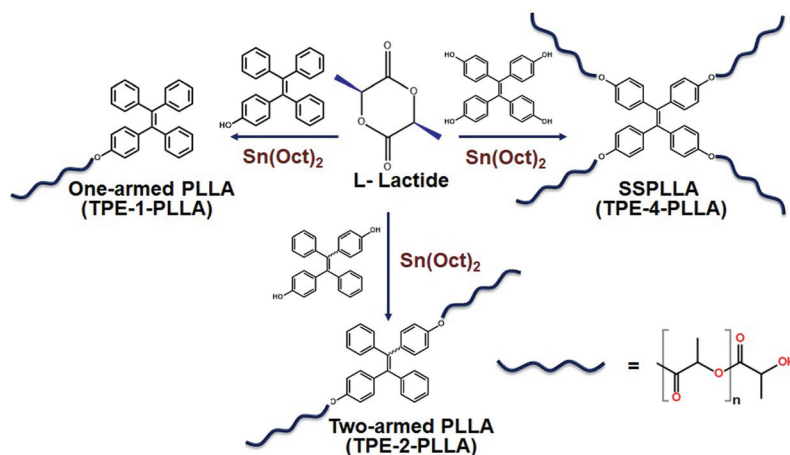
As for the AIE molecules, a few polymers carrying these molecules have been synthesized and tested for their emission behavior in response to multiple external stimuli.<sup>22,25–28,34,36,41,46,47</sup> For example, Taniguchi *et al.* synthesized poly(dimethylsiloxane) carrying TPE molecules and demonstrated the stimuli-sensitive fluorescence behavior of the hybrid system against organic solvents and temperature.<sup>34</sup> Zhang *et al.* synthesized AIE-active core cross-linked star polymers with polystyrene (PS), polyethylene (PE) or polyethylene-*b*-polycaprolactone (PE-*b*-PCL) and these polymers exhibited temperature-responsive emission behavior in tetrahydrofuran (THF)/*n*-hexane mixtures.<sup>27</sup> Using TPE-functionalized PE-based polymers, it was demonstrated that the micelle formation restricts the intramolecular rotation of TPE to enhance the fluorescence emission.<sup>25</sup> Xu *et al.* showed the reversible thermal-induced fluorescence behavior of TPE-labeled Nylon 6 and at a higher temperature, a blue shift in fluorescence was reported due to the rotation of phenyl rings of TPE.<sup>36</sup> Liang *et al.* reported the tuning of the fluorescent behavior by polymer crystallization using poly( $\epsilon$ -caprolactone) capped with TPE molecules and showed that these hybrid materials are sensitive to explosives.<sup>47</sup> Although significant works have been reported on AIE-labeled polymers by several groups, investigation on AIE-incorporated biodegradable and biocompatible synthetic polymers is extremely limited. In particular, the development of AIE in biomedicine and bio-imaging is of utmost importance and AIE-incorporated biodegradable and biocompatible polymers have great potential as bioprobes for real-time imaging and sensor applications.<sup>22,48,49</sup> Poly(L-lactide) (PLLA) is one of the most successful biodegradable polymers produced from renewable biomass. It exhibits five major crystalline forms, namely,  $\alpha$ ,  $\beta$ ,  $\gamma$ ,  $\delta$  ( $\alpha'$ ), and  $\epsilon$ .<sup>50–55</sup> Because of its intrinsic properties, many fluorescent molecules

have been incorporated into PLLA to afford unique functionalities.<sup>22,56–62</sup> Hsiao *et al.* showed that the crystallization of PLLA chains determines the AIE properties of 1,2-bis(2,4-dihydroxybenzylidene)hydrazine after incorporation into the backbone of PLLA.<sup>57</sup> Zhao *et al.* incorporated TPE into the PLLA chains by living chain transfer polymerization and demonstrated that these polymers exhibit unique emission properties in the aggregated states.<sup>22</sup> They have demonstrated that star-shaped PLLA (SSPLLA) was non-luminescent in good solvents like tetrahydrofuran (THF) and emits strongly when a poor solvent (water) was added due to aggregate formation. However, the influence of polymer chain packing and crystal structure of PLLA on the AIE behavior of core molecules in star-shaped polymers has rarely been reported. Furthermore, the influence of solvent molecules on the crystal structure and fluorescent behavior of SSPLLA has not been studied. In addition, the influence of crystalline transitions of PLLA on the fluorescent behavior of core molecules in SSPLLA was investigated using temperature-dependent wide-angle X-ray scattering (WAXS), UV-vis spectroscopy, and photoluminescence (PL) spectroscopy measurements.

This paper focuses on the role of polymer chain packing in the emission behavior of TPE molecules in one-armed, two-armed and four-armed PLLAs. Hydroxyl-modified tetraphenylethylenes (TPE) were used as macroinitiators to carry out the ring-opening polymerization of L-lactide. Compared to one-armed and two-armed PLLAs, four-armed PLLA (SSPLLA) shows strong emission in the aggregate and gel states. For that reason, SSPLLA was selected for a detailed study to understand the role of polymer chain packing in the emission behavior of the core molecule TPE. SSPLLA shows non-emissive behavior in good solvents (*e.g.*, chloroform) and typical AIE behavior in the aggregate and gel states. The fluorescence behavior of SSPLLA could be regulated by multiple factors, including solvents, polymer chain conformation, crystal-to-crystal transition of the host polymer and temperature. The change in the emission behavior of SSPLLA is attributed to the restriction of intramolecular rotation of the peripheral phenyl rings of core molecules induced by the chain conformation of arm PLLAs. We believe that the marriage of AIE molecules with biocompatible/biodegradable polymers will impart remarkable fluorescent properties and lead to a new way with fascinating functions and applications in medical and pharmaceutical fields and bio-imaging.

## Results and discussion

One-armed, two-armed and four-armed PLLAs were synthesized by ring-opening polymerization of L-lactide using TPE-1-OH, TPE-2-OH and TPE-4-OH, respectively, as macroinitiators and tin(II)ethylhexanoate (Sn(Oct)<sub>2</sub>) as the catalyst as depicted in Scheme 1. The chemical structures of various PLLAs were confirmed by <sup>1</sup>H NMR (Fig. 1 and Fig. S1†), <sup>13</sup>C NMR (Fig. S1 and Table S1†) and FTIR (Fig. S2 and Table S1†). The number average molecular weights ( $M_n$ ) and molecular



**Scheme 1** Synthesis of one-armed, two-armed and four-armed PLLAs with tetraphenylethylene.

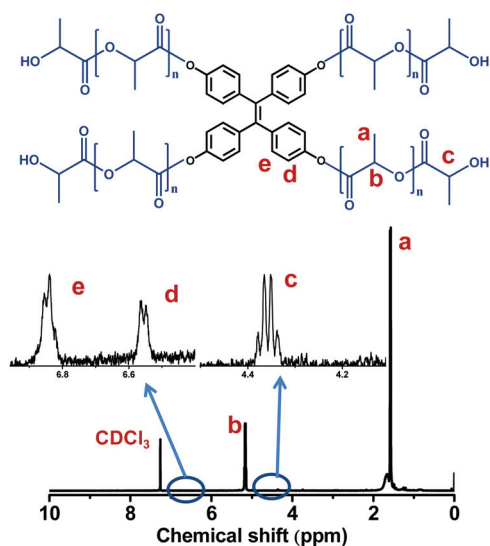


**Fig. 1**  $^1\text{H}$  NMR spectrum of SSPLLA with tetraphenylethylene as the core molecule.

weight distributions ( $D$ ) of various PLLAs were measured using GPC (Table 1 and Fig. S3†). The absolute molecular weights of various PLLAs were estimated from  $^1\text{H}$  NMR using the reported procedure.<sup>63</sup> Differential scanning calorimetry (DSC) thermograms (Fig. 2a) of one-armed PLLA, two-armed PLLA and SSPLLA show no peaks during cooling, indicating that the crystallization rates of various PLLAs are relatively slow and upon

reheating, multiple transitions corresponding to glass transition ( $T_g$ ), cold-crystallization ( $T_{cc}$ ) and melting ( $T_m$ ) are observed (Table 1). No traces of crystallization and melting of TPE molecules were observed. The wide-angle X-ray scattering (WAXS) patterns of the cold-crystallized PLLAs (Fig. 2b) show X-ray reflections corresponding to the  $\alpha$  form of PLLA at  $2\theta = 14.8^\circ$  (010),  $16.8^\circ$  (110/200),  $19.1^\circ$  (203),  $20.8^\circ$  (204),  $22.4^\circ$  (015), and  $27.7^\circ$  (207)<sup>50</sup> and no additional crystalline reflections were observed, indicating the purity of the synthesized samples. In the  $\alpha$  form, left-handed  $10_7$  helical chains are packed in the orthorhombic unit cell.<sup>50,64</sup> Sakamoto and Tsuji investigated the effect of branching on the crystallization behavior of one-armed PLLA, two-armed PLLA and branched PLLA and demonstrated that the crystal growth mechanism is not affected by the presence of branching.<sup>63,65</sup> PLLA is known to form crystalline complexes or co-crystals ( $\epsilon$  form) with particular solvents such as  $N,N$ -dimethylformamide (DMF), cyclopentanone (CPO), and THF at temperatures below  $-5^\circ\text{C}$ .<sup>53,55</sup> It was recently reported that the solvents favoring the  $\epsilon$  form could form PLLA gels by dissolving PLLA at higher temperatures and subsequent cooling of the solutions to room temperature or sub-ambient temperatures.<sup>66</sup> Fig. 2c shows the WAXS patterns of one-armed PLLA, two-armed PLLA and SSPLLA gels in DMF at room temperature. All the WAXS patterns show X-ray reflections at  $2\theta = 9.8^\circ$  (111),  $11.9^\circ$  (200),  $14.1^\circ$  (020),  $15.7^\circ$  (121/114),  $18.5^\circ$  (123),  $19.5^\circ$  (223),  $20.8^\circ$  (116) and  $23.8^\circ$  (117) corresponding to the  $\epsilon$  form of PLLA.<sup>53</sup> In the  $\epsilon$  form, PLLA chains are packed in the orthorhombic unit cell

**Table 1** Characterization of PLLAs synthesized in this study

Sample	$M_n^a$ (g mol $^{-1}$ )	$M_n^b$ (g mol $^{-1}$ )	$D^b$	$T_g$ ( $^\circ\text{C}$ )	$T_{cc}$ ( $^\circ\text{C}$ )	$T_m$ ( $^\circ\text{C}$ )	$X_c^c$ (%)
One-armed PLLA	8800	9195	1.28	46	90	159	27
Two-armed PLLA	13 800	14 600	1.32	50	105	162	23
SSPLLA	8900	9100	1.4	46	91	159	17

<sup>a</sup>  $M_n$  was estimated using  $^1\text{H}$  NMR. <sup>b</sup>  $M_n$  and  $D$  were estimated using GPC. <sup>c</sup>  $X_c$  was estimated using the WAXS patterns shown in Fig. 2(c).



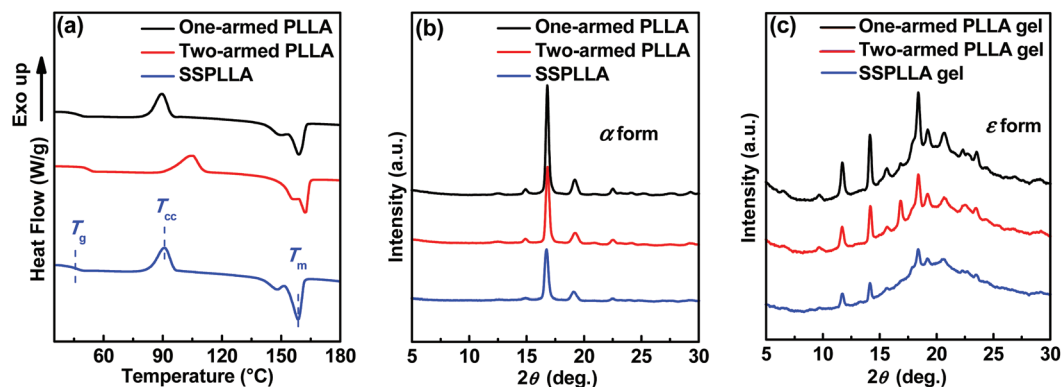


Fig. 2 (a) DSC reheating thermograms obtained at a rate of  $10\text{ }^{\circ}\text{C min}^{-1}$ , WAXS patterns of (b) cold-crystallized samples and (c) gels (in DMF) of one-armed PLLA, two-armed PLLA and SSPLLA.

and take the  $10_7$  helical chain conformation. SSPLLA gel formed is quite stable at room temperature.<sup>53</sup> The degree of crystallinity ( $X_c$ ) of PLLA decreased with the increase of the number of arms connected to the TPE (Table 1) and  $X_c$  of one-armed PLLA, two-armed PLLA and SSPLLA gels were estimated to be 27, 23 and 17%, respectively.

With the TPE-incorporated PLLAs in hand, we systematically characterized the influence of polymer chains on the optical properties of TPE by UV-vis absorption spectroscopy and the circular dichroism of SSPLLA as depicted in Fig. 3. The absorption spectrum of SSPLLA (Fig. 3a) in chloroform solution (good solvent) shows two bands around 244 nm and 325 nm corresponding to the  $n \rightarrow \pi^*$  transition of the carbonyl groups in PLLA<sup>67</sup> and the  $\pi \rightarrow \pi^*$  transition of the TPE unit, respectively.<sup>34,68</sup> When the poor solvent (hexane) was added into the SSPLLA solution, a hypsochromic shift of the C=O absorption band (236 nm) occurred due to the aggregation (formation of helical chains of PLLA). Wang *et al.* reported such a blue shift of the carbonyl band upon the crystallization of PLLA in bulk.<sup>69</sup> To further confirm the formation of helical PLLA chains, the CD spectrum of SSPLLA was measured in chloroform and a mixture of solvents (chloroform/hexane: 25/75 v/v) (Fig. 3b). The CD spectra show a positive Cotton effect

at 236 nm corresponding to the  $n \rightarrow \pi^*$  transition of the carbonyl group of PLLA and polymer chains adopt left-handed helical chain conformation.<sup>67</sup> It has to be noted that in a good solvent such as chloroform, SSPLLA chains adopt majorly random coil conformation (with a few short helices) because of the molecular level dissolution and the corresponding CD spectrum is less intense. This is labeled as the solution state. On the other hand, the addition of the poor solvent shows a large positive Cotton effect and the intensity of the CD band is significantly amplified compared to the chloroform solution due to the aggregation of PLLA chains (formation of more number of helical chains of PLLA). This situation is labeled as the aggregate state, where no crystals of PLLA are formed. For the purpose of comparison, the CD spectrum of SSPDLA was obtained under similar conditions, as shown in Fig. S4.† It is obvious that the CD spectrum of SSPDLA showed a mirror-imaged Cotton effect compared to SSPLLA, indicating the opposite handedness in the helical chains. On the basis of the coupled oscillator method, it was assigned that PLLA and PDLA adopt left- and right-handed helical chain conformations, respectively.<sup>70</sup> A similar observation was made in the cases of one-armed and two-armed PLLAs.

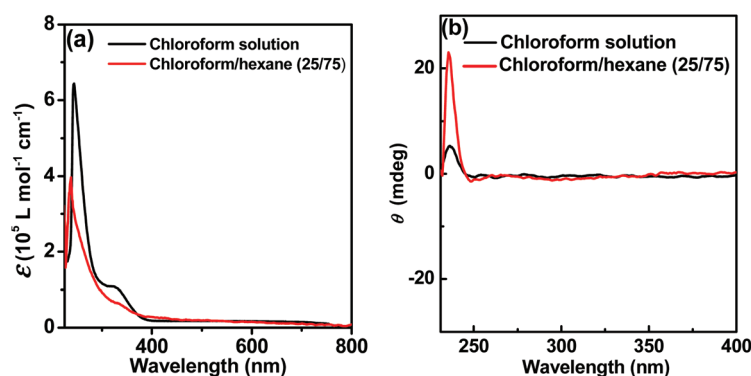


Fig. 3 (a) UV-vis absorption spectra (in the solution and aggregate states) and (b) CD spectra (in the solution and aggregate states) of SSPLLA with TPE core molecules.

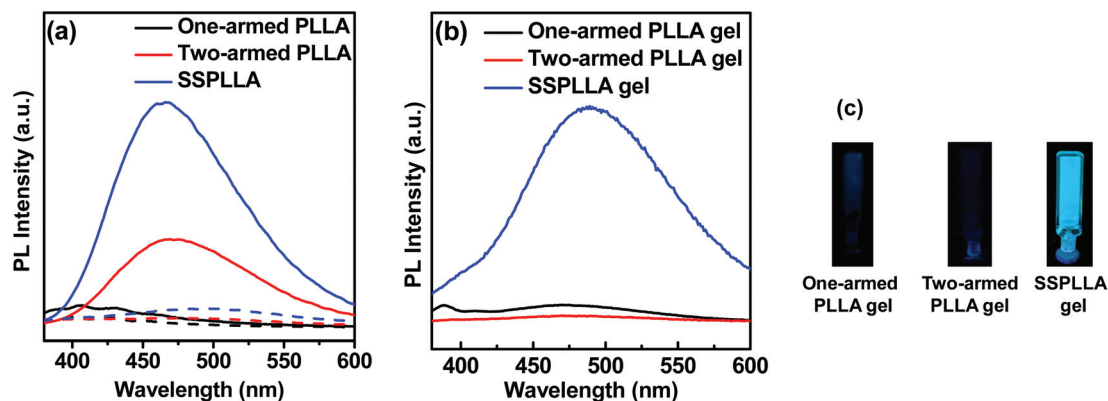


Fig. 4 PL emission spectra of one-armed PLLA, two-armed PLLA and SSPLLA (a) in the solution state (dashed lines), in the aggregate state (in the mixture of solvents chloroform/hexane 25/75 v/v) (thick lines), and (b) in the gel state. (c) Photographs of gels under UV light illumination.

Fig. 4 shows the emission spectra of one-armed PLLA, two-armed PLLA and SSPLLA in different states. As seen, the PL spectra of all the PLLAs dissolved in chloroform (solution state) show almost flat lines (dashed lines in Fig. 4a) indicating that the TPE-incorporated polymer is non-emissive in the completely dissolved state where most of the PLLA chains adopt random coil conformation with less number of aggregated helical chains. Interestingly, the emission intensity increased gradually with the increase of poor solvent (hexane) content in all the three polymers (the PL emission spectra of SSPLLA is shown in Fig. S5† as a representative) and the maximum emission was observed when the poor solvent content is around 75% (chloroform/hexane: 25/75 v/v) (aggregate state). However, the increase is quite significant in the case of SSPLLA. Similar to the aggregate state, SSPLLA emits strongly in the gel state (crystalline state) compared to the one-armed and two-armed PLLA gels (Fig. 4b) and the corresponding photographs of gels under UV-light illumination (Fig. 4c) further confirms the different emission behavior. In the gel state, the physical networks are formed through the crystallization of polymer chains and fiber-like structures exist. It was shown that PLLA takes  $10_7$  helical conformations both in aggregate and gel states.<sup>56,66</sup> It means that the change in the conformation of PLLA from random to helical chains has a significant influence on the TPE molecules and it is expected that the covalently linked PLLA chains alter the torsion angles of the peripheral phenyl rings and restrict their intramolecular rotation.<sup>1</sup> In the case of one-armed and two-armed PLLAs, the excited-state energy of TPE can be dissipated through the rotations of its free phenyl rings<sup>35</sup> (that are not covalently connected to PLLA) and that can result in the lower emission. In the gel state, the emission behavior of one-armed and two-armed PLLAs is almost similar because of the free rotations of the phenyl rings of TPE in the solvated amorphous phase (higher mobility of PLLA chains). On the other hand, in SSPLLA, all the phenyl rings are covalently connected to PLLA chains and these chains strongly restrict the intramolecular rotations of phenyl rings. Such a situation leads to the strong aggregation-induced emission of SSPLLA compared to one-armed and two-

armed PLLAs with TPE molecules. Zhao *et al.* reported a similar behavior in TPE-labeled star PLLA in a THF/water mixture, where the PLLA chains are connected to the TPE core through two ethylene glycol units.<sup>22</sup> In this way, we found that SSPLLA emits strongly both in the aggregate and gel states. Because of this reason, we have used this particular system for further studies. The fluorescence lifetime-decay profiles of SSPLLA with the TPE core in the aggregated state (in a chloroform/hexane mixture) and the gel state are shown in Fig. S6 and Table S2.† Both aggregated and gel states exhibited tri-exponential decay, with average lifetimes of 1.3 and 0.56 ns, respectively (see the ESI†). A slight increase in the lifetime of the aggregated state than that of the gel state may be due to the local environments caused by the restriction of intramolecular rotation of the peripheral phenyl rings with the branched polymer chains. To further get insights into the role of PLLA helical chains on the emission behavior of the TPE core, different crystalline forms of SSPLLA were prepared and systematically investigated using variable temperature UV-vis, PL and WAXS measurements.

The gel formation of SSPLLA in DMF was further confirmed by performing the viscoelastic measurements. Fig. 5a shows the dynamic frequency sweep tests conducted at 20 °C. The observed storage modulus ( $G'$ ) is higher than the loss modulus ( $G''$ ) in the frequency range of 0.1–100 rad s<sup>-1</sup>, a typical feature of supramolecular gels. These results are in good agreement with the reported data on PLLA/DMF gels.<sup>66</sup> Atomic force microscopy (AFM) image of the SSPLLA/DMF gel shows the entangled fibrillar networks having a length of a few micrometers as shown in Fig. 5b. The formation of fibrillar morphology is mainly responsible for the SSPLLA gels in DMF. As discussed in the preceding section, PLLA crystallized into the  $\epsilon$  form in SSPLLA/DMF gels. On the other hand, as shown in Fig. 5c, SSPLLA formed aggregate particle morphology in *N,N*-dimethylacetamide (DMA) and no gelation was observed in DMA, which might be due to the difference in the interactions between the polymer and solvent. In this case, SSPLLA leads to the formation of a precipitate and the WAXS pattern of this precipitate shows the typical  $\alpha$  form, as shown in a later

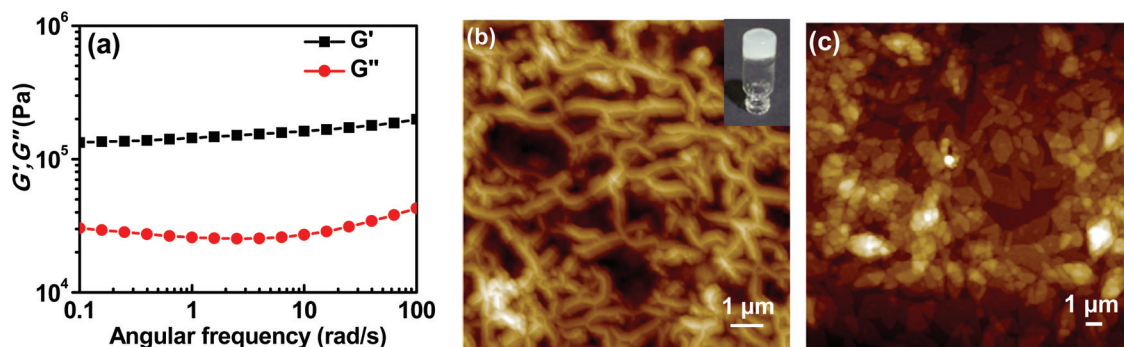


Fig. 5 (a) Plot of angular frequency ( $\omega$ ) versus dynamic storage modulus ( $G'$ ) and loss modulus ( $G''$ ) for PLLA gel in DMF at 20 °C, AFM height images of (b) PLLA gel in DMF ( $\epsilon$  form) (the inset shows the photograph of gel under room light) and (c) PLLA precipitate in DMA ( $\alpha$  form). The surface roughness of dried PLLA gel and PLLA precipitate are 10 and 8 nm, respectively.

section. In this way, solvents play a significant role in determining the crystal structure, morphology and physical state of SSPLLA.

To further understand the influence of PLLA chains on the aggregation properties of TPE, temperature-dependent UV-vis absorption and PL emission studies of SSPLLA/DMF gels and SSPLLA/DMA precipitates were carried out. Fig. 6 depicts the temperature-dependent UV-vis absorption spectra and PL emission spectra of SSPLLA/DMF gel. At 20 °C, the absorption spectrum of SSPLLA/DMF gel (Fig. 6a) shows two bands around 272 nm and 331 nm corresponding to the  $n \rightarrow \pi^*$  transition of the carbonyl groups in PLLA<sup>67</sup> and the  $\pi \rightarrow \pi^*$  transition of the TPE unit, respectively.<sup>34,68</sup> The band corresponding to the carbonyl groups in PLLA is red-shifted from 244 nm to 272 nm compared to the SSPLLA/chloroform solution, which may be due to the change in the polarity of solvent used (DMF) and the interactions between PLLA and DMF. Marini *et al.* reported that the polarity of the solvent plays a role in the fluorescent properties of solvated molecular probes.<sup>71</sup> As DMF is a polar solvent, the absorption spectrum of SSPLLA/DMF gel is red-shifted compared to the SSPLLA/

chloroform solution. Besides, the UV-vis spectrum showed a Mie scattering effect for the gel, indicating the existence of nanofibers. Upon heating, no change in the absorption spectra is observed up to 35 °C and above this temperature, a slight decrease in the intensity of bands is observed. At higher temperatures, above 80 °C, the Mie scattering effect disappeared, indicating the formation of a homogeneous solution. Fig. 6b shows the temperature-dependent PL emission spectra of SSPLLA/DMF gel. At low temperatures, gel emits strongly at 472 nm and the PL intensity decreased with the increase in the temperature. At around 35 °C, the emission peaks blue-shifted to 415 nm. Around 45 °C, a sudden quench in the PL emission is observed. To further understand the reason for these observations, we have carried out DSC and temperature-dependent WAXS studies of SSPLLA/DMF gels.

Fig. 7 shows the DSC thermogram and temperature-dependent WAXS patterns of the SSPLLA/DMF gel in the heating process. As seen in Fig. 7a, two transitions are observed in the temperature range of 30–120 °C. Matsuda *et al.* demonstrated the formation of  $\epsilon$  gels using PLLA in DMF and showed that the  $\epsilon$  to  $\alpha$  transition occurs over a broad temperature range of

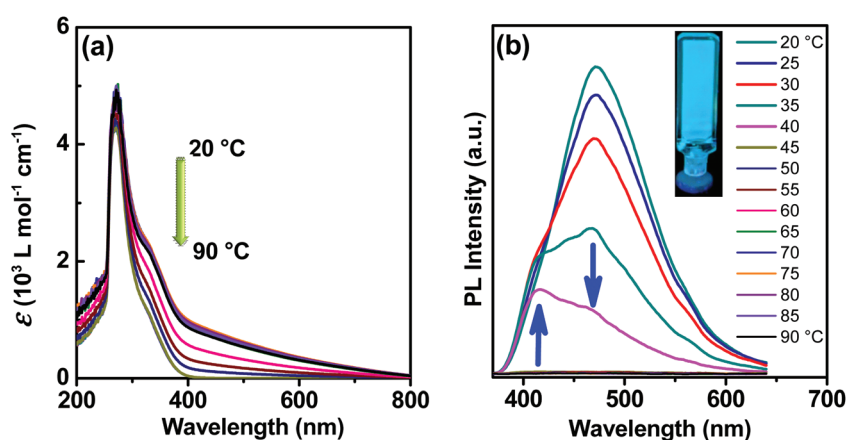


Fig. 6 Temperature-dependent (a) absorption and (b) emission spectra of the SSPLLA/DMF gel. The inset of (b) shows the photograph of gel under UV light illumination.

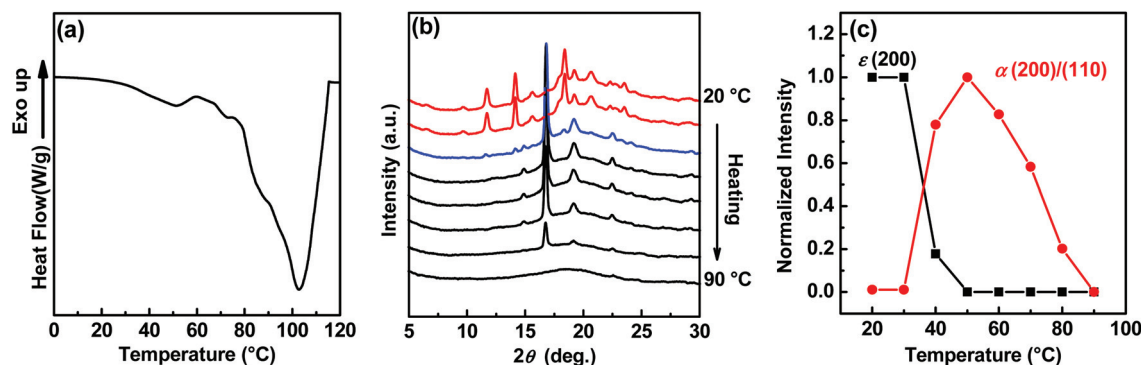


Fig. 7 (a) DSC thermogram during heating at  $10\text{ °C min}^{-1}$ , temperature-dependent (b) WAXS patterns and (c) normalized intensity of the reflections at  $2\theta = 11.2^\circ$  ( $\epsilon$ ), and  $16.6^\circ$  ( $\alpha$ ) evaluated from (b) during the heating process of SSPLLA/DMF gel.

27–42 °C.<sup>66</sup> The transition at 30–40 °C can be assigned to the crystal-to-crystal transition ( $\epsilon$  to  $\alpha$  form) and the onset of the transition temperature is around 30 °C. On further heating, a broad endothermic peak is observed at 104 °C, corresponding to the melting of the  $\alpha$  form. As seen in Fig. 7b, at 20 °C, several X-ray reflections corresponding to the  $\epsilon$  form appeared at  $2\theta = 11.7^\circ, 14.1^\circ, 15.6^\circ, 18.3^\circ, 19.2^\circ, 20.6^\circ, 22.3^\circ, 23.5^\circ,$  and  $29.1^\circ$  similar to the PLLA. This observation suggested that the presence of covalently linked TPE core molecules in SSPLLA has no influence on the formation of the  $\epsilon$  form in the gel state. As the TPE molecule is quite large in size, it is expected that these molecules will be excluded out of the crystalline lamellae and reside at the interface of the crystalline and amorphous phases or in the amorphous phase. In the  $\epsilon$  form (gel), DMF molecules are distributed both in the crystalline and amorphous phases. Upon heating, the intensity of the  $\epsilon$  form reflections started to decrease from 30 °C and completely disappeared at 50 °C. It was demonstrated that the mobility in the amorphous region (*i.e.*, glass transition temperature) triggers the  $\epsilon$  to  $\alpha$  transition upon heating.<sup>55</sup> At this transition temperature, DMF molecules residing within the crystal lattice of the  $\epsilon$  form are excluded into the amorphous state through the locally disordered helical chains and the structure is transformed to the new crystalline form. Based on the X-ray reflections ( $2\theta = 14.8^\circ, 16.8^\circ, 19.1^\circ, 20.8^\circ, 22.4^\circ, 25.0^\circ$  and  $27.7^\circ$ ), the new form was assigned to the  $\alpha$  form and it started appearing from 40 °C. At around 90 °C, the reflections corresponding to the  $\alpha$  form disappeared, indicating the melting of  $\alpha$  crystals. Fig. 7c shows the changes in the normalized intensities of representative reflection (200) of the  $\epsilon$  form and (200/110) of the  $\alpha$  form against temperature. Both DSC and WAXS results indicated that the structural reorganization in the crystal lattice occurred in a broad temperature range from 30–45 °C and in this temperature range, conformational reorganization of helical chains ( $10_7$  (left-handed  $10_3$ )) occurred within the crystal lattice due to the exclusion of DMF molecules from the crystal lattice of the  $\epsilon$  form to the amorphous phase of the  $\alpha$  form. In the case of gels, the solvent molecules reside in the polymer-poor phase or solvent phase (amorphous phase). It is

also worth mentioning here that the  $\epsilon$  to  $\alpha$  transition is irreversible as the obtained  $\alpha$  form is a stable form.

Based on the insights from temperature-dependent UV-vis spectroscopy, PL spectroscopy, WAXS and DSC, it is now possible to summarize the emission behavior of TPE in SSPLLA upon heating of the SSPLLA/DMF gel. Fig. 8 depicts the schematic representation of structural changes occurring upon heating of the SSPLLA/DMF gel. At 20 °C, SSPLLA/DMF gel forms the  $\epsilon$  form and the DMF molecules are distributed both in the crystalline and amorphous phases (Fig. 8a). In this case, polymer chains take the  $10_7$  (left-handed  $10_3$ ) helical conformation. In the  $\epsilon$  form, covalently linked TPE core molecules are excluded from the crystal lattice due to their large size and stabilized at the interface of the crystalline and amorphous phases or in the amorphous phase. As a result, all the covalently linked phenyl ring intramolecular rotations are restricted to give higher emissions. When heated, as evident from the DSC and WAXS, the crystal-to-crystal transition ( $\epsilon$  to  $\alpha$  transition) occurred in the broad temperature range of 30–40 °C and as a result, the solvent molecules residing in the crystal lattice of the  $\epsilon$  form are excluded into the amorphous phase of the  $\alpha$  form (Fig. 8b). Such a situation resulted in the change in the torsion angles of the peripheral phenyl rings. At the same time, the covalently linked PLLA chains still restrict the intramolecular rotation of the peripheral phenyl rings. As a result, PL emission blue-shifted due to the decrease in the conjugation length of TPE. Xu *et al.* reported a similar situation in the case of two-armed nylon labeled TPE.<sup>36</sup> It was also reported that the blue shift in TPEs occurred due to the change in the twist angle of the aromatic rings with respect to the ethylenic stator in the case of columnar liquid-crystalline materials based on TPEs and piezofluorochromic materials based on TPEs.<sup>72,73</sup> Such a twist changes the torsion angle of phenyl rings; as a result, the conjugation length reduces, resulting in the blue emission. On further heating, just above the transition temperature, drastic quenching in the PL emission is observed (Fig. 6b) even though the structure remained in the crystalline state ( $\alpha$  crystal) (Fig. 8c). We might have two possibilities to explain the quenching behavior of TPE above

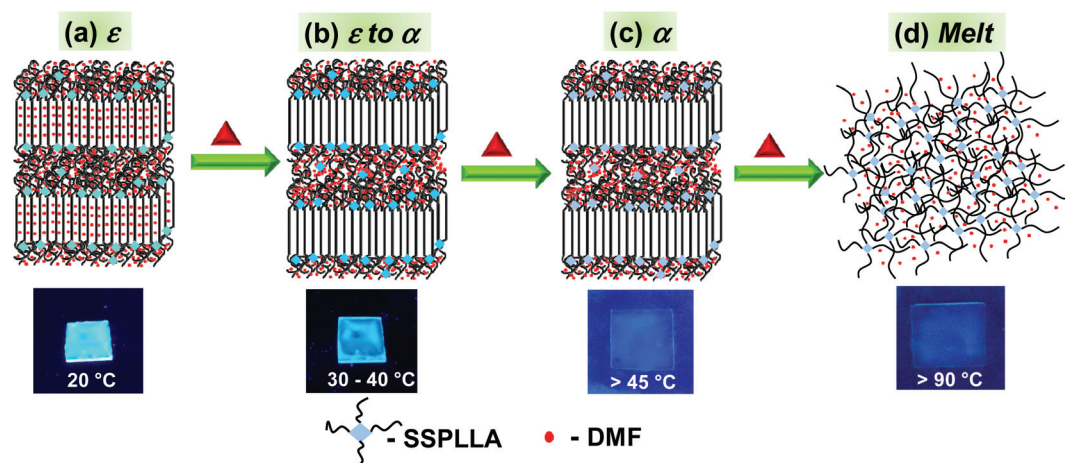


Fig. 8 Schematic representation of structural changes and emission behavior of SSPLLA/DMF gel during the heating process.

the transition temperature. For example, the thickness of the solvated amorphous phase may increase due to the expulsion of solvents from the crystal lattice of the  $\epsilon$  form above the  $\epsilon$  to  $\alpha$  transition, and this situation leads to the reduction of the concentration of TPE molecules in the solvated amorphous phase. Another possibility is that the vigorous mobility of the amorphous chains at higher temperatures results in the free rotation of the phenyl rings of TPE in the solvated amorphous phase to completely quench PL emission even though the PLLA is in the semicrystalline state ( $\alpha$  crystal). On further heating, around 90 °C, the crystals melt and a clear solution is formed in which phenyl ring free rotation is possible (Fig. 8d). Until today, solvents forming PLLA gels with  $\alpha$  crystals are not reported. To further prove that the PL emission quenching is happening mainly due to the mobility of the amorphous chains and not due to the arrangement of polymer chains in the  $\alpha$  form, further investigations were carried out using the  $\alpha$  form of SSPLLA.

Fig. 9 shows the temperature-dependent UV-vis absorption spectra, PL emission spectra and WAXS patterns of the SSPLLA/DMA precipitate in the heating process. At 20 °C, the

absorption spectrum of the SSPLLA/DMA precipitate (Fig. 9a) shows two bands at 264 nm and 330 nm corresponding to the carbonyl groups in the PLLA and TPE units, respectively. Upon heating, no change in the absorption spectra is observed in the entire temperature range. Unlike SSPLLA/DMF gel, in this case, no Mie scattering effect is observed due to the absence of the nanofibrillar morphology (Fig. 5c). Room temperature PL emission spectrum (Fig. 9b) of the SSPLLA/DMA precipitate shows strong emission at 472 nm and the PL intensity decreased gradually with the increase in the temperature. Unlike the SSPLLA/DMF gel ( $\epsilon$  form), the precipitate ( $\alpha$  form) shows emission peaks even at 70 °C. Similar to the observations made in the  $\epsilon$  gel case, the emission peak is blue-shifted to 415 nm (with lesser intensity) but at a higher temperature, *i.e.*, 50 °C. This blue-shift is mainly due to the change in the torsion angle of phenyl rings, which resulted in the reduction of the conjugation length of TPE. On further heating, above 75 °C, complete quenching of PL emission was observed. Fig. 9c shows the temperature-dependent WAXS patterns of the SSPLLA/DMA precipitate. As discussed in the preceding section, SSPLLA precipitates in DMA and shows aggre-

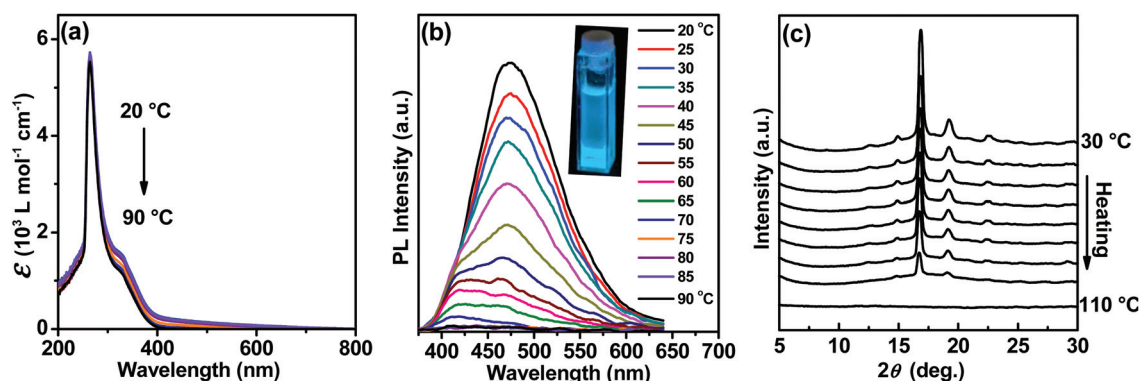


Fig. 9 Temperature-dependent (a) absorption and (b) emission spectra and (c) WAXS patterns of the SSPLLA/DMA precipitate. The inset of (b) shows the photograph of the precipitate under UV light illumination.

gate particle morphology, as shown in Fig. 5c. The room temperature WAXS pattern shows reflections corresponding to the typical  $\alpha$  form. Upon heating, the structure remained in the  $\alpha$  form until melting at 110 °C. Unlike SSPLLA/DMF gel, no crystal transition was observed in the case of the SSPLLA/DMA precipitate. As observed in Fig. 9b, the PL emission decreases gradually with temperature and a small shoulder at 417 nm was observed due to the change in the torsion angle of the phenyl rings in the temperature range of 50–70 °C. It means that even in the  $\alpha$  form (precipitate), at room temperature, the intramolecular rotations of phenyl rings of TPE are restricted to give higher emission similar to the SSPLLA/DMF gel ( $\epsilon$  form). At the higher temperatures (above 50 °C), because of the higher mobility of the amorphous chains, the torsion angles of phenyl rings change, which resulted in the blue shift due to the change in the conjugation length of TPE molecules. The different emission behavior of  $\alpha$  form at the higher temperature in the case of SSPLLA/DMF and SSPLLA/DMA is mainly due to the difference in the polarity of the solvents and the interactions between PLLA and solvent molecules. On further heating, above 75 °C, complete quenching of PL emission was observed due to two possible reasons. For example, above 75 °C, partial melting of  $\alpha$  crystals and the segmental mobility of PLLA chains in the amorphous phase cause complete quenching. Another possibility is the conventional thermal-induced fluorescence decay at higher temperatures.

To further evaluate the biocompatibility of SSPLLA, cytotoxicity assessment and antibacterial studies were carried out. Cytotoxicity of the SSPLLA was examined using the human lung fibroblast cell line WI-38. The viability of the WI-38 cell line was evaluated by the 3-(4,5-dimethylthiazol-2-yl)-2,5-diphenyltetrazolium bromide (MTT) assay as previously reported by Maiti and co-workers.<sup>74</sup> WI-38 cells were incubated at various concentrations of SSPLLA (1, 5, 10, 50, 100  $\mu\text{g mL}^{-1}$ ) for 6, 12 and 24 h. The insoluble formazan crystals formed were solubilized by the addition of 100  $\mu\text{L}$  of MTT lysis buffer followed by an incubation of 4 h; the absorbance was measured at 570 nm using a microplate spectrophotometer (BioTek, Power Wave XS). As shown in Fig. S7,† SSPLLA did not exhibit any noticeable toxicity, whereas Dox-induced toxicity was observed. The bacterial growth on SSPLLA/DMF gel was tested against three species of pathogens: *E. coli* DH5 $\alpha$ , *E. coli* and *S. aureus*, as shown in Fig. S8.† DMF was used as a control. After spreading the bacteria, the plates were sealed and incubated at 37 °C for 36 h. The uniform growth of bacteria was observed both on sample and control, suggesting that the SSPLLA possessed bacterial activity of both the Gram-negative and Gram-positive pathogens. These experiments further confirm the nontoxic nature of SSPLLA.

## Conclusions

In summary, we have synthesized one-armed PLLA, two-armed PLLA and SSPLLA with a fluorophore TPE and investigated their AIE characteristics in the solution, aggregate and gel

states. The synthesized polymers are non-emissive in good solvents and emit in the aggregated state. Compared to one-armed and two-armed PLLAs, SSPLLA emits strongly in the aggregated and gel states. In SSPLLA, four arms of TPE molecules are held covalently with PLLA chains and therefore, the emission behavior of the TPE core is sensitive to the conformational changes (structural changes) of PLLA. In the case of SSPLLA gels in DMF, PLLA crystallized into the  $\epsilon$  form and the large TPE molecules are excluded out of the crystalline phase. These gels emitted cyan light at 20 °C because the intramolecular rotations of the covalently linked phenyl rings are restricted. Upon heating, over a broad temperature range (30–40 °C), a significant blue-shift in its fluorescence is observed. WAXS and DSC revealed that the structure of SSPLLA was transformed from the  $\epsilon$  to  $\alpha$  form in this temperature range by the expulsion of solvents from the crystal lattice. The solvent expulsion and the segmental mobility of amorphous chains (above  $T_g$ ) induce the rotation of the phenyl rings of TPE and are responsible for the blue shift of emission due to the change in the conjugation length of TPE. At higher temperatures, the enhanced mobility of the amorphous chains leads to the complete quenching of emission due to the free rotation of the phenyl rings of TPE. In the case of the SSPLLA precipitate in DMA, PLLA was crystallized into the  $\alpha$  form at room temperature. The fluorescence emission decreased gradually with temperature and the blue shift was observed relatively at higher temperatures (above 50 °C) due to the vigorous mobility of the amorphous chains. The combination of biocompatible and biodegradable polymers and AIE fluorophores is expected to open a new horizon in the biomedical area, such as the medical and pharmaceutical fields and bioimaging.

## Experimental

### Materials

L-Lactide monomer, tin(II) ethylhexanoate Sn(Oct)<sub>2</sub>, chloroform, dry toluene and hexane were purchased from the Sigma-Aldrich chemical company. D-Lactide was supplied by Jinan Daigang Biomaterials, China. Methanol, ethyl acetate, N,N-dimethylformamide (DMF), and N,N-dimethylacetamide (DMA) were purchased from Merck Chemicals. The L-Lactide monomer was recrystallized before polymerization with ethyl acetate as solvent. Hydroxyl-modified tetraphenylethylenes (TPE-1-OH, TPE-2-OH and TPE-4-OH) were purchased from TCI chemicals and used without further purification.

### Synthesis of one-armed, two-armed and SSPLLA

Ring-opening polymerization was used to synthesize one-armed PLLA (TPE-1-PLLA), two-armed PLLA (TPE-2-PLLA) and SSPLLA (TPE-4-PLLA). Details of the polymerization of SSPLLA are as follows. A mixture of L-lactide (3.7 g), TPE-4-OH (10.4 mg), Sn(Oct)<sub>2</sub> (2 drops) and dry toluene (40 ml) was stirred under an inert atmosphere at room temperature for 1 h to remove air. Then the reaction was carried out at 140 °C for

4 h under a nitrogen atmosphere. The obtained polymer was dissolved in chloroform and purified twice by re-precipitation using methanol as a precipitant. The resultant precipitate was filtered and dried under reduced pressure at 40 °C for 12 h. For the purpose of comparison, SSPDLA was synthesized with comparable molecular weight ( $M_n = 9400 \text{ g mol}^{-1}$ ) by the same procedure, using D-lactide as the monomer. The same procedure was used to synthesize the other two polymers, TPE-1-PLLA and TPE-2-PLLA using TPE-1-OH and TPE-2-OH as macroinitiators, respectively. The chemical structures of the polymers were confirmed by  $^1\text{H}$  NMR. The number-average molecular weights of polymers were determined by GPC. In this work, we have prepared the lower molecular weight PLLAs in order to maintain a high concentration of TPE core molecules, so that the influence of polymer chain packing on the emission properties of the core molecules can be studied effectively.

### Sample preparation

**Preparation of SSPLLA gel.** 10 wt% of SSPLLA (TPE-4-PLLA) was dissolved in DMF at 120 °C and the solution was poured into a container. It was placed in a freezer overnight at  $-4$  °C for gelation. Gel formation was confirmed by the failure of the solvent to flow while inverting the container. Furthermore, the thermoreversible nature of the gels was confirmed by repeated heating and cooling processes. A similar procedure was used to prepare gels with one-armed PLLA (TPE-1-PLLA) and two-armed PLLA (TPE-2-PLLA).

**Preparation of SSPLLA precipitate.** 10 wt% of SSPLLA was dissolved in DMA at 120 °C and the solution was poured into a container. It was placed in a freezer overnight at  $-4$  °C. Unlike in DMF, SSPLLA forms precipitate in DMA.

### Characterization

$^1\text{H}$  NMR spectra were recorded using a 500 MHz Bruker Advance DPX spectrometer using tetramethylsilane (TMS) as an internal reference. The molecular weight and polydispersity ( $\mathcal{D}$ ) of the polymer were determined by GPC using an Agilent Technologies-1260 instrument with an RI detector, which is equipped with a PL-gel 20  $\mu\text{m}$  mixed bed column operated at 30 °C with THF as solvent (flow rate of  $1 \text{ mL min}^{-1}$ ). Molecular weight was measured using a standard calibration curve obtained using narrow polystyrene standards. DSC thermograms of solids and gels were carried out using a thermal analyzer (TA instrument Q2000) at a heating and cooling rate of  $10 \text{ }^\circ\text{C min}^{-1}$  under a  $\text{N}_2$  atmosphere. TGA thermogram was measured using a thermogravimetric analyzer (TA instruments Q50) under a nitrogen atmosphere and the polymer is thermally stable up to 205 °C (Fig. S9†). CD measurements were collected using a JASCO-J-810 spectrometer with Peltier thermostatic cell holders using a quartz cuvette of 1.0 cm path length. The concentration of the solution was fixed at  $1 \text{ mg mL}^{-1}$  for an SSPLLA chloroform/hexane mixture. Photophysical properties were measured using a 1 cm or 1 mm quartz cuvette. The emission spectra at room temperature were recorded using a SPEX-Fluorolog-3 FL3-221 spectrofluorimeter.

Variable temperature fluorescence spectra were recorded using the Spex-Fluoromax FL22 spectrofluorimeter equipped with a double grating 0.22 m Spex 1680 monochromator, a 450 W Xe lamp as the excitation source and a Hamamatsu R928P photomultiplier tube detector. The excitation wavelength was 330 nm. Emission spectra were corrected for source intensity (lamp and grating) by standard correction curves. The absorption spectra were recorded using a Shimadzu UV-2600 UV-vis spectrophotometer. Variable temperature absorption spectra were recorded using a Shimadzu model S-1700 temperature controller. The sample was allowed to reach thermal equilibrium at every temperature ( $\pm 0.1$  °C) in a Hellma Analytics 1 cm path length quartz cell in thermostated cell holder of the spectrophotometer. Wide-angle X-ray scattering (WAXS) measurements were carried out using a XEUS SAXS/WAXS system from Xenocs (operated at 50 kV and 0.60 mA) in transmission geometry using Cu  $\text{K}\alpha$  radiation (wavelength,  $\lambda = 1.54 \text{ \AA}$ ). The two-dimensional patterns were recorded using a Mar 345 image plate system (detector) and the data were processed using the Fit2D program. Silver behenate was used to calibrate the sample to detector distance. The variable temperature measurements of SSPLLA gels were carried out using a Linkam THMS 600 hot stage fitted to the X-ray system. Rheological measurements were performed using an Anton Paar modular compact (MCR 150) stress-controlled rheometer equipped with a parallel plate geometry (20 mm diameter) and striated cone. The gap between the cone and the plate was kept fixed between 0.25 mm. AFM images were collected using a multimode SPM (Bruker Nanoscope V) in the tapping mode. Antimony doped silicon cantilever with a resonant frequency of 300 kHz and a spring constant of  $40 \text{ N m}^{-1}$  was used. Samples were prepared by dropcasting the diluted gel dispersion on a cleaned silicon wafer surface and dried in the air for 48 hours in a closed Petri dish at room temperature. An MTT assay was performed using human lung fibroblast cell line WI-38. WI-38 cells were kindly gifted from CSIR-IICB, Kolkata, India. The cells were maintained in Dulbecco's modified Eagle's medium (DMEM) with 10% fetal bovine serum (FBS) and 5%  $\text{CO}_2$  at 37 °C. The growth inhibition capacity was evaluated by MTT assay. Cell suspensions of  $5 \times 10^3$  cells per well (100  $\mu\text{L}$ ) were seeded in a 96 well plate and 100  $\mu\text{L}$  of SSPLLA was added to that at various concentrations ( $1 \mu\text{g mL}^{-1}$  to  $100 \mu\text{g mL}^{-1}$ ). The plain medium was used as a negative control, while the clinically used anti-cancer chemotherapeutic agent doxorubicin (Dox,  $1 \mu\text{M}$ ) was employed as a positive control. The plates were incubated for a period of 6 h, 12 h and 24 h in a  $\text{CO}_2$  incubator. After incubation, 20  $\mu\text{L}$  of MTT ( $5 \text{ mg mL}^{-1}$ ) was added to each well and incubation was continued for an additional 2 h. The insoluble formazan crystals formed were solubilized by the addition of 100  $\mu\text{L}$  of MTT lysis buffer followed by an incubation of 4 h and the absorbance was measured at 570 nm using a microplate spectrophotometer (BioTek, Power Wave XS). The bacterial growth of SSPLLA against selected Gram-negative and Gram-positive pathogens was carried out by spreading the bacterial strains aseptically on LB agar plates using a sterile cotton swab. Four

wells were prepared on the culture smeared agar plates using a sterile cork borer. The disks were loaded with 25  $\mu\text{L}$  of SSPLLA gel in DMF and DMF as the control (2 replicates for each). The disks were then dried inside the biosafety cabinet and incubated at 37  $^{\circ}\text{C}$  for 36 h.

## Author contributions

Virat and Bhoje Gowd contributed equally in conceptualization, visualization and investigation. Virat contributed to data curation, methodology and writing – original draft preparation and Bhoje Gowd contributed to supervision and writing – reviewing and editing.

## Conflicts of interest

The authors declare no competing financial interest.

## Acknowledgements

The authors greatly appreciate Dr K. K. Maiti and Dr N. Ramesh Kumar for PL studies and biocompatibility studies. The authors thank Dr Subrata Das, Dr Sreejith Shankar, Dr V. K. Praveen, Dr U. S. Hareesh, Mr Peer Mohamed, Ms Saumini, Dr Yoosaf, Dr Karunakaran Venugopal and Mr Robert for PL, UV, CD, rheology, NMR, fluorescence lifetime decay and AFM measurements. The authors thank Mr Amal Raj and Mr Vipin Krishnan for their technical help. The authors also thank Dr Joshy Joseph for his valuable inputs. Virat is grateful to the Council of Scientific and Industrial Research (CSIR), Government of India, New Delhi for the Research Associate Fellowship. E. B. G. acknowledges the financial support from the CSIR.

## References

- J. Mei, N. L. C. Leung, R. T. K. Kwok, J. W. Y. Lam and B. Z. Tang, *Chem. Rev.*, 2015, **115**, 11718–11940.
- Y. Yang, Q. Zhao, W. Feng and F. Li, *Chem. Rev.*, 2013, **113**, 192–270.
- J. Wu, W. Liu, J. Ge, H. Zhang and P. Wang, *Chem. Soc. Rev.*, 2011, **40**, 3483–3495.
- X. Feng, L. Liu, S. Wang and D. Zhu, *Chem. Soc. Rev.*, 2010, **39**, 2411–2419.
- F. Cicoira and C. Santato, *Adv. Funct. Mater.*, 2007, **17**, 3421–3434.
- L. Tong, R. R. Gattass, J. B. Ashcom, S. He, J. Lou, M. Shen, I. Maxwell and E. Mazur, *Nature*, 2003, **426**, 816–819.
- J. Y. Zheng, Y. Yan, X. Wang, Y. S. Zhao, J. Huang and J. Yao, *J. Am. Chem. Soc.*, 2012, **134**, 2880–2883.
- M. Bredol, U. Kynast and C. Ronda, *Adv. Mater.*, 1991, **3**, 361–367.
- Y. Chen, A. J. H. Spiering, S. Karthikeyan, G. W. M. Peters, E. W. Meijer and R. P. Sijbesma, *Nat. Chem.*, 2012, **4**, 559–562.
- T. Jüstel, H. Nikol and C. Ronda, *Angew. Chem., Int. Ed.*, 1998, **37**, 3084–3103.
- S. S. Babu, V. K. Praveen and A. Ajayaghosh, *Chem. Rev.*, 2014, **114**, 1973–2129.
- A. P. de Silva, H. Q. N. Gunaratne, T. Gunnlaugsson, A. J. M. Huxley, C. P. McCoy, J. T. Rademacher and T. E. Rice, *Chem. Rev.*, 1997, **97**, 1515–1566.
- M. A. Baldo, D. F. O'Brien, Y. You, A. Shoustikov, S. Sibley, M. E. Thompson and S. R. Forrest, *Nature*, 1998, **395**, 151–154.
- J. B. Birks, *Photophysics of Aromatic Molecules*, Wiley, New York, 1970.
- T. M. Figueira-Duarte, P. G. Del Rosso, R. Trattnig, S. Sax, E. J. W. List and K. Müllen, *Adv. Mater.*, 2010, **22**, 990–993.
- S. W. Thomas, G. D. Joly and T. M. Swager, *Chem. Rev.*, 2007, **107**, 1339–1386.
- J. Mei, Y. Hong, J. W. Y. Lam, A. Qin, Y. Tang and B. Z. Tang, *Adv. Mater.*, 2014, **26**, 5429–5479.
- Y. Hong, J. W. Y. Lam and B. Z. Tang, *Chem. Commun.*, 2009, 4332–4353, DOI: 10.1039/B904665H.
- Y. Hong, J. W. Y. Lam and B. Z. Tang, *Chem. Soc. Rev.*, 2011, **40**, 5361–5388.
- R. Hu, N. L. C. Leung and B. Z. Tang, *Chem. Soc. Rev.*, 2014, **43**, 4494–4562.
- Q. Zeng, Z. Li, Y. Dong, C. A. Di, A. Qin, Y. Hong, L. Ji, Z. Zhu, C. K. W. Jim, G. Yu, Q. Li, Z. Li, Y. Liu, J. Qin and B. Z. Tang, *Chem. Commun.*, 2007, 70–72, DOI: 10.1039/B613522F.
- W. Zhao, C. Li, B. Liu, X. Wang, P. Li, Y. Wang, C. Wu, C. Yao, T. Tang, X. Liu and D. Cui, *Macromolecules*, 2014, **47**, 5586–5594.
- Y. Dong, J. W. Y. Lam, A. Qin, J. Liu, Z. Li, B. Z. Tang, J. Sun and H. S. Kwok, *Appl. Phys. Lett.*, 2007, **91**, 011111.
- A. Ajayaghosh and S. J. George, *J. Am. Chem. Soc.*, 2001, **123**, 5148–5149.
- Y. Jiang and N. Hadjichristidis, *Macromolecules*, 2019, **52**, 1955–1964.
- X.-H. Wang, N. Song, W. Hou, C.-Y. Wang, Y. Wang, J. Tang and Y.-W. Yang, *Adv. Mater.*, 2019, **31**, 1903962.
- Z. Zhang, P. Bilalis, H. Zhang, Y. Gnanou and N. Hadjichristidis, *Macromolecules*, 2017, **50**, 4217–4226.
- G. Das, R. Thirumalai, B. Vedhanarayanan, V. K. Praveen and A. Ajayaghosh, *Adv. Opt. Mater.*, 2020, **8**, 2000173.
- X. Qi, H. Li, J. W. Y. Lam, X. Yuan, J. Wei, B. Z. Tang and H. Zhang, *Adv. Mater.*, 2012, **24**, 4191–4195.
- G. Yu, S. Yin, Y. Liu, J. Chen, X. Xu, X. Sun, D. Ma, X. Zhan, Q. Peng, Z. Shuai, B. Tang, D. Zhu, W. Fang and Y. Luo, *J. Am. Chem. Soc.*, 2005, **127**, 6335–6346.
- Q. Chen, D. Zhang, G. Zhang, X. Yang, Y. Feng, Q. Fan and D. Zhu, *Adv. Funct. Mater.*, 2010, **20**, 3244–3251.
- B.-K. An, J. Gierschner and S. Y. Park, *Acc. Chem. Res.*, 2012, **45**, 544–554.



- 33 M. Martínez-Abadía, R. Giménez and M. B. Ros, *Adv. Mater.*, 2018, **30**, 1704161.
- 34 R. Taniguchi, T. Yamada, K. Sada and K. Kokado, *Macromolecules*, 2014, **47**, 6382–6388.
- 35 N. L. C. Leung, N. Xie, W. Yuan, Y. Liu, Q. Wu, Q. Peng, Q. Miao, J. W. Y. Lam and B. Z. Tang, *Chem. – Eur. J.*, 2014, **20**, 15349–15353.
- 36 J. Xu, W. Ji, C. Li, Y. Lv, Z. Qiu, L. Gao, E. Chen, J. W. Y. Lam, B. Tang and L. Jiang, *Adv. Opt. Mater.*, 2018, **6**, 1701149.
- 37 Z. Qiu, X. Liu, J. W. Y. Lam and B. Z. Tang, *Macromol. Rapid Commun.*, 2019, **40**, 1800568.
- 38 Y.-G. He, S.-Y. Shi, N. Liu, Y.-S. Ding, J. Yin and Z.-Q. Wu, *Macromolecules*, 2016, **49**, 48–58.
- 39 X. Guan, D. Zhang, L. Meng, Y. Zhang, T. Jia, Q. Jin, Q. Wei, D. Lu and H. Ma, *Ind. Eng. Chem. Res.*, 2017, **56**, 680–686.
- 40 J. Xue, W. Bai, H. Duan, J. Nie, B. Du, J. Z. Sun and B. Z. Tang, *Macromolecules*, 2018, **51**, 5762–5772.
- 41 A. C. B. Rodrigues, J. Pina, W. Dong, M. Forster, U. Scherf and J. S. Seixas de Melo, *Macromolecules*, 2018, **51**, 8501–8512.
- 42 Y.-D. Jiu, C.-F. Liu, J.-Y. Wang, W.-Y. Lai, Y. Jiang, W.-D. Xu, X.-W. Zhang and W. Huang, *Polym. Chem.*, 2015, **6**, 8019–8028.
- 43 Y. Jiu, J. Wang, J. Yi, C.-F. Liu, X.-W. Zhang, W.-Y. Lai and W. Huang, *Polym. Chem.*, 2017, **8**, 851–859.
- 44 C.-F. Liu, M. Sang, W.-Y. Lai, T. T. Lu, X. Liu and W. Huang, *Macromolecules*, 2018, **51**, 1325–1335.
- 45 C.-F. Liu, Y. Jiu, J. Wang, J. Yi, X.-W. Zhang, W.-Y. Lai and W. Huang, *Macromolecules*, 2016, **49**, 2549–2558.
- 46 W. Huang, M. Bender, K. Seehafer, I. Wacker, R. R. Schröder and U. H. F. Bunz, *Macromolecules*, 2018, **51**, 1345–1350.
- 47 G. Liang, L.-T. Weng, J. W. Y. Lam, W. Qin and B. Z. Tang, *ACS Macro Lett.*, 2014, **3**, 21–25.
- 48 Z. Wang, S. Chen, J. W. Y. Lam, W. Qin, R. T. K. Kwok, N. Xie, Q. Hu and B. Z. Tang, *J. Am. Chem. Soc.*, 2013, **135**, 8238–8245.
- 49 H. Wang, G. Liu, H. Gao and Y. Wang, *Polym. Chem.*, 2015, **6**, 4715–4718.
- 50 S. Sasaki and T. Asakura, *Macromolecules*, 2003, **36**, 8385–8390.
- 51 J. Zhang, Y. Duan, H. Sato, H. Tsuji, I. Noda, S. Yan and Y. Ozaki, *Macromolecules*, 2005, **38**, 8012–8021.
- 52 H. Marubayashi, S. Akaishi, S. Akasaka, S. Asai and M. Sumita, *Macromolecules*, 2008, **41**, 9192–9203.
- 53 H. Marubayashi, S. Asai and M. Sumita, *Macromolecules*, 2012, **45**, 1384–1397.
- 54 D. Sawai, K. Takahashi, A. Sasashige, T. Kanamoto and S.-H. Hyon, *Macromolecules*, 2003, **36**, 3601–3605.
- 55 P. Shaiju, N. S. Murthy and E. B. Gowd, *Macromolecules*, 2016, **49**, 224–233.
- 56 S. Nagarajan and E. B. Gowd, *Macromolecules*, 2017, **50**, 5261–5270.
- 57 T.-S. Hsiao, P.-C. Huang, L.-Y. Lin, D.-J. Yang and J.-L. Hong, *Polym. Chem.*, 2015, **6**, 2264–2273.
- 58 S. K. Nisha and S. K. Asha, *ACS Appl. Mater. Interfaces*, 2014, **6**, 12457–12466.
- 59 S. K. Nisha and S. K. Asha, *J. Mater. Chem. C*, 2014, **2**, 2051–2060.
- 60 M.-C. Li, H.-F. Wang, C.-H. Chiang, Y.-D. Lee and R.-M. Ho, *Angew. Chem., Int. Ed.*, 2014, **53**, 4450–4455.
- 61 K. Kan, M. Fujiki, M. Akashi and H. Ajiro, *ACS Macro Lett.*, 2016, **5**, 1014–1018.
- 62 N. M. Praveena, S. Nagarajan and E. B. Gowd, *CrystEngComm*, 2021, **23**, 2122–2132.
- 63 Y. Sakamoto and H. Tsuji, *Macromol. Chem. Phys.*, 2013, **214**, 776–786.
- 64 K. Wasanasuk, K. Tashiro, M. Hanesaka, T. Ohhara, K. Kurihara, R. Kuroki, T. Tamada, T. Ozeki and T. Kanamoto, *Macromolecules*, 2011, **44**, 6441–6452.
- 65 Y. Sakamoto and H. Tsuji, *Polymer*, 2013, **54**, 2422–2434.
- 66 Y. Matsuda, A. Fukatsu, Y. Wang, K. Miyamoto, J. W. Mays and S. Tasaka, *Polymer*, 2014, **55**, 4369–4378.
- 67 R. W. Newberry and R. T. Raines, *Chem. Commun.*, 2013, **49**, 7699–7701.
- 68 T. Mori and Y. Inoue, *J. Phys. Chem. A*, 2005, **109**, 2728–2740.
- 69 H.-F. Wang, C.-H. Chiang, W.-C. Hsu, T. Wen, W.-T. Chuang, B. Lotz, M.-C. Li and R.-M. Ho, *Macromolecules*, 2017, **50**, 5466–5475.
- 70 N. Berova, L. D. Bari and G. Pescitelli, *Chem. Soc. Rev.*, 2007, **36**, 914–931.
- 71 A. Marini, A. Muñoz-Losa, A. Biancardi and B. Mennucci, *J. Phys. Chem. B*, 2010, **114**, 17128–17135.
- 72 J. Kim, S. Cho and B.-K. Cho, *Chem. – Eur. J.*, 2014, **20**, 12734–12739.
- 73 X. Zhang, Z. Chi, H. Li, B. Xu, X. Li, W. Zhou, S. Liu, Y. Zhang and J. Xu, *Chem. – Asian J.*, 2011, **6**, 808–811.
- 74 M. M. Joseph, A. N. Ramya, V. M. Vijayan, J. B. Nair, B. T. Bastian, R. K. Pillai, S. T. Therakathinal and K. K. Maiti, *Small*, 2020, **16**, 2003309.